Failure Mechanism Analysis and Life Prediction based on Atmospheric Plasma-Sprayed and Electron Beam-Physical Vapor Deposition Thermal Barrier Coatings

Bochun Zhang

A thesis submitted to the Faculty of Graduate and Postdoctoral Studies in partial fulfillment of the requirement for the degree of

MASTER OF APPLIED SCIENCE

In Mechanical Engineering

Ottawa-Carleton Institute for Mechanical and Aerospace Engineering
University of Ottawa
Ottawa, Canada

January 2017

Abstract

Using experimentally measured temperature-process-dependent model parameters, the failure analysis and life prediction were conducted for Atmospheric Plasma Sprayed Thermal Barrier Coatings (APS-TBCs) and electron beam physical vapor deposition thermal barrier coatings (EB-PVD TBCs) with Pt-modified β-NiAl bond coats deposited on Ni-base single crystal superalloys. For APS-TBC system, a residual stress model for the top coat of APS-TBC was proposed and then applied to life prediction. The capability of the life model was demonstrated using temperature-dependent model parameters. Using existing life data, a comparison of fitting approaches of life model parameters was performed. The role of the residual stresses distributed at each individual coating layer was explored and their interplay on the coating's delamination was analyzed. For EB-PVD TBCs, based on failure mechanism analysis, two newly analytical stress models from the valley position of top coat and ridge of bond coat were proposed describing stress levels generated as consequence of the coefficient of thermal expansion (CTE) mismatch between each layers. The thermal stress within TGO was evaluated based on composite material theory, where effective parameters were calculated. The lifetime prediction of EB-PVD TBCs was conducted given that the failure analysis and life model were applied to two failure modes A and B identified experimentally for thermal cyclic process. The global wavelength related to interface rumpling and its radius curvature were identified as essential parameters in life evaluation, and the life results for failure mode A were verified by existing burner rig test data. For failure mode B, the crack growth rate along the topcoat/TGO interface was calculated using the experimentally measured average interfacial fracture toughness.

Table of Contents

List of Figures

List of Tables

Abbreviations and Definitions

TBC	Thermal barrier coating or topcoat within thermal barrier coating system
TBCs	Thermal barrier coating system
APS-TBC	Atmospheric plasma sprayed-Thermal barrier coating
EB-PVD TBC	Electron beam-Physical vapor deposition Thermal barrier coating
TC	Topcoat
TGO	Thermal grown oxide
BC	Bond coat
MCrAlY	A composition of bond coat that consists of M(M = Co, Ni or Co/Ni), Chromium, Aluminum, Yttrium.
Pt-Al	A composition of bond coat that consists of Platinum-modified Aluminum overlays
SEM	Scanning Electron Microscopy
FEA	Finite element analysis
CTE	Coefficient of thermal expansion
YSZ	Yttria-stabilized Zirconia
Lifetime	failure time of Thermal barrier coating systems that equal to life in context
Matlab	High-level technical computing language and interactive environment

Acknowledgements

First and foremost I would first like to thank my thesis advisor Natalie Baddour, Chair of the Mechanical engineering department at University of Ottawa. The door to Professor Baddour's office was always open whenever I ran into a trouble spot or had a question about my research or writing. She consistently allowed this paper to be my work, but steered me in the right the direction whenever she thought I needed it. She also offered me an opportunity to participate in the 2016 Canada society for mechanical engineering international congress (2016 CSME). By addressing a presentation and talking to the researchers in the conference, I obtained lots of information that was useful for my research as well as my thesis. Thanks you again for the reimbursement of my travelling expense.

I would also like to thank the expert who worked as my co-supervisor and was involved as technical support for my research survey, Professor Kuiying Chen. During a year and half of my research, he required me to give a project meeting weekly which promoted the proceeding of my research work and many technical challenges and difficulties were tackled from the effort by both of us. At the beginning of my research work, he taught me about the basic method to read the journal paper and conduct analysis based on existing experimental data. I appreciated that the ideas during discussion we had in each project meeting inspired me and many theories presented in my thesis came from further work after each discussion. Professor Chen also guide me with my journal papers acting as essential role in my thesis. Thanks again for all the contribution he made during my research work.

I wish I can thank my friend, Zekun Zhou and Wentian Wang. Zhou has been amazing help with Matlab, the software I mainly used in my research work. He was never bored to answer my phone and inspired me in an unexpected way when I was at a deadlock during my research work. Wang was willing to help me with my presentation when I prepared to participate in 2016 CSME. He made lots of suggestion on slides that were extremely helpful and some tips he told me worked well when I presented my slides in the congress. They are my best friends and I want to thank you again.

Finally, I must express my very profound gratitude to my parents and to my aunt for providing me with unfailing support and continuous encouragement throughout my years of study and through the process of researching and writing this thesis. This accomplishment would not have been possible without them. Thank you.

1. Introduction

Thermal barrier coating systems (TBCs) used as a thermal isolator between substrate metal and the external environment in gas turbines have been developed for decades. The TBC is typically applied to the inner parts of a gas turbine that undergo severe operating conditions, for example, a large temperature gradient in a very short time as well as an extremely high holding temperature. The coating system is used to sustain high thermal gradients and provide an adequate backside cooling, which prolongs the lifetime of components [1]–[8]. The TBCs typically consists of a ceramic topcoat layer, a metallic bond coat layer and the substrate metal that needs to be protected. Based on the difference of deposition methods, the ability and mechanism of the topcoat to sustain a high thermal gradient in the presence of backside cooling could be variable. As of this writing, atmospheric plasma spray (APS) as well as electron beam-physical vapor deposition (EB-PVD) are considered as the two main methods to fabricate the topcoat in TBCs. Meanwhile, strain-tolerance is also integrated into the design of the topcoat in order to avoid instantaneous delamination of the topcoat due to large thermal stress which is to be expected at the topcoat and bond coat interface during thermal cyclic serving conditions. The bond coat of TBCs is applied onto the substrate before the deposition of the topcoat. To strengthen the interfacial adhesion, the bond coat is used to provide sufficient chemical and mechanical bonding between the topcoat and substrate. Similar to the fabrication of topcoat, the material of bond coat (diffusion aluminide coating or MCrAlY overlay coating) and the deposition parameters (either heavy or light surface grit-blast) are both selected depending on topcoat deposition

methods. Another important feature of the bond coat is the ability to prevent oxidation of the substrate under extremely high temperatures by forming a thin oxide layer known as thermal grown oxide (TGO). The preferred α-alumina layer is mainly found at the interface between topcoat and bond coat due to the oxidation mechanism of TBC, and is governed by inward diffusion of anions (oxygen ions or oxygen). Oxidation occurs at the surface of the bond coat which acts as a sufficient aluminide reservoir to facilitate the oxidation. However, large stresses could be introduced based on the mechanism of TGO formation. The failure mechanism of different TBCs is also related to TGO layer formation as consequence of the progressive oxidation of the bond coat. It is usually considered that the spallation of the topcoat from the bond coat marks the failure of TBCs. For engineering applications, a reliable lifetime prediction model is required to estimate the average lifetime corresponding to various external serving conditions. However, the failure mechanism and related lifetime model can vary from APS to EB-PVD TBCs since their microstructure and thermal characteristics of the topcoats do not possess many similarities. An analysis based on the different TBC fabrication methods should therefore be conducted before development of a detailed lifetime model.

1.1. Atmospheric plasma sprayed thermal barrier coating system

1.1.1. APS-TBCs general background (scientific background)

The typical microstructure from a cross-section of a APS-TBC specimen is shown in Figure 1-1.

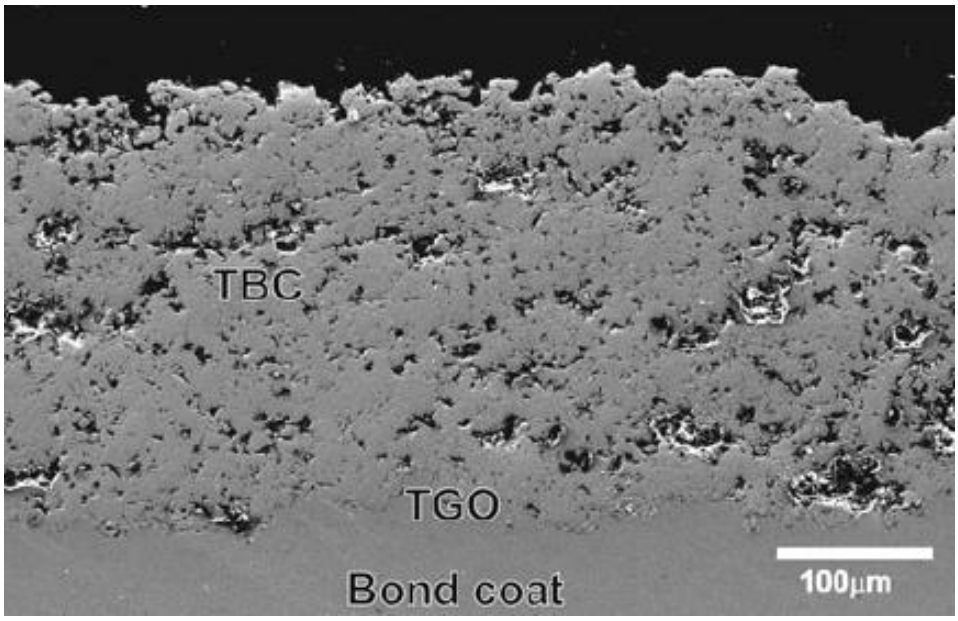

Figure 1-1 Typical microstructure of APS-TBCs, the intra/intersplat voids could be observed within topcoat that lower the conductivity of topcoat

The geometrical parameters of splats (size and depositing position) that result from the impact of high speed Yttria-stabilized Zirconia (YSZ) particles to the bond coat surface are the most significant factors that determine the microstructure of topcoat. This, in turn plays a major role in the chemical and mechanical properties of the topcoat. For example, the intersplat pores and voids formed by overlapping splats could provide a high strain tolerance, the higher porosity of the topcoat also indicates a lower thermal conductivity implying that the capability of the thermal isolator could be improved. It has to be mentioned that the cost of APS-TBCs fabrication is much lower than TBCs deposited by EB-PVD, thus APS-TBCs is always considered as a preferred thermal isolator.

The bond coat of APS-TBCs is based on the MCrAlY system, which is a bond coat that consists of M (M = Co, Ni or Co/Ni), Chromium, Aluminum and Yttrium. The Y indicates the yttrium that is used to improve the adhesion between TGO and bond coat.

The surface of the bond coat from APS-TBCs typically has a roughness which is integrated in the design since it provides sufficient mechanical bonding between the topcoat and substrate.

The TGO layer is formed as a consequence of progressive oxidation of the bond coat. Apart from α-alumina observed between the topcoat and bond coat, it is generally considered heterogeneous within a TGO based on the MCrAlY system. This is partially related to the oxidation of yttrium, which is easier to be oxidized compared with other elements. Thus, the yttrium aluminum garnet or namely, peg observed from a cross-section of SEM usually indicates an area with a high distribution of yttria.

1.1.2. Failure mechanism analysis of APS-TBCs

The failure mechanism of APS-TBCs is largely dependent on the thickness of the TGO. Based on the results from thermal cycling experiments, a crack is initiated at the peak location of bond coat roughness and propagates along the interface as a consequence of the coefficient of thermal expansion mismatch between TGO and bond coat. As theTGO thickens, the crack generate at a valley of the topcoat where stress inversion occurs. The spallation of the topcoat occurs when neighboring cracks coalescence and marks the failure of TBCs. The details of the failure mechanism analysis of APS-TBCs are described in Section 3 part 2.

1.1.3. Lifetime prediction model of APS-TBCs

The residual stress integrated model (Residual stress - crack driving force - lifetime prediction model) is currently considered as the preferred lifetime prediction model based on APS-TBCs. The residual stress is generated as consequence of either the

coefficient of thermal expansion (CTE) mismatch strain between topcoat, TGO and bond coat or as a consequence of TGO volume expansion strain. These two phenomena applications were considered as a significant development. The introduction of geometrical parameters describing the roughness profile of the interface into the stress model was the first essential application where the capacity of the stress model was improved compared with those stress models based on a flat assumption. The benefit of those geometrical parameter integrated stress models also resulted from their ability to be used in finite element analysis. The matrix could be set based on the geometrical parameters measured from SEM and better simulation results could thus be obtained. The second essential application was attributed to the integration of process and/or temperature dependent parameters. Compared with the average value approximated by a constant, the correlation of time or temperatures with model parameters could be more precisely described by those process/temperature dependent parameters. These two applications are considered in the development of stress models in the present work. The crack driving force is used to evaluate the effect of stress on cracking behavior, which is usually given by the form of energy release rate or residual stress related term. The correlation of those crack driving forces to the crack length related parameters is expressed by introducing a fitting parameter. This significant parameter will be discussed in later sections that relate to the lifetime prediction model. To date, several attempts have been made although large discrepancy from predicted lifetime to experimental lifetime indicates the need for better lifetime prediction models.

1.2. Electron beam-physical vapor deposition

1.2.1. EB-PVD TBCs general background

A typical microstructure from a cross-section of a EB-PVD TBC specimen is shown in Figure 1-2. The most attractive characteristics is the columnar grain structure in the topcoat which, with segmentation vertical cracks, could provide a large strain tolerance. Similar to the topcoat fabricated by APS, multi-scale porosity is able to lower the thermal conductivity. However, the cost of EB-PVD fabrication is much higher compared to TBCs deposited by traditional APS.

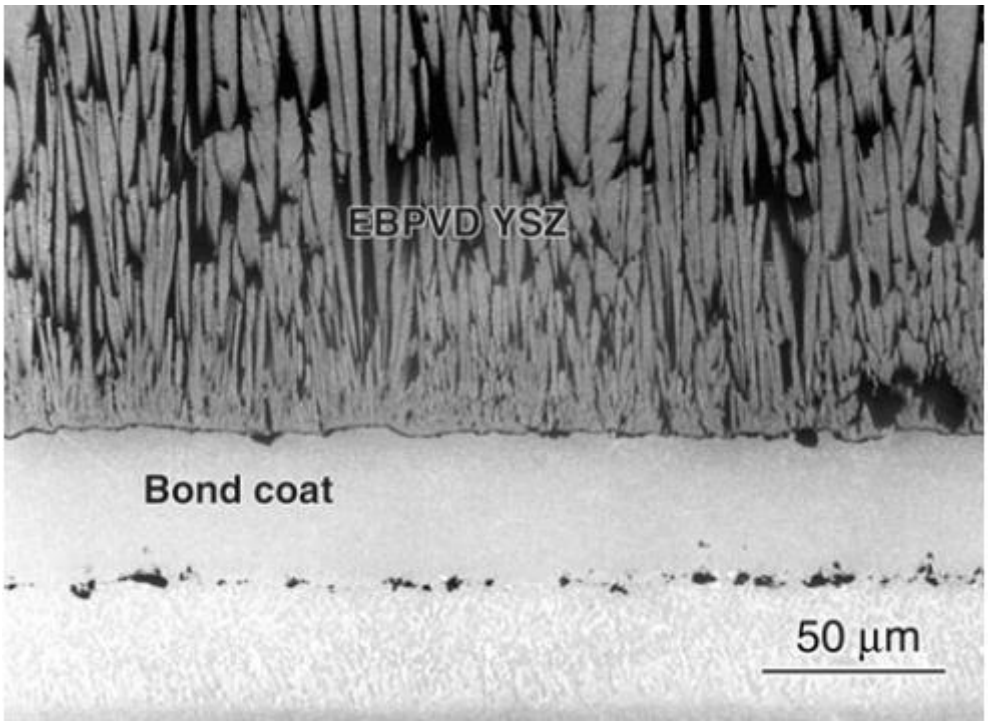

Figure 1-2 Typical microstructure of EB-PVD TBCs, topcoat shows the columnar structure with vertical cracks

There are two different type of bond coats for EB-PVD TBCs, MCrAlY overlay coating or diffusion aluminide coating. The previous type has been discussed in the preceding section. For the latter, the bond coat usually consists of platinum modified diffusion aluminide. Platinum is used to improve the ability to provide better adhesion between the topcoat and TGO. The surface of the bond coat, unlike the sinusoidal interfacial

profile of APS-TBCs, is relative flat which is deliberately designed to reduce the effect of large imperfections by sand-blasting the bond coat surface before further topcoat deposition.

The type of TGO layer formed between topcoat and bond coat is dependent on the selection of the bond coat. As described in the preceding section, apart from typical α-alumina, the yttrium aluminum garnet is used for the Pt-Al bond coat. For the present research in EB-PVD, the failure mechanism analysis and lifetime prediction model are only conducted for the Pt-Al bond coat TBC system.

1.2.2. Failure mechanism analysis of EB-PVD TBCs

Until now, there were mainly two failure mechanisms identified for the EB-PVD TBCs based on the Pt-Al bond coat. For the failure mode A, the relative small rumpling effect from the bond coat dominates the failure process. Due to its thermal instability at high temperature, small downward displacements could be found at the surface of the bond coat and followed by TGO, leaving voids at the interface between the topcoat and TGO. The failure could be expected as neighboring voids expand horizontally and crack forms leading to spallation of the topcoat from TGO.

Failure mode B is similar to that of APS-TBCs, the cracks generate at a peak of TGO/BC interface and penetrate the TGO until reaching the voids at an interface between topcoat/TGO. The failure then occurs as neighboring cracks coalescence. The details for the failure mechanism analysis of EB-PVD TBCs are described in section 5 part 2. Moreover, the relationship between failure mechanism and sand-blasting process that is used to flatten the surface of bond coat will be discussed.

1.2.3. Lifetime prediction model of EB-PVD TBCs

Although there were plenty of data for the experimental lifetime of EB-PVD TBCs conducted by both isothermal and thermal cycling process, it is rare that analytical lifetime prediction models can be found. One damage model proposed by Courcier *et al* [9] is a semi-quantitative model based on observation results from experiments where the elastic strain as well as TGO volume expansion were considered in order to describe damage related parameters. Another important model proposed by Evans [10] was based on film theory. Lifetime was estimated via TGO critical thickness measured by experiments or calculated by a parabolic growth law. The model does not contain factors that describe the effect of stress on lifetime based on EB-PVD TBCs. The present work develops a stress model as well as a lifetime prediction model by using temperature and process-dependent parameters described in section 4 and section 5.

1.3. Objectives and Outline of the thesis

This thesis has three objectives that will be addressed in turn.

1. To improve the capability of lifetime prediction models for APS-TBC systems by proposing a new APS-TBC stress model and incorporating temperature-dependence into the fitting parameters.
2. To develop stress models on different layers within EB-PVD TBC systems by using temperature process-dependent model parameters.
3. To estimate the lifetime and crack growth rate for EB-PVD TBC systems by using the stress models and temperature process-dependent model parameters

developed in objective 2.

Apart from the introduction of background about thermal barrier coating system, the development methodology to be used in this thesis for the stress model and lifetime prediction is presented in Chapter 2. The results for lifetime prediction by using temperature-dependent parameters based on atmospheric plasma sprayed thermal barrier coating system is described in Chapter 3 (objective 1). The stress modelling process is shown in Chapter 4 (objective 2) and the development of the proposed lifetime prediction model along with the predicted lifetime is presented in Chapter 5 (objective 3). A summary is given in Chapter 6.

2. Methodology

2.1. Brief discussion of existing lifetime prediction models

It is generally considered that the lifetime of a coating system will decrease nonlinearly with increasing service temperature. For engineering applications, it is necessary to acquire each temperature-dependent lifetime. To date, several lifetime prediction models have been proposed based on various assumptions of the failure mechanisms of the coating system or the type of data measured experimentally. A general description for each type of lifetime model will be discussed in the subsequent section.

An early model developed by Miller [11][12] is considered as the first generation of lifetime prediction model. A significant empirical model in which the measured TGO thickness as well as the measured strain were used to estimate the lifetime by comparing with the critical TGO thickness as well as critical strain, respectively. The lifetime model attempt to describe an essential role of the TGO thickness in APS-TBCs life prediction based on experimental observation. However, the relative simple configuration of the lifetime function in this model indicates that the lifetime was estimated empirically based on a large experimental dataset as well as failure analysis.

The TGO growth, as the source of strain generated by volume expansion, was recognized as a critical factor affecting the lifetime of coating system. The damage by interfacial rumpling was also identified as a factor and both related parameters were integrated into the second generation of lifetime prediction model, for example the model proposed by Courcier *et al* [9]. In this mode, the TGO growth was described by a parabolic law. However, an analytical function for the rumpling effect was not

identified. The rumpling effect was measured by the average roughness at the surface between the TGO and the bond coat in the following lifetime model.

As can be seen in the preceding discussion, lifetime models have gradually evolved to relate to the identified failure mechanism for each different coating system. The rumpling effect, for example, is generally considered as the significant failure mechanism in EB-PVD TBCs with platinum modified aluminum BC. The voids formed within the topcoat close to the TGO are due to the rumpling effect of the bond coat at high hold temperature. The failure occurs when these voids extend parallel to the surface of the TGO followed by separation crack formation and spallation of the topcoat. The function for evaluating the stress intensity factor for EB-PVD TBCs was developed by Mumm et al [1][13] which could be used for the third generation of lifetime prediction model. Another failure mechanism-dependent lifetime prediction model working on APS-TBCs was developed by Evans et al [10]. The remnant ligament theory was built into the failure mechanism described for APS-TBCs, and the corresponding analytical critical TGO thickness function was developed as time fracture occurs. The lifetime could be estimated combining the critical TGO function with parabolic law that was used to estimate the TGO growth. It should be remarked that the discrepancy between the second and third generation of lifetime prediction model depends on whether all parameters integrated into the lifetime model could be described by an analytical function, which also marks the transformation of lifetime prediction from an empirical model to an analytical model.

Up to the model described above, the lifetime was estimated from the critical

characteristics of interfacial morphology profile (rumpling amplitude or TGO thickness). Nevertheless, the reason that the failure occurs in practice, as indicated by the spallation of the topcoat from the bond coat, is that a large radial stress is generated between the layers. The stress could be estimated numerically by finite element analysis and it is reasonable that the lifetime could also be estimated based on the stress-dependent energy-related parameters. The fourth generation of lifetime prediction model, represented by the model developed by Vaßen et al [14], consists of a subcritical crack growth law, where the stress generated by the coefficient of thermal expansion mismatch is integrated into the lifetime model. The physical implication of the fitting parameter was illustrated and estimated by experimental lifetime measurements. This also marks the combination of empirical results with analytical solutions. It should be mentioned that the capability of lifetime models was determined by the variation of significant parameters involved. For example, for APS-TBCs, a regular roughness profile from the interface between the topcoat and BC could be expected due to the spray parameters controlled during TBC fabrication. The geometrical roughness of the interface could be estimated by a sinusoidal function with a roughness amplitude A, as well as wavelength L, both of which are integrated into lifetime estimation as average value though, the roughness amplitude A and global wavelength L vary as a function of temperature and cycle numbers. Thus, temperature process-dependent model parameters are integrated into the analytical stress function in the present research work and simulated stress is determined by fitting the residual stress-related parameters based on the FE analysis.

Some critical points about the lifetime prediction model discussed above are listed in Table 2-1.

Table 2-1 Lifetime prediction model categorized by generations

Generation Number	Model Configuration	Critical Parameters	Empirical →Analytical	Capability
I	$N = \left(\frac{\Delta\varepsilon_c \left(d/d_C \right)}{\Delta\varepsilon} \right)^a$	(Critical) TGO thickness/(Critical) strain range	Empirical function based on experimental lifetime data	Low
II	$D = 1 - \left(1 - D_{ox}\right)\left(1 - D_r\right)$ Global damage equation	Damage caused by isothermal(TGO growth)/thermal cyclic process(rumpling effect)	Empirical function Based on measured damage data	medium
III	$K \approx \frac{E_{TBC}(dA/dN)}{2\sqrt{\pi}(1-\nu_{TBC}^{\ 2})\sqrt{L}}\left(\frac{L}{a}\right)^{1.5} N$ $h_c = \frac{2\sqrt{\pi}\left(1 - \upsilon^2\right) m d^{1.5} K_{Ic}^{TBC}}{\left(m - 1\right) R E_{TBC}}$	Rumpling amplitude; Global wavelength/Critical TGO thickness	Analytical model based on different failure mechanism	high
IV	$\int_{a_0}^{a_f} \frac{da}{a^{m/2}} = \frac{A^* Y^m}{K_{IC}^m} \cdot \int_{t_0}^{t_f} \sigma(T)^m dt$ Subcritical crack growth law	Temperature-process-dependent parameters, fitting parameter $\frac{A^* Y^m}{K_{IC}^m}$	Analytical model based on stress analysis with FEA results	high

Proposed lifetime prediction models started from empirical models represented by an early strain model and gradually transformed to semi-analytical models, such as the subcritical crack growth law. For the empirical model, the experimental data, such as measured lifetime and damage percentage to the total area, play a major role in evaluating the predicted lifetime. As the models approach an analytical model, the dependence on experimental data decreases, more analysis is put into the newly proposed functions that attempt to illustrate the essence of factors determining the lifetime of the coating system. The experimental data in the analytical model are used to fit the lifetime prediction model parameters as fitting parameters, as will be discussed in the following section.

2.2. The use of critical parameter of analytical lifetime prediction model in the present work——Fitting parameter

It should be noted that all the analytical models discussed in the preceding section belong to the semi-empirical model class. Here, existing experimental data (such as temperature-process dependent geometrical parameters or measured lifetime from thermal cyclic experiments) play a significant role in affecting the estimated results of lifetime model related parameters or fitting parameters. These fitting parameter are used to equate the physical units from both sides of a lifetime prediction model, as well as provide a reasonable estimated value to facilitate the evaluation process of lifetime prediction. The fitting parameter is generated from the lifetime prediction model. Assume that the general form of an analytical lifetime prediction model is described by

$$A(t,T) = B(t,T)C(T) \qquad \text{eq 2-1}$$

where *A(t,T)* is a temperature-process model parameter for which both analytical and experimentally measured data have been obtained. *B(t,T)* is a temperature-process model parameter for which only an analytical expression is obtained. For the *C(T)*, neither analytical expression nor experimental measured data could be found.

Based on these assumptions, the function *C(T)* is considered to be the fitting parameter within the presented lifetime prediction model. By integrating the temperature-process-dependent experimental data into the analytical expression of *A(t,T)* and related temperature-process information into the analytical expression of *B(t,T)*, it is possible that the value of the temperature-dependent fitting parameter *C(T)* can be obtained and fitted by an appropriate analytical expression which is used to predict the temperature-dependent lifetime within the range of temperatures provided by the experimental measured data.

Since the correlation between the temperature-dependent lifetimes to other parameters are given by eq 2-*1*, the fitting parameter could be directly identified by estimating the "unknown" part *C(T)* through a mathematical expression. In order to ensure the accuracy of predicted lifetime, it is necessary to verify the capability of the fitting parameters. Assume that the fitting parameter *C(T)* consists of *D(T)* and *E(T)* described as

$$C(T) = D(T)E(T) \qquad \textit{eq 2-2}$$

where the value of *D(T)* and *E(T)* could be qualitatively estimated. As *C(T)* is calculated by using the method discussed above, a comparison between the result of *C(T)* and

D(T)E(T) could be used to evaluate the capability of the fitting parameters.

The fitting parameter discussed above was generated by a lifetime prediction model where the implication of the fitting parameter was identified. Researchers attempted to establish the lifetime prediction model by including all the lifetime related parameters, such as failure mode related parameters, the type of stress generated at a specific layer, the surface geometrical parameter to the lifetime, etc. Nevertheless, there should be many unexpected factors that failed to integrate into the expression of lifetime prediction model. It is expected that the capability of lifetime prediction model is determined by the number of factors involved. It has to be mentioned again that the fitted mathematical expression for fitting parameters only works for predicted lifetime within the experimental data range.

2.3. The application of lifetime prediction model used in the present work

The generation III and IV of lifetime prediction models are the main focus of the present work, where the failure mechanisms related to the different topcoat fabrication method, i.e. APS-TBC, EB-PVD, are identified and incorporated into the lifetime model. Based on the analysis of the subcritical crack growth law, a lifetime prediction model for APS-TBCs with temperature-dependent fitting parameters is presented in Chapter 3. As discussed in the preceding section, the stress at the interface between the topcoat, TGO and bond coat generated during thermal cyclic experiments plays a significant role, affecting cracking behavior. The analysis of thermal stress in EB-PVD TBCs which is generated as a consequence of the coefficient of thermal expansion mismatch is described in Chapter 4. A specific rumpling-dependent failure mechanism and related lifetime model is detailed in the Chapter 5, and based on the contribution of stress

analysis, a method to quantitatively evaluate the crack growth rate within layers is provided.

3. Lifetime prediction based on Atmospheric Plasma-sprayed Thermal Barrier Coating system

This chapter addresses objective 1 (estimate lifetime for APS-TBC system) by using temperature-dependent fitting parameters.

The content of this chapter has been submitted for publication to the Journal of Thermal Spray Technology in 2016.

[a]*B. Zhang,* [b*]*K. Chen,* [a] *N. Baddour,* [c] *P. C. Prakash*

[a] *Department of Mechanical Engineering, the University of Ottawa, Ottawa, Canada*

[b] *Structures, Materials and Manufacturing Laboratory, Aerospace Portfolio, National Research Council Canada, Ottawa, Canada*

[c] *Gas Turbine Laboratory, Aerospace Portfolio, National Research Council Canada, Ottawa, Canada*

**Corresponding author*

Aerospace Portfolio

National Research Council Canada

Ottawa, Ontario, K1A 0R6

Canada

Fax 1-613-949-8165

E-mail: kuiying.chen@nrc-cnrc.gc.ca

Abstract

The failure analysis and life prediction of Atmospheric Plasma Sprayed Thermal Barrier Coatings (APS-TBCs) were carried out for a thermal cyclic process. A residual stress model for the top coat of APS-TBC was proposed and then applied to life prediction. This residual stress model shows an inversion characteristic versus thickness of Thermally Grown Oxide (TGO). The capability of the life model was demonstrated using temperature-dependent model parameters. Using existing life data, a comparison of fitting approaches of life model parameters was performed. A larger discrepancy was found for the life predicted using linearized fitting parameters versus temperature compared to those using non-linear fitting parameters. A method for integrating the residual stress was proposed by using the critical time of stress inversion. A residual stress relaxation of topcoat was examined through using a viscosity parameter in the model, and this relaxation effect on fatigue crack growth was discussed. The role of the residual stresses distributed at each individual coating layer was explored and their interplay on the coating's delamination was analyzed.

Keywords: life prediction, CTE mismatch, fitting parameter, critical time for stress inversion

3.1. Introduction

Thermal barrier coatings (TBCs), consisting of an Yttria partially Stabilized Zirconia (YSZ) topcoat and a metallic bond coat (BC) deposited onto a superalloy substrate, are favourably used as the protective coatings of hot section components such as combustion chambers, turbine nozzle guide vanes and turbine blades in advanced gas turbine engines. These coatings can withstand high inlet temperatures, thus increasing engine efficiency and improving the life of the components [5]–[8], [15]–[18]. While the YSZ layer has low thermal conductivity and provides thermal insulation to the component, the metallic bond coat enhances the adhesion of the YSZ layer to the substrate and also provides oxidation and corrosion protection to the substrate metal [1], [19]–[23].

One general understanding about TBC failure is that biaxial compressive stresses are built up at the interface between the ceramic top coat and the bond coat during cooling from elevated to ambient temperature because of the thermal expansion mismatch between the two constituents. The biaxial compressive stresses produce a tensile stress normal to the coating plane, due to local tortuosity of the interface plane morphology. The tensile stress that acts on pre-existing flaws and defects and thus promotes crack initiation and delamination in the coating system [24]–[34].

It has been understood that the failure of TBC systems is largely attributed to the formation of Thermally Grown Oxide (TGO) as large stresses could be generated while TGO thickens upon progressive oxidation of the bond coat [35]–[40]. Meanwhile, extensive cracks nucleate from the sites where transient mixed oxides such as spinel form, leading to a reduction of fracture toughness [41]–[49]. Based on the identified

failure mechanisms, various life models of APS-TBCs have been explored. One early model developed by Miller[11][12] attempted to describe an essential role of the TGO thickness in APS-TBCs life prediction. The life of APS-TBCs was evaluated using ratios of TGO thickness over the critical TGO thickness, as well as the ratio of the strain over the critical strain.

Another life model proposed by Beck *et al* [50] divided the entire life of APS-TBCs into two parts associated with crack incubation and propagation, where the trends of TGO thickness as well as crack length were used to define the boundary between these two life periods. The residual stress generated due to a difference of Coefficient of Thermal Expansion (CTE) between the topcoat and TGO together with TGO growth stress were integrated into the life model. The life in [50] was numerically evaluated by calculating the crack growth rate iteratively during thermal cycles up to the specific measured failure crack length.

Busso *et al.* [51] developed a life model for APS TBCs on the basis of fatigue damage parameters. The fatigue damage is driven by the maximum out-of-plane interfacial stress, which was obtained from the finite element analysis of a representative cell of a TBC system. The maximum out-of-plane interfacial stress comprised the combined stresses including the thermal stress during cycles and stresses due to oxide growth and sintering of the top coat. In their work, the effects of thermo-elastic and visco-plastic deformation, bond coat progressive oxidation and topcoat sintering were

considered to play significant roles in evaluating the out-of-plane stress.

Evans *et al*. [10] proposed an analytical life model in which TGO growth kinetics combined with the delamination of the topcoat were integrated to evaluate the life based on assumed cracking patterns. The physics beyond the model is that the failure of the TBC system occurs upon a detachment of ligament with available transverse load on the system. The curvature radius describing the roughness of imperfection was introduced into the life model.

Va ßen et al [14] investigated the life of APS-TBC systems through examining fatigue crack growth rate via

$$\int_{a_0}^{a_f} \frac{da}{a^{m/2}} = \frac{A^* Y^m}{K_{IC}^m} \cdot \int_{t_0}^{t_f} \sigma(T)^m \, dt \qquad \text{eq 3-1}$$

where $\sigma(T)$ is the residual stress acting on the APS topcoat, *a* is the crack length and *m* is an exponent parameter to be fitted to experimental data. *A** is a constant and $K_{I,c}$ is the critical stress intensity factors. *T* is the high temperature at holding period and *t* is time. In their stress model, the coating interface profile such as the roughness amplitude, the wavelength and TGO thickness were included in the stress model. However, in their life model, the fitting parameter $A^* Y^m / K_{IC}^m$ in

$$\int_{a_0}^{a_f} \frac{da}{a^{m/2}} = \frac{A^* Y^m}{K_{IC}^m} \cdot \int_{t_0}^{t_f} \sigma(T)^m \, dt \qquad \text{eq 3-1}$$

was fitted as a constant independent of testing temperatures of APS-TBCs, and consequently does not reflect a high temperature cyclic effect of APS-TBC systems[14].

In this paper, temperature-dependent model parameters are identified and fitted to the testing life data. A newly-proposed stress model is used to describe the stress state at the valley of the top coat, where a CTE mismatch strain is considered to be the main contributor of residual stress in the vicinity of the top coat/TGO interface. The stress model parameters were fitted to the 3-D FEA calculation [52], while the life model parameters were fitted to existing burner rig test results of APS-TBC systems [53].

3.2. Failure analysis and stress

3.2.1. Failure Analysis

For a flat coating interface, there is no residual stress normal to the interface. However, the imperfection or roughness occurring in a coating redistributes the residual stress. As a result, at the location of both valley and peak, a tensile stress is incurred due to interfacial roughness, and this in turn could cause crack nucleation and subsequent propagation, eventually leading to coating spallation. In the present paper, the life prediction of APS-TBCs relies primarily on roughness analysis of the coating interface between the top coat and TGO, Figure 3-1.

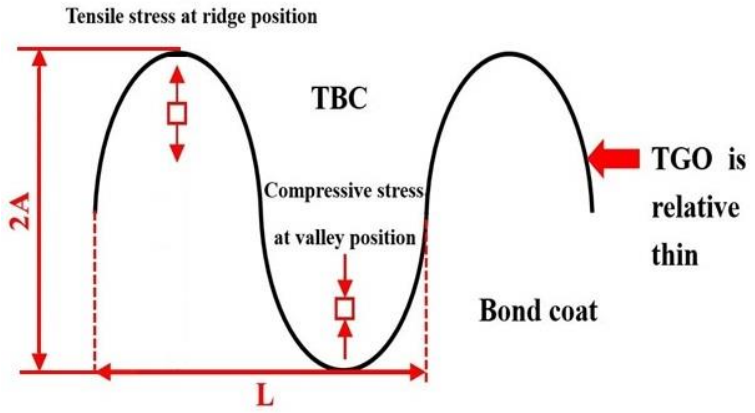

(a)

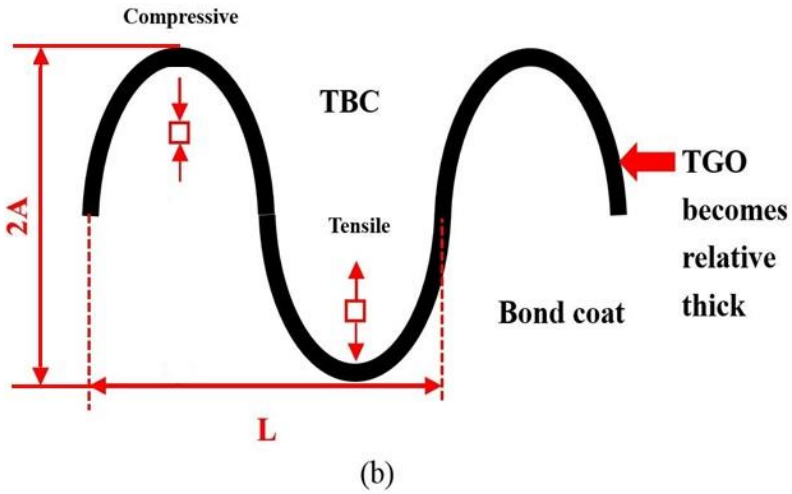

Figure 3-1 Failure mechanism of APS-TBCs, the crack initiate at valley of topcoat as TGO thickens where a stress inversion was considered as thermal cycle proceeds [14]

To study residual stress upon cooling and its effect on crack nucleation and propagation, it is assumed that the coating exhibits a stress-free state at high dwell temperatures. Upon cooling, a large tensile stress normal to the coating interface develops at the imperfection where crack nucleation is initiated, and subsequent propagation proceeds along the interface until inhibited at the valley of the top coat due to compressive stress. As the thermal cycle continues, the TGO thickens due to progressive oxidation of the bond coat. The compressive stress normal to the interface at the valley attenuates, and at a critical thickness of TGO, the top coat at the valley location is under tensile stress, Figure 3-1. This tensile stress will, in turn, promote fatigue crack nucleation and propagation. A spallation of the top coat occurs when these neighboring cracks link and coalescence, which indicates a failure of APS-TBCs.

3.2.2. Stress model

A stress model for the top coat at the valley location is proposed as

$$\sigma_{valley}(y) = -\alpha\Lambda\left\{(\alpha_{TGO} - \alpha_{TBC}) + (\alpha_{BC} - \alpha_{TGO})\left(1 - \beta\frac{d_{TGO}}{A}\frac{R}{y}\right)^3\right\}\exp\left(-\frac{R}{y}\right) \quad \text{eq 3-2}$$

where α_{TGO} α_{BC} and α_{TBC} represent the CTEs of TGO, bond coat and top coat respectively, and d_{TGO} is the TGO thickness. *A* is the amplitude of interfacial roughness, *y* is the valley location of the top coat, where the residual stress will be evaluated for crack propagation. *R* is the curvature radius of the roughness (radius of imperfection) in Figure 3-1. In eq 3-*2*, Λ is a parameter describing a combination of elastic moduli and temperature effect, with $\Lambda = 4\kappa\mu\Delta T/(\kappa + 4\mu/3)$, $\mu = E_{TBC}/2(1+\upsilon)$, and $\kappa = E_{TBC}/3(1-2\upsilon)$, where ΔT is used to describe the difference between the high holding temperature and room temperature. υ is the Poisson ratio of the topcoat. The sintering effect of Young's modulus E_{TBC} of the top coat was also taken into consideration [14] when applying the crack growth rate eq 3-*1*,

$$E_{TBC}(t) = \frac{\beta E_{TBC}^0 E_{TBC}^\infty}{\beta E_{TBC}^0 + E_{TBC}^\infty - E_{TBC}^0} \quad with \quad \beta = 1 + A_{\sin t}\exp\left(-\frac{E_{\sin t}}{\kappa_B T}\right)t^p \quad \text{eq 3-3}$$

κ_B is the Boltzmann constant, $A_{\sin t}$ and $E_{\sin t}$ are the sintering coefficient and sintering activation energy of the top coat in APS-TBC, respectively. Here, *t* is the high temperature holding time,

Although eq 3-*1* describes the residual stress located at the topcoat, it involves the effect of TGO, BC and topcoat through combined parameters such as the difference of CTEs between TGO and topcoat, CTE difference between BC with TGO, TGO thickness, as

well as the elastic moduli of topcoat. In the present paper, it is assumed that TGO growth follows a parabolic-like law [14] given by

$$d_{TGO} = A_{TGO} \exp\left(-\frac{E_{TGO}}{\kappa_B T} \right) t^p \qquad \text{eq 3-4}$$

where A_{TGO}, E_{TGO} and p are the TGO growth rate coefficient, TGO growth activation energy and TGO growth exponent, respectively. *T* is a temperature during a hold period, and *t* is an exposure holding time. κ_B is the Boltzmann constant. The interfacial profile can be approximately described as a sinusoidal curve, thus the curvature radius of imperfection is given as $R = L^2 / 4\pi^2 A$, where *L* represents the mean value of the wavelength. The valley location of y=20μm was selected according to the Scanning Electron Microscope (SEM) measurement of the top coat [14].

As previously explained, the radial stress at the valley of topcoat develops initially under compressive state for at thinner TGO. Upon TGO thickening, this stress develops into a tensile state at a critical TGO thickness, i.e., the sign change of residual stress occurs from an initially negative compressive stress to a positive tensile stress. The corresponding critical TGO thickness can be derived as the vanishing point of the second order derivative of the stress given by,

$$d_{TGO}^{C} = \frac{1}{\beta} A \frac{y}{R} \left[1 - \left(\frac{\alpha_{TBC} - \alpha_{TGO}}{\alpha_{BC} - \alpha_{TGO}} \right)^{1/3} \right] \qquad \text{eq 3-5}$$

This equation is then used to predict the critical time when the stress conversion occurs. The physical implication of all parameters used in stress model and lifetime prediction are listed in Table 3-1 to Table 3-3.

Table 3-1 Related parameters within stress model

Parameters	A	R	y	α_{TGO}	α_{BC}
Abbreviation	Amplitude	curvature radius	valley location	CTE of TGO	CTE of BC
Value	7μm	15.3μm	10μm	$8\times10\text{-}6K^{-1}$	$1.6\times10\text{-}5K^{-1}$
Parameters	α_{TBC}	α	β	\	\
Abbreviation	CTE of TBC	Residual stress related coefficient		\	\
Value	$1\times10\text{-}5K^{-1}$	5.5577	0.37736	\	\

Table 3-2 Temperature-dependent model parameter

Parameters	d_{TGO}	A_{TGO}	E_{TGO}	p	T
Abbreviation	TGO thickness	TGO growth rate coefficient	TGO growth activation energy	TGO growth exponent	Temperature during a hold period
Value	\	7.48×10^{-4}m/s^{p}	0.907eV	0.25	1273.15K
Parameters	t	E_{TBC}	υ	E_{TBC}^{0}	E_{TBC}^{∞}
Abbreviation	exposure holding time	Young's modulus of TBC	Poisson ratio of TBC	Initial modulus of TBC	Bulk modulus of TBC
Value	\	\	0.33	20GPa	136GPa
Parameters	κ_B	$A_{\sin t}$	$E_{\sin t}$	P	d_{TGO}^{C}
Abbreviation	Boltzman constant	sintering coefficient	sintering activation energy	Sintering exponential coefficient	Critical TGO thickness
Value	1.38×10^{-23}J/K	2×1010s^{-p}	3eV	0.25	4.4μm

Table 3-3 Lifetime prediction model related parameters

Parameters	a	a_f	a_0	$\sigma(T)$	t_0
Abbreviation	Crack length	Full crack length(Entire wavelength)	Initial crack length (half wavelength)	Temperature-process dependent stress	Initial time that tensile stress developed
Value	\	65μm	32.5μm	\	74.2358h
Parameters	t_f	m	$\frac{A^* Y^m}{K_{IC}^m}$	\	\
Abbreviation	Estimated lifetime	Exponential fitting coefficient	Temperature-dependent fitting parameter	\	\
Value	\	18	\	\	\

3.2.3. Life prediction Procedure

Vaßen et al. [14]proposed an empirical stress model for the topcoat of APS-TBC system, and by combining their stress model and fatigue crack growth formula eq 3-*1*, the life was evaluated numerically. The right hand side of eq 3-*1* is an integral of the residual stress on the topcoat from an initial time t_0 to t_f, the failure life time to be estimated. The left hand side of eq 3-*1* is an integral of the crack length initially starting from a_0, an assumed half wavelength, to the a_f of the entire wavelength, indicating the spallation of the topcoat from the bond coat completely. Equation eq 3-*1*

can be interpreted as follows: the right hand side of eq 3-*1* represents a driving force of the fatigue crack growth during a cyclic process, while the left hand side of eq 3-*1* is a consequence of fatigue crack growth driven by the right side during thermal cycles, leading to crack propagation. When the crack length a reaches the critical a_f, the cracks coalesce, resulting in spallation of the top coat, where the failure time t_f can be consequently obtained for coating. This is the procedure that was used in estimating the life of APS-TBC systems [14] in this paper.

3.3. Model parameters

The burner rig test result of failure life of APS-TBC system [54] was used to fit model parameters of eq 3-1, Figure 3-*2*.

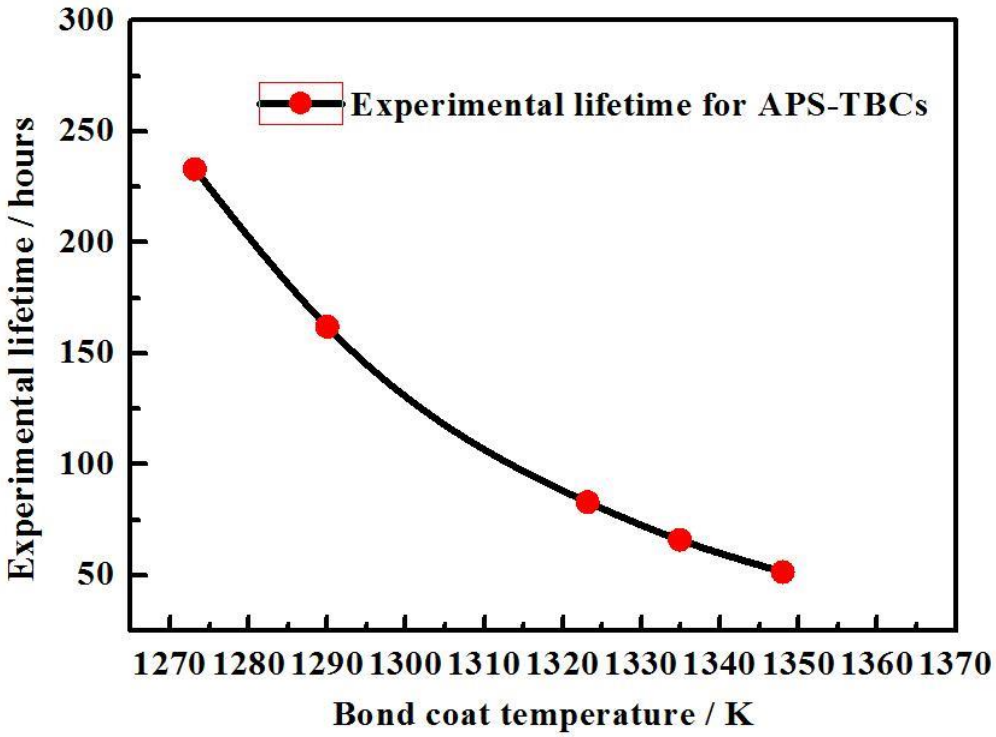

Figure 3-2 Experimental lifetime as a function of bond coat temperature, the lifetime standing by red marks was measured based on burner rig tests described in [54]

Normally, a high cycle frequency of the burner rig test will cause more fatigue damage than using a normal cycle frequency test, which in turn shortens the APS-TBC life [53].

The thermal radial stress versus the TGO thickness at the valley of the top coat simulated using FEA [52] is shown in Figure 3-3, together with the plotted curve using the proposed stress model of eq 3-*2*.

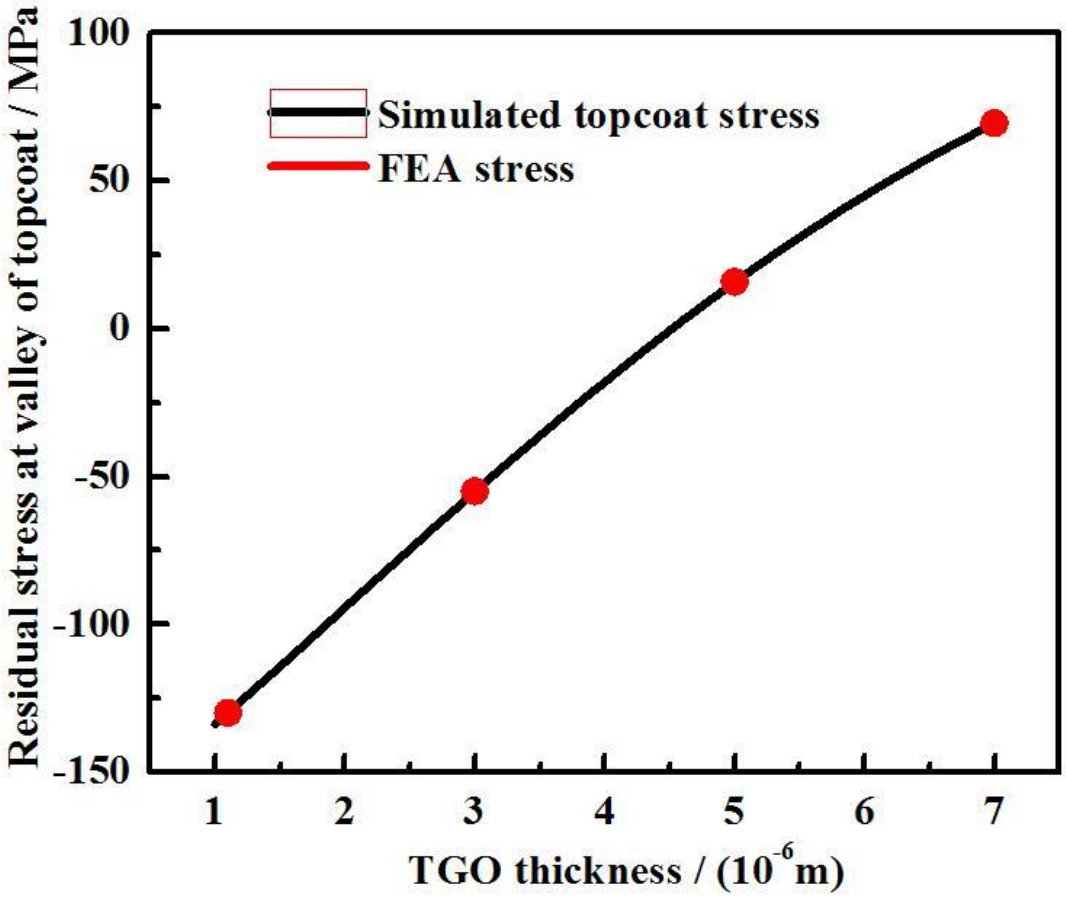

Figure 3-3 Simulated stress as a function of TGO thickness, a perfect reproduction could be made between the stress estimated by eq 3-2 and fitted by FEA

It can be seen that the stress conversion takes place from compressive to tensile state at a TGO thickness of d_{TGO} = 4.6μm. In this paper, the amplitude of A = 5μm and wavelength of λ =65μm in describing the roughness interface were used to fit residual stress model parameters of α, β and γ in eq 3-*2*. In this research, it is assumed that the residual stress model parameters of α, β, γ are temperature-independent, while the temperature-dependent characteristics of the life model is reflected by the fitting parameters $A^* Y^m / K_{IC}^m$ in the fatigue crack growth formula of eq 3-*1*, where temperature-

dependent life data from burner rig test was used.

In Ref.[14], the fitting parameter $A^{*}Y^{m}/K_{IC}^{m}$ in the fatigue crack growth formula of eq 3-*1* was treated as a constant although the life data was obtained at different temperatures. As a result, this led to large deviations in life prediction of APS-TBCs. In the present paper, based on the burner rig test life results at five temperatures, the fitting parameter $A^{*}Y^{m}/K_{IC}^{m}$ was fitted accordingly and shows a temperature-dependent characteristic, Figure 3-4. This temperature-dependent parameter can be well described by an exponential function (straight line on a log plot).

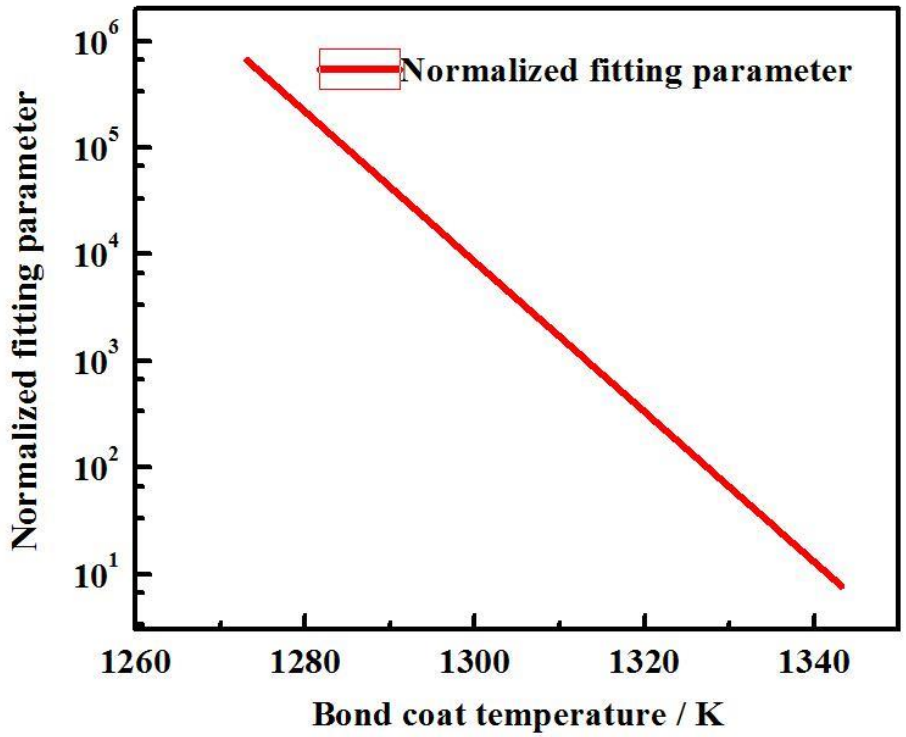

Figure 3-4 Normalized lifetime fitting parameters as function of BC temperature, the normalized fitting parameter decreases exponentially as temperature increases

3.4. Life prediction and discussions

Using this temperature-dependent model parameter, the predicted life between 1000℃ to 1075℃ is shown in Figure 3-5.

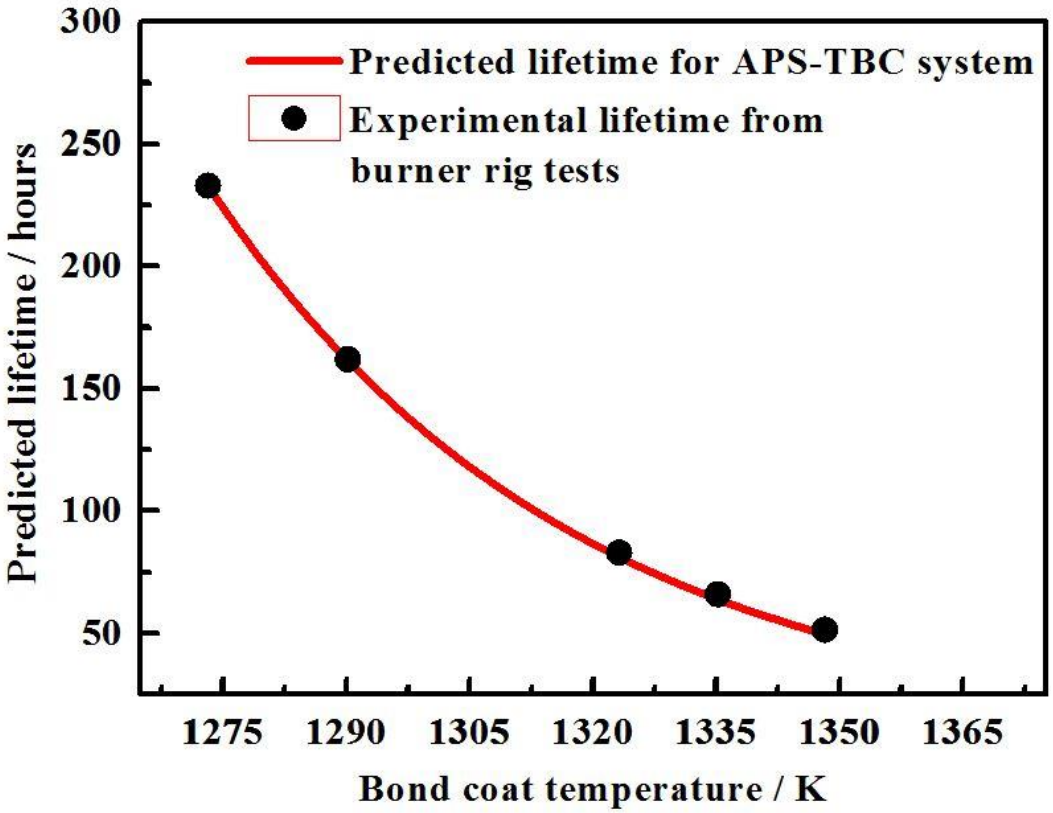

Figure 3-5 Predicted lifetime as function of BC temperatures, the general predicted lifetime drop dramatically as bond coat temperature increase

The average life of the APS-TBCs decreases versus the bond coat temperatures. In order to examine the capability of the life model, a comparison between the experimental data [54] and the predicted lifetime was made, Table 3-4. A maximum error of 2-hours (3.72%) in life prediction was found at high temperatures.

Table 3-4 Comparison between the experimental data with predicted lifetime

Experimental Temp / Kelvin	Experimental lifetime / hours	Calculated Temp / Kelvin	Predicted lifetime / hours	Deviation $\Delta t/t_f$
1273.15	233	1273.15	232.9167	0.036%
1289.99	162	1290.15	161.3333	0.412%
1323.15	83	1323.15	81.1667	2.21%
1334.9	66	1335.15	63.8333	3.28%
1347.98	51.5	1348.15	49.5833	3.72%

As analyzed in the preceding sections, the life of APS-TBCs can be evaluated by integrating eq 3-*1*, and the capability of the life model can be improved upon using

temperature-dependent fitting parameters in the model. Thermal cyclic testing was also performed on specimens of various microstructures of topcoats[14], and the life results are presented in Figure 3-6 versus the bond coat temperature.

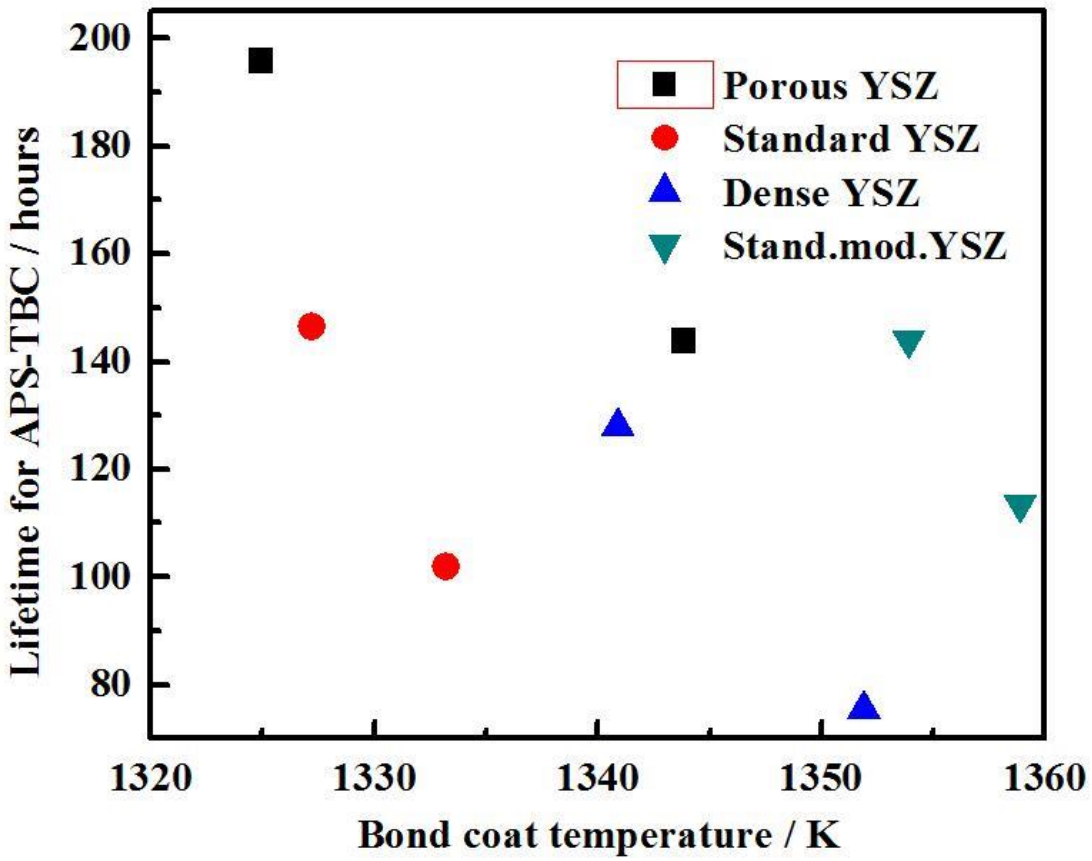

Figure 3-6 various lifetime for APS-TBCs as function of bond coat temperature categorized by different type of topcoat, two lifetimes was measured for a specific TBC system and large discrepancy of lifetime could be observed based on different YSZ properties [14]

In Figure 3-6, four pairs of the selected specimens were measured for their coating's evaluation, presented by specific symbols and colors. Each pair of specimens was assumed to have the same topcoat microstructure but measured for life at different bond coat temperatures. The measured life for each pair of specimens was initially used to evaluate the fitting parameter $A^* Y^m / K_{IC}^m$ in eq 3-*1*. A linear correlation of the $A^* Y^m / K_{IC}^m$ with the bond coat temperature was fitted to each pair of life data.

Upon having the fitted linear correlation of A^*Y^m / K_{IC}^m with the bond coat temperature for each pair of tested life data, a life prediction at the testing temperatures where the model parameters A^*Y^m / K_{IC}^m were fitted can also be performed in principle by using eq 3-*1*. This procedure can be realized through the following steps using eq 3-6 and eq 3-*7* by re-arranging eq 3-*1*, respectively,

$$B = \left[\int_{a_0}^{a_f} \frac{da}{a^{m/2}}\right] \Big/ \frac{A^* Y^m}{K_{I,c}^m} \qquad \text{eq 3-6}$$

$$\int_{t_0}^{t_i} \sigma(T)^m dt = B \qquad \text{eq 3-7}$$

Using the fitted temperature-dependent model parameter A^*Y^m / K_{IC}^m, the B value in Eq. eq 3-6 can be calculated at specific temperature to within the temperature range of testing life data. The failure life, t_i at the upper limit of the integral eq 3-*7* at this temperature To can be obtained through a numerical procedure that a tentative t_i was initially set up, and then used to integrate eq 3-*7* until the value of eq 3-*7* at this specific temperature equals to the B value of eq 3-6 at a given precision. However, this numerical procedure for a convergence life t_i failed, whereas a series of t_i was obtained resulting in the same B value in eq 3-*7*.

To further evaluate this uncertainty of life t_i, another procedure for evaluating the parameter A^*Y^m / K_{IC}^m was also performed. For a given pair of life data shown in Figure 3-6 such as a pair of red solid circle data, if a linear correlation of life data was assumed within this temperature range, a temperature-dependent parameter A^*Y^m / K_{IC}^m can be

developed in principle using eq 3-*1*. Therefore, the temperature-dependent fitting parameter $A^{*}Y^{m} / K_{IC}^{m}$ s can be calculated using

$$\frac{A^{*}Y^{m}}{K_{I,c}^{m}} = \int_{a_0}^{a_f} \frac{da}{a^{m/2}} \Big/ \int_{t_0}^{t_i} \sigma(T)^{m} dt \qquad \text{eq 3-8}$$

However, this numerical procedure for determining $A^{*}Y^{m} / K_{IC}^{m}$ also failed if the life data t_i at the upper limit of the integral eq 3-*8* was selected based on the assumed linear correlation for the test life, i.e., the convergence of determining $A^{*}Y^{m} / K_{IC}^{m}$ was not achieved. This failure also indicates that more test life data are required to fit the temperature-dependent model parameter $A^{*}Y^{m} / K_{IC}^{m}$ so that a non-linear correlation for $A^{*}Y^{m} / K_{IC}^{m}$ with the temperature could be established, and consequently a reliable and convergent life can be predicted. This result was confirmed upon using a non-linear test life data presented in Figure 3-5, where a non-linear fitting parameter $A^{*}Y^{m} / K_{IC}^{m}$ was also established.

This could be explained by an integral characteristic of large negative compressive stress having no effect on crack nucleation and propagation at early life of cyclic process. At this stage, the positive tensile stress which is responsible for promoting the crack formation fails to play a major role in the stress integral due to its smaller amount compared to the negative compressive stress, Figure 3-7.

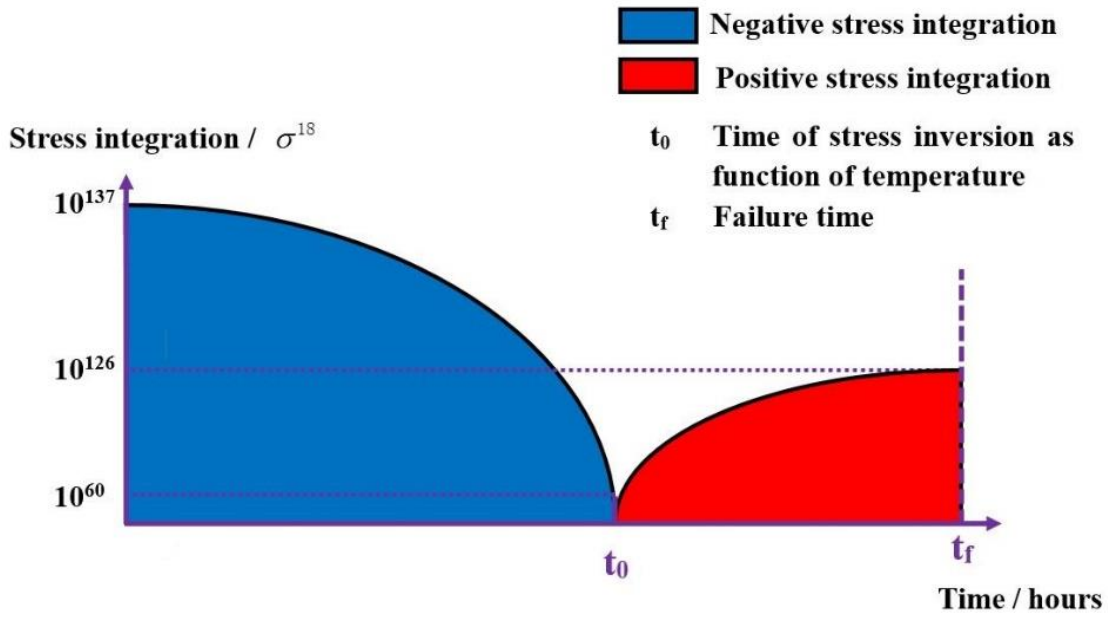

Figure 3-7 the schematic diagram of full-time scale stress integration, the stress estimated by eq 3-2 was integrated from first cycle (t =0) to assumed failure times (t=t_f)

A selected stress integral was applied to the life prediction model where only the positive stress is integrated starting from the critical time.

The time for stress inversion at the valley of topcoat is required for integrating the tensile-residual stress. The critical time for stress inversion could be found by combining eq 3-*4* and eq 3-*5* is described as,

$$t_0 = \left\{ d_{TGO}^c \Big/ \left[A_{TGO} exp\left(-\frac{E_{TGO}}{\kappa_B T} \right) \right] \right\}^{\frac{1}{p}} \qquad \text{eq 3-9}$$

According to eq 3-*9*, the critical time for stress inversion shows the temperature-dependent characteristics, which should be used in estimating each temperature-dependent lifetime. A schematic diagram used to describe the selected stress integration is shown in Figure 3-8.

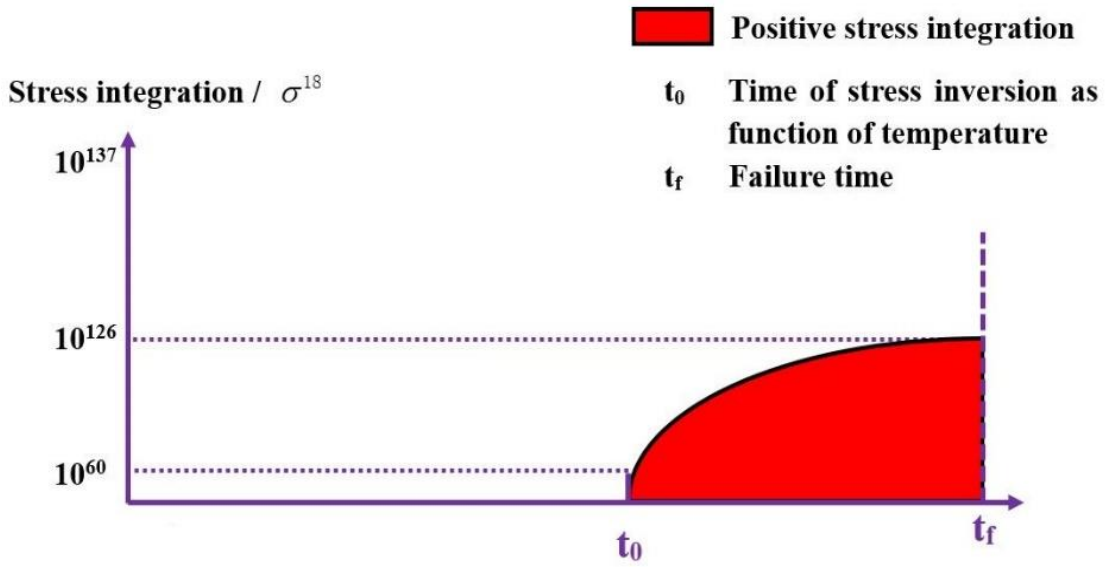

Figure 3-8 the schematic diagram of half-time scale stress integration, the stress estimated by eq 3-2 was integrated from critical time point that stress inversion occurred (t= t0) to assumed failure times (t= t_f)

The schematic diagram of calculated lifetime model parameters using the selected stress integration is shown in Figure 3-9.

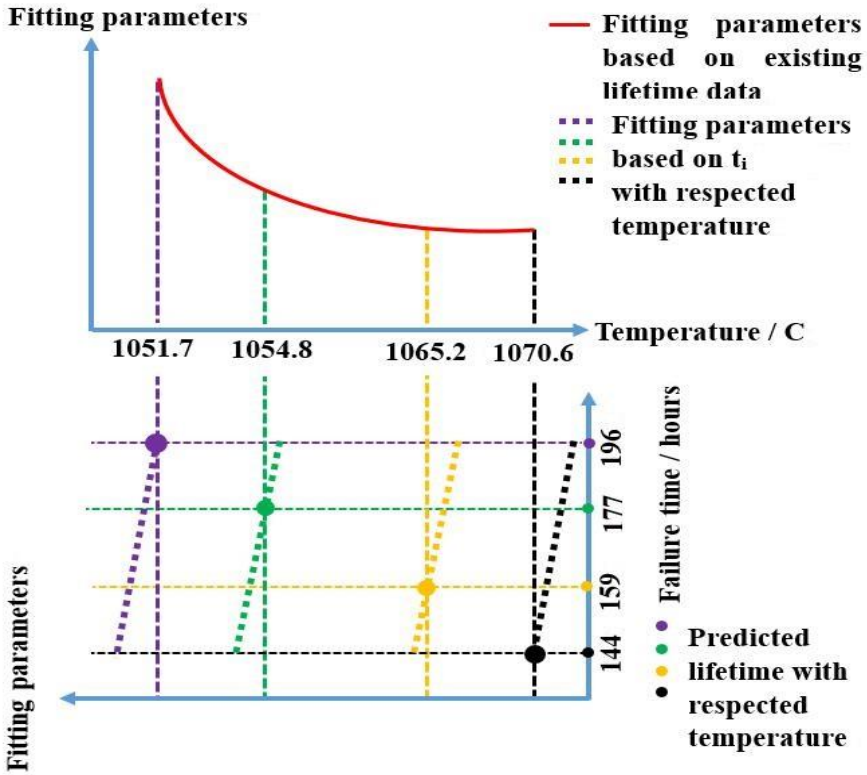

Figure 3-9 Fitting parameters based on unlinear assumption with half-time scale stress integration and corresponding predicted lifetime as function of bond coat temperatures

As the tensile stress plays a major role in integration of residual stress, a significant distinction of temperature-dependent fitting parameters could be found versus thermal cycles. The life could then be estimated by incorporating the specific temperature into life prediction model and the result is presented in Figure 3-5.

3.5. Interactions between residual stresses and contributions to the life

As analyzed before, the residual tensile stress located at the valley of the top coat/TGO interface promotes crack nucleation and propagation as TGO reaches a certain critical thickness. Calculation of the total residual stress of eq 3-*1* involves properties of the TGO, bond coat and topcoat. This total residual stress also reflects the geometry characteristics of TGO/bond coat interface. It illustrates a combination of properties of TGO, bond coat and topcoat, it reflects interactions among these stresses. More importantly, this total stress can be divided into two contributions based on the CTE differences such as $\alpha_{TGO}-\alpha_{TBC}$ and $\alpha_{BC}-\alpha_{TGO}$, in which these two stresses are expressed as,

$$\sigma_{TBC-TGO}(y)=-\alpha\Lambda(\alpha_{TGO}-\alpha_{TBC})\exp\left(-\frac{R}{y}\right) \qquad \text{eq 3-10}$$

$$\sigma_{BC-TGO}(y)=-\alpha\Lambda(\alpha_{BC}-\alpha_{TGO})\left(1-\beta\frac{d_{TGO}}{A}\frac{R}{y}\right)^{3}\exp\left(-\frac{R}{y}\right) \qquad \text{eq 3-11}$$

Here, σ_{BC-TGO} stands for the residual stress associated with the CTE difference between the TGO and bond coat. Similarly, $\sigma_{TBC-TGO}$ represents the residual stress associated with the CTE difference between the topcoat and TGO. These individual stress components are shown in Figure 3-10.

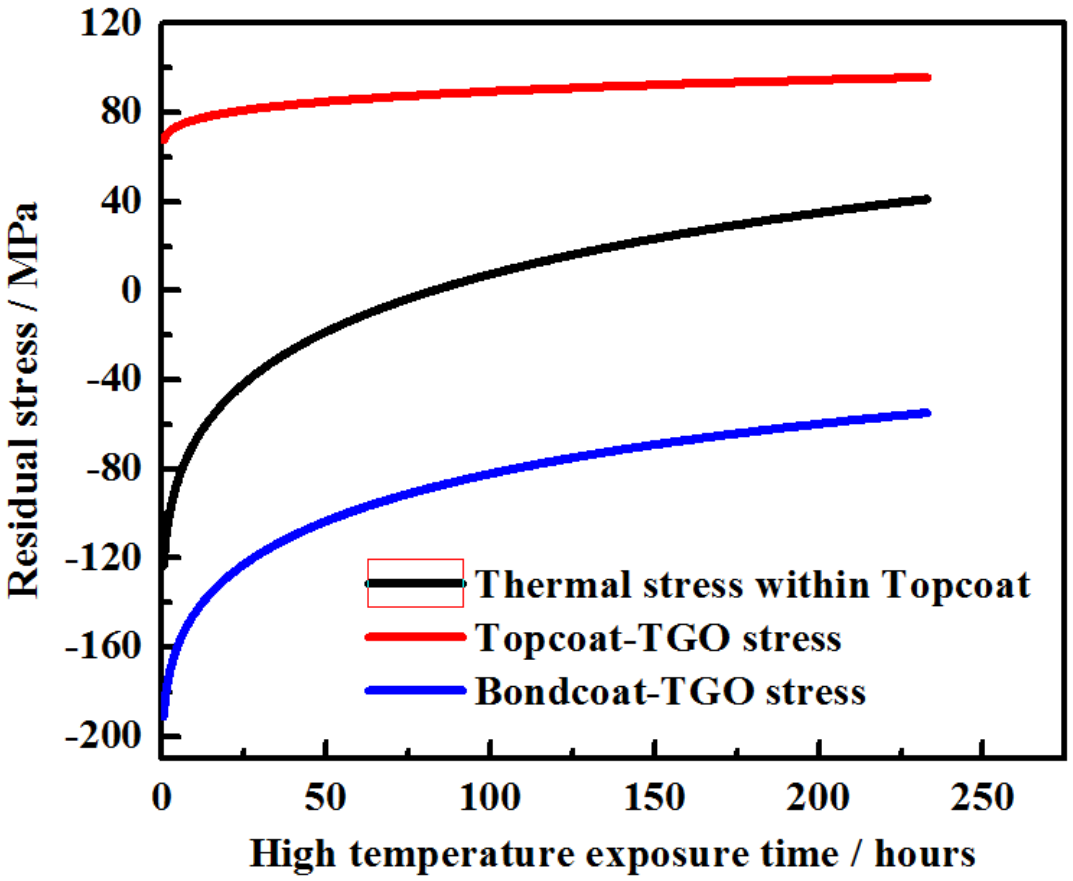

Figure 3-10 Stress distribution based on CTE mismatch between different layers, the stress describing the interplay between the topcoat and TGO is responsible for crack initiation and propagation where the stress generated from interplay between TGO and bond coat inhibit the crack formation

It was noticed that the stress representing the CTE mismatch between the topcoat/TGO is always tensile, while the stress due to CTE mismatch between TGO/bond coat is compressive. It should be pointed out that the term of $\sigma(T)^m$ of eq 3-*1* at right hand side can be expanded in three terms,

$$\sigma^m_{Valley}(y) = \sigma^m_{TBC-TGO}(y) + \sigma^m_{TGO-BC}(y) + \Delta(\sigma_{TBC-TGO}, \sigma_{TGO-BC}) \qquad \text{eq 3-12}$$

The term $\Delta(\sigma_{TBC-TGO}, \sigma_{TGO-BC})$ represents a combination of aforementioned two stresses in eq 3-*10* and eq 3-*11*, it reflects their complicated interactions among TGO, bond coat and topcoat. By integrating each individual part, the effect of these stresses on

crack propagation can be shown in Table 3-5 and Figure 3-11.

Table 3-5 Stress integration analysis, noticed that stress integration between TBC/TGO and TBC-TGO-BC play essential role in crack formation

T[℃]	t_f[h]	Integral results by different stress sources			
		$I_1(\sigma_1)$ TBC-TGO $[10^{149}]$	$I_2(\sigma_2)$ BC-TGO $[10^{147}]$	$I_3(\Delta\sigma)$ TBC-TGO-BC $[10^{149}]$	Total $[10^{141}]$
1000	232.9167	1.4620	-4.9795	-1.4122	4.9236
1020	151.4167	9.6903	-22.922	-9.4611	126.42
1040	99.5833	75.485	-116.90	-74.316	3183.9
1060	66.4167	656.46	-781.60	-648.64	82078
1075	49.5833	3383.2	-2544.8	-3357.7	902462

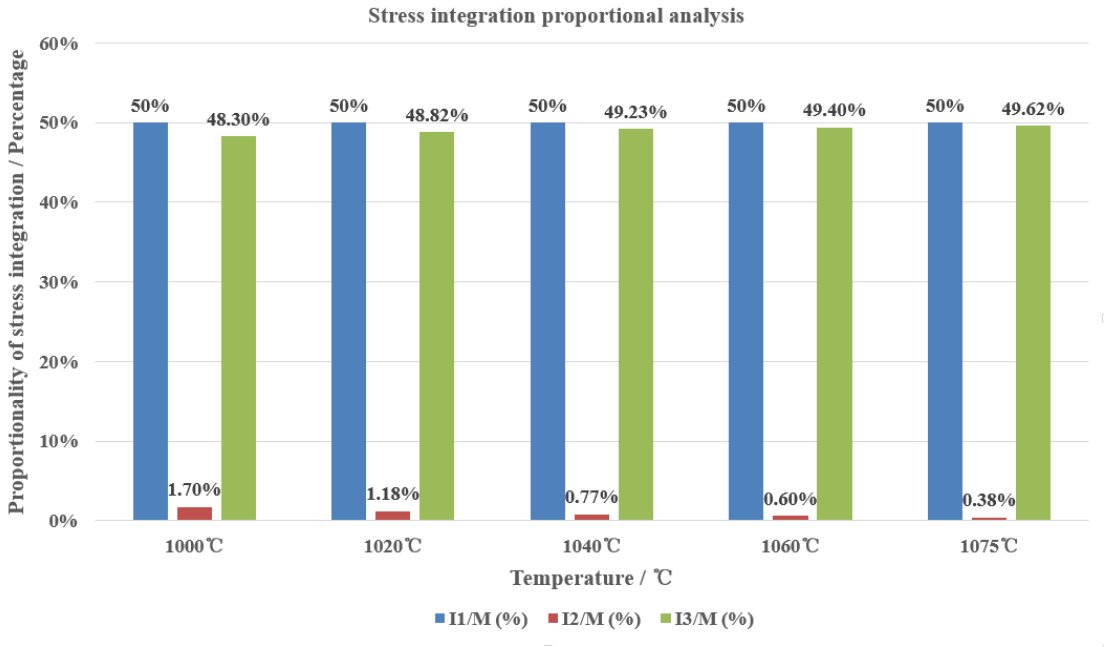

Figure 3-11 Stress integration proportional analysis according to Table 3-2 as function of temperatures

It is interesting to note from Table 3-5 and Figure 3-11 that the residual stress due to a CTE mismatch between the top coat/TGO is positive, responsible for crack nucleation and propagation. While the residual stresses due to a CTE mismatch between the bond coat/TGO as well as their combination are negative, responsible for inhibiting crack propagation. The interaction of top coat with TGO plays a major role in promoting crack formation, and accounts for up to 50% of the predicted lifetime. On the other hand, the interplay of top coat-TGO-bond coat accounts for the other 50%, responsible for inhibiting crack propagation.

3.6. Conclusions

Life prediction of APS-TBC was conducted by using a proposed residual stress model and existing burner rig test life data. The stress model demonstrates a combination of properties of TGO, bond coat and topcoat, the model also involves geometric characteristics of TGO/bond coat/topcoat interfaces. Stress model parameters were obtained by fitting to stress data calculated by 3-D FEA calculations. Temperature-dependent model parameters in evaluating fatigue crack propagation were obtained by fitting to burner rig test data for APS-TBC systems. The life prediction was conducted by using temperature-dependent model parameters, and the capability for life prediction was improved by combining stress integration with a critical time for stress inversion. The interactions of residual stresses representing the top coat, TGO and bond coat were examined. The residual stress associated with the top coat and TGO were identified as responsible for crack nucleation and propagation in the topcoat, while the residual stress associated with the TGO/bond coat and their interplay among TGO/bond coat/top coat are responsible for inhibiting crack propagation. Therefore, properly controlling the

stresses due to CTE mismatch between the top coat and TGO could be a way to extend APS-TBC life.

4. The development of stress models that used in lifetime prediction model in EB-PVD TBCs

This chapter addresses objective 2 (develop the stress model on different layers within EB-PVD TBC system) by using temperature process-dependent model parameters.

The content of this chapter has been submitted for publication in Materials Sciences and Engineering A in 2016.

Stress Models for Electron Beam-Physical Vapor Deposition Thermal Barrier Coatings With Temperature-process-dependent Model Parameters

[a]*BC. Zhang,* [b]*KY. Chen,* [a] *N. Baddour*

[a]*Department of Mechanical Engineering, the University of Ottawa, Ottawa, Canada*

[b]*Structures, Materials and Manufacturing Laboratory, Aerospace Portfolio, National Research Council Canada, Ottawa, Canada*

Abstract

Electron Beam-Physical Vapor Deposition Thermal Barrier Coatings (EB-PVD TBCs) are nowadays an essential part in gas turbines. The failure mechanism of Electron Beam-Physical Vapor Deposition Thermal Barrier Coatings (EB-PVD TBCs) were analyzed for thermal cyclic process. Based on the site where cracks initiate, two newly analytical stress models from the valley position of the top coat and ridge of the bond coat were proposed describing stress levels generated as consequence of the coefficient of thermal expansion (CTE) mismatch between each layers. The thermal stress within TGO was evaluated based on composite material theory where effective parameters were calculated. Bond coat (BC) and thermal grown oxide (TGO) were treated as inclusion and matrix based on Eshelby's model described somewhere else. The capability of the stress model was improved by using temperature-process dependent model parameters. A reduction of stress levels at valley of topcoat and ridge of bond coat were explained due to crack formation at interface according to the failure mechanism of EB-PVD TBCs. A difference on stress levels was found between the peak of bond coat and within TGO, which was considered as result of a difference on creep properties and fracture toughness of bond coat and TGO. The capability of wavelength parameter in analytical models in EB-PVD TBC system was detailed and discussed.

Keywords: Stress model, CTE mismatch, temperature-process dependent model parameters, creep behavior, wavelength.

4.1. Introduction

Electron beam-physical vapor deposition Thermal Barrier Coatings (EB-PVD TBCs) used as thermal isolators between metallic substrates and the external environment in gas turbines have been developed for decades [1]–[4]. These materials consists of 8%-YSZ topcoat, a metallic bond coat and metal substrate. Compared with the traditional plasma-sprayed thermal barrier coatings, a relative high strain tolerance could be achieved [55]–[60] by its columnar microstructure of the topcoat, especially during thermal cycling process where large thermal strain generated due to coefficient of thermal expansion mismatch (CTE mismatch) between each layer. The bond coat made by either Pt-modified nickel aluminide or NiCoCrAlY overlay is deposited onto the substrate prior to topcoat fabrication. A relative strong bonding between topcoat and substrate [61]–[63] could be achieved, in which the bond coat plays an essential role in strengthening the chemical interaction between topcoat and substrate. The bond coat is also used to prevent further oxidation of the substrate during high temperatures by forming a thin oxide layer as thermal grown oxide (TGO) [64]–[69]. It is well-known that failure of TBC systems is largely attributed to the formation of TGO where a large stress could be generated due to volume expansion, led by progressive oxidation of the bond coat [70]–[75]. Meanwhile, the extensive crack will nucleate from the site where the transient mixed oxide, for example, spinel formed due to its brittleness characteristics and reduced fracture toughness compared to the preferred TGO of α-alumina [76]–[83]. In order to improve the durability of the coating system, many efforts has been made to identify the basic failure mechanism of EB-PVD TBCs [84]–[87] and different possible crack paths have been suggested. According to the SEM measured from cross sections of EB-PVD TBC specimens conducted by thermal cyclic experiment, Courcier et al believed that cracks nucleate at voids found at the valley of the topcoat where the

roughness of the interfacial surface on the surface of TGO is due to the downward displacement of the bond coat as rumpling at high temperature and followed by downward growth of the TGO layer. The cracks form as voids expand parallel to the interface and propagate between topcoat and thermal grown oxide (TGO) [9][88][89]. On the other hand, Vaidyanathan et al suggested that the failure of EB-PVD TBCs was triggered by convergence of multi-layer cracks which nucleate from each site of the ridge of bond coat, two neighboring cracks convergence occur by penetrating the TGO layer and propagating within topcoat parallel with boundary of TGO [90][91]. Based on those two identified failure mechanisms, various numerical models describing stress levels at different layers of EB-PVD TBCs have been explored. One early model developed by E.P. Busso [92] simulated the stress at different positions close to the rough interface between each layer, where the related parameters describing the thermal dynamic properties of each layers, geometrical roughness of interface and volumetric strains associated with the formation of the thermal grown oxide (TGO) are incorporated into the stress analysis based on FE calculations. The position of largest out-of-plane tensile stress was identified either during high temperature or after cooling down to room temperature, and the order of magnitude of tensile stress was determined semi-quantitatively, which large discrepancy could be found based on three elastic assumptions for topcoat materials which indicates that the anisotropic property of YSZ plays the significant role in stress levels. Vaidyanathan et al. [90]also categorized the life of EB-PVD TBCs into three groups corresponding to different failure crack paths, the radial tensile stress level was estimated at ridge top of bond coat (BC) where the failure crack nucleate.

However, the models described so far were concentrated on estimating the stress state close to TGO within the bond coat and a generalized analytical function used to describe the stress level at topcoat as well as TGO was not seen. Meanwhile, as for the

parameters used in the previous semi-quantitative stress model, the given value, for example, the amplitude of interfacial roughness, the thickness of TGO as well as approximate curvature radius of bond coat roughness, were treated as constants independent of temperature and thermal cycles, which does not reflect the high temperature cyclic characteristics of EB-PVD systems.

In the present paper, all temperature-process-dependent model parameters are identified and integrated into the newly proposed stress models which are used to describe the stress levels at the valley of topcoat, as well as ridge of the bond coat. The CTE mismatch strain is considered to be the main contributor of residual stress for all layers. The results of stress level showed temperature-process dependent characteristics. A comparison is made between stress levels on the bond coat and within the TGO. The reason for lower stress levels on the bond coat is attributed to increasing creep behavior during high temperature holding time and lower bond coat fracture toughness compared with TGO. The capability of wavelength parameter in stress model is briefly discussed.

4.2. Stress model description

As discussed in the preceding section, the failure mechanism of EB-PVD TBCs is partially based on the roughness of the coating interface, i.e., the cracks nucleates from the voids formed at the topcoat/TGO interface, or from the separation at ridge at bond coat/TGO interface as indicated in Figure 4-1. For the crack within the topcoat, it is considered that voids generated at the topcoat close to the interface are embryonic formations of a crack, which is introduced by the rumpling effect of the bond coat followed by downward displacement of TGO. As the thermal cycle proceeds, larger voids form and expand parallel to the interface as a consequence of the downward growth of the TGO.

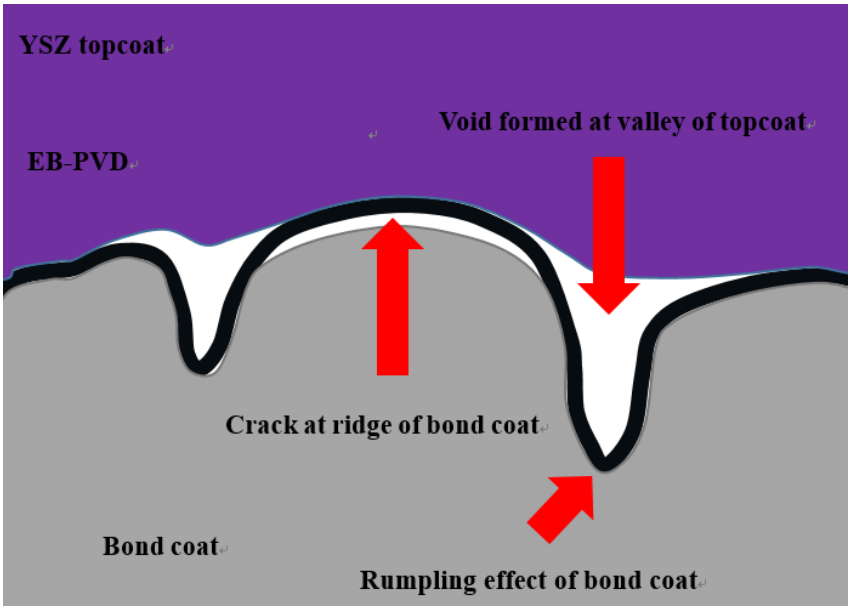

Figure 4-1the ridge of bond coat and valley of topcoat could be sites where crack nucleates in EB-PVD TBCs due to the rumpling effect of bond coat [90]

Once two neighboring voids coalescence, the failure-induced crack forms followed by spallation of topcoat. Failure is assumed when the neighboring cracks coalescence, Figure 4-2.

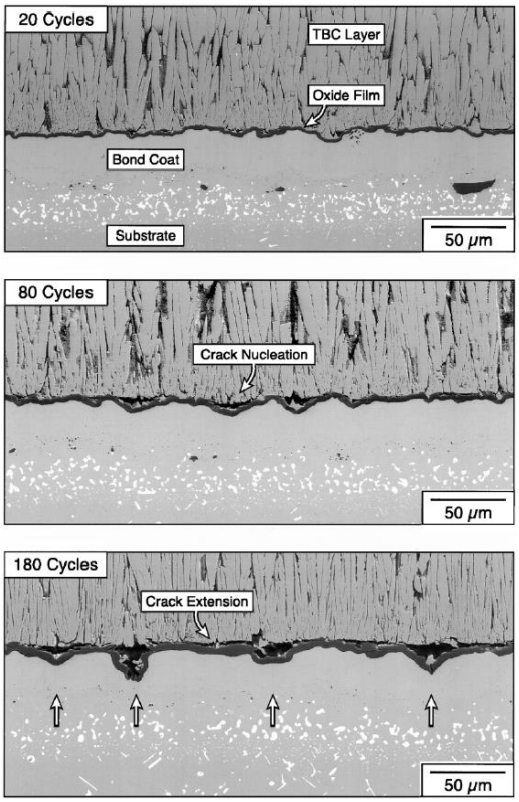

Figure 4-2 Crack nucleate / propagate from the voids at topcoat and TGO interface as thermal cycle proceeds [1]

For the crack initiating from the ridge of the bond coat, it is considered that the crack nucleating from the ridge of the bond coat meets the crack generated from voids at the topcoat, where a large in-plane stress generated upon cooling leads to out-of-plane tensile stress within the TGO. As the consequence, the neighboring cracks penetrate the TGO layer and convergence within topcoat close to the interface, Figure 4-3.

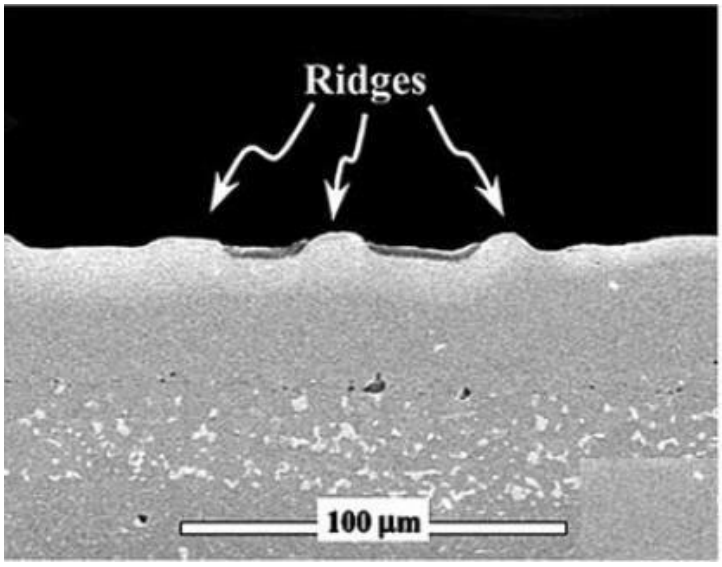

Figure 4-3 SEM indicates the failure was due to the separation generated by crack nucleating and propagating from the at ridge of bond coat [90]

Based on the failure mechanism and crack paths, three stress models are outlined, which are used to estimate the stress level at the interface between layers as well as within the TGO. It should be mentioned that stress models are used to describe the CTE mismatch between each layer upon cooling, the additional dilatational stress generated from TGO formation due to progressive oxidation of BC are not taken into account as they could be calculated based on equations described elsewhere [1]. The model parameters are measured at different stages of thermal cycles which are extracted from thermal cyclic experimental data. The interfacial amplitude, TGO thickness, Young's modulus for topcoat and bond coat are fitted by using the data for EB-PVD TBC systems [89]. The radius at imperfections are measured by SEM taken from cross sections on failed specimens [13][85][90][93][94], where those parameters plays significant role in

estimating stress at different positions. It is noted that the analytical stress function is not only used to describe the stress state for each layer, but also to be a critical part of work for developing the lifetime prediction model for future research.

4.2.1. Stress within TBC close to TC/TGO interface

As discussed in the preceding section, the stress model within the TBC close to the TBC/TGO interface is relying on an assumption that the spallation of the topcoat is due to crack nucleation from voids generated by the rumpling effect of the BC. The propagation of horizontal crack is only possible with radial tensile stress generated at the interface between topcoat and TGO. It is evident that the size of voids becomes larger as the thermal cycle proceeds, where these local deficiencies form as consequence of large CTE radial stress generate at topcoat/TGO interface. The newly proposed stress model for the top coat describing stress state at the valley location can be expressed as

$$\sigma_{\text{valley}} = \alpha\Lambda\left[(\alpha_{TGO}-\alpha_{BC})(\beta\frac{d_{TGO}A}{y_{TBC}R}-1)+(\alpha_{TGO}-\alpha_{TBC})\right](e^{\gamma\frac{A}{R}}-1) \qquad \text{eq 4-1}$$

where α_{TGO} , α_{BC} and α_{TBC} are temperature-dependent parameters, representing coefficient of thermal expansion of the TGO, bond coat and top coat. d_{TGO} is the TGO thickness. A is the amplitude of BC roughness, y_{TBC} is the valley location of the top coat, where the samples in Figure 4-2 shows cracks running in the TBC close to the TBC/TGO interface at a distance close to the one selected in the stress model (20μm). R is the curvature radius of the voids from the top coat. The sintering effect of Young's modulus E_{TBC} of the top coat was considered into the stress model. The temperature-dependent residual stress model parameters of α, β, γ are fitted by FEA results in specific temperature.

In the present stress function, it is assumed that the CTE mismatch stress between

topcoat and bond coat will be calculated as the TGO thickness equal to zero. On the other hand, it is assumed that the coating has a stress-free state at a high dwell temperature due to creep on both the top coat and the bond coat (BC) at the beginning of thermal cycles, indicated by flat interface (*R* tend to infinite). The exponential factor will lead to a fast reduction of stress state for large value of R/A, which could be used to simulate the stress relaxation caused by creep behavior of bond coat.

The Λ is a factor describing a combination of elastic moduli and temperature effects for the topcoat, where $\Lambda = 4\kappa\mu\Delta T/(\kappa + 4\mu/3)$ with $\mu = E_{TBC}/2(1+\upsilon)$, and $\kappa = E_{TBC}/3(1-2\upsilon)$. υ is the Poisson ratio of the topcoat. The sintering effect of Young's modulus E_{TBC} for the topcoat was considered into the stress model.

4.2.2. Stress within BC close to TGO/BC interface

According to [95] and [96], the maximum value of stress at ridge of bond coat based on the approximation of axisymmetric hemispherical surface is given by

$$\sigma_N = \frac{2\sigma_{TGO} d_{TGO}}{R} \qquad \text{eq 4-2}$$

where σ_{TGO} represents the in-plane stress within TGO measured using photoluminescence piezospectroscopy (PLPS) technique. The equation was used to evaluate the stress level at ridge of bond coat, where the given value of in-plane compressive stress, TGO thickness and curvature radius are only mean value estimated from experimental data [90]. The calculated residual stress at failure is nearly constant (approximately 0.3Gpa). However, the results of calculation using eq 4-2 depend on the measured in-plane compressive stress, where the model does not contain factors which describe the stress (strain) introduced by CTE mismatch. With the presented approach, the stress level is calculated using eq 4-3 which has a similar form

to the stress function in topcoat:

$$\sigma_{ridge} = a_{BC}\Lambda_{BC}\left[(\alpha_{TBC}-\alpha_{TGO})(\frac{1}{b_{BC}}\frac{d_{TGO}A}{y_{BC}R}-1)+(\alpha_{BC}-\alpha_{TGO})\right](e^{c_{BC}\frac{A}{R}}-1) \qquad \text{eq 4-3}$$

It should be noted that the Λ_{BC} is a factor describing a combination of elastic moduli and temperature effect for bond coat, where $\Lambda_{BC} = 4\kappa_{BC}\mu_{BC}\Delta T/\left(\kappa_{BC}+4\mu_{BC}/3\right)$ with $\mu_{BC} = E_{BC}/2\left(1+\upsilon_{BC}\right)$ and $\kappa_{BC} = E_{BC}/3\left(1-2\upsilon_{BC}\right)$. υ_{BC} is the Poisson ratio of the bond coat. Unlike the sintering effect of topcoat, the BC is dominated by high temperature creep behavior which is considered and integrated into the expression of BC Young's modulus E_{BC}. The temperature-dependent residual stress model parameters of a_{BC}, b_{BC}, c_{BC} are fitted by FEA results in specific temperature.

Similar to the stress function described by eq 4-1, it is assumed that the CTE mismatch stress between topcoat and bond coat will be calculated as the TGO thickness equals zero. On the other hand, it is assumed that the coating has a stress-free state at a high dwell temperature due to creep on the bond coat (BC) during the beginning of thermal cycles, indicated by flat interface (*R* tend to infinite). The exponential factor $\exp(\gamma_{BC}A/R)$ will lead to a fast reduction of stress state for large value of R/A, which could be used to reflect the stress relaxation caused by creep behavior of bond coat.

4.2.3. Stress within TGO

The model described so far focused on the stress state within topcoat and bond coat close to TGO. As indicated from preceding sections, the crack nucleating from ridge of the BC and valley of voids within the topcoat will converge where the crack penetrates the TGO layer as large tensile stresses generated within TGO due to the CTE mismatch. The analytical function for the stress is proposed based on a composite of bond coat and TGO [95] is described as

$$\sigma_* = \frac{(\alpha_{TBC} - \alpha_{COMP})\Delta T}{(1-\nu_{TBC})/2E_{TBC} + (1-2\nu_{COMP})/E_{COMP}} \quad \text{eq 4-4}$$

where σ_* is the radial stress within bond-coat/TGO composite sphere. ΔT is the temperature difference between the high temperature during holding time and environmental temperature. ν_{TBC} and E_{TBC} are Poisson's ratio and young's modulus for topcoat. The α_{COMP} ν_{COMP} and E_{COMP} are effective parameters where the TGO and BC are considered as composite materials. Their Young's modulus and coefficient of thermal expansion combining with geometrical factors are incorporated into Eshelby's model and given in eq 4-5 to eq 4-8. The effective Poisson's ratio followed by a rule of mixture relation is given in eq 4-9.

$$E_{COMP} = 3K_{COMP}(1-2\nu_{comp}) \quad \text{eq 4-5}$$

where K_{COMP} is bulk modulus for composite material.

$$\alpha_{COMP} = \alpha_{TGO} + \frac{P_3(\alpha_{BC}-\alpha_{TGO})}{P_2} \quad \text{eq 4-6}$$

The functions P_2 and P_3 are defined in [97] as

$$P_2 = \frac{R^3(1+\nu_{TGO}) + 2(R-d_{TGO})^3(1-2\nu_{TGO})}{2R^3 - 2(R-d_{TGO})^3} + \frac{E_{TGO}(1-2\nu_{BC})}{E_{BC}} \quad \text{eq 4-7}$$

and

$$P_3 = \frac{3R^3(1-\nu_{TGO})}{2R^3 - 2(R-d_{TGO})^3} \quad \text{eq 4-8}$$

$$\nu_{COMP} = \frac{a^3}{b^3}\nu_{BC} + \frac{(b^3-a^3)}{b^3}\nu_{TGO} \quad \text{eq 4-9}$$

where a is the radius of spherical inclusion in Eshelby's model, indicating the curvature radius for bond coat. b is the radius of sphere in Eshelby's model, indicating the sum of curvature radius and TGO thickness, Figure 4-4.

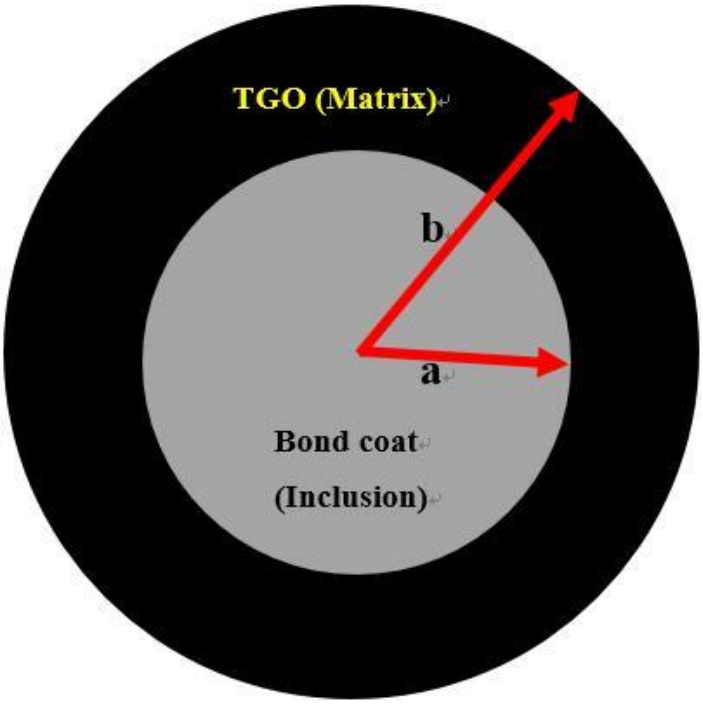

Figure 4-4 Eshelby's model incorporated into the TGO stress function where a and b indicates the curvature radius of inclusion (bond coat) and matrix (bond coat plus TGO) respectively

ν_{TGO} and ν_{BC} are Poisson's ratio for TGO and bond coat. The parameters used in the stress function will be discussed in following section.

4.3. Data source

As discussed in the preceding sections, three stress models are outlined which describe the CTE stress as function of thermal cycles for different layers. An essential part of models are temperature-process-dependent parameters which are integrated into stress functions. The related parameters at different layers are listed in Table 4-1.

Table 4-1 Related parameters for different layers

TBC

Parameters	Young's modulus	Coefficient of thermal expansion	Poisson's ratio	Valley position for stress calculation	Residual stress model parameters
Abbreviation	E_{TBC}	α_{TBC}	ν_{TBC}	y_{TBC}	α, β, γ

TGO

Parameters	Coefficient of thermal expansion	TGO thickness	Young's modulus	Poisson's ratio
Abbreviation	α_{TGO}	d_{TGO}	E_{TGO}	ν_{TGO}

Bond coat

Parameters	Young's modulus	Coefficient of thermal expansion	Ridge position for stress calculation	Amplitude of interfacial roughness
Abbreviation	E_{BC}	α_{BC}	y_{BC}	A

Parameters	Poisson's ratio	Curvature radius	Residual stress model parameters
Abbreviation	ν_{BC}	R	a_{BC}, b_{BC}, c_{BC}

Composite materials

Parameters	Bulk modulus for composite material	Effective coefficient of thermal expansion
Abbreviation	K_{COMP}	α_{COMP}

A key feature of our model is the assumption of similarities in the roughness profile between TC/TGO interface and TGO/BC interface, which avoids a further measurement for curvature radius of roughness at the TC/TGO interface as a function of thermal cycles and BC temperatures. The simplification is deliberately made to keep the number of parameters small within the stress expressions. The curvature radius was

measured on a cross section of a failed specimen by SEM for three different BC temperatures shown in Figure 4-5.

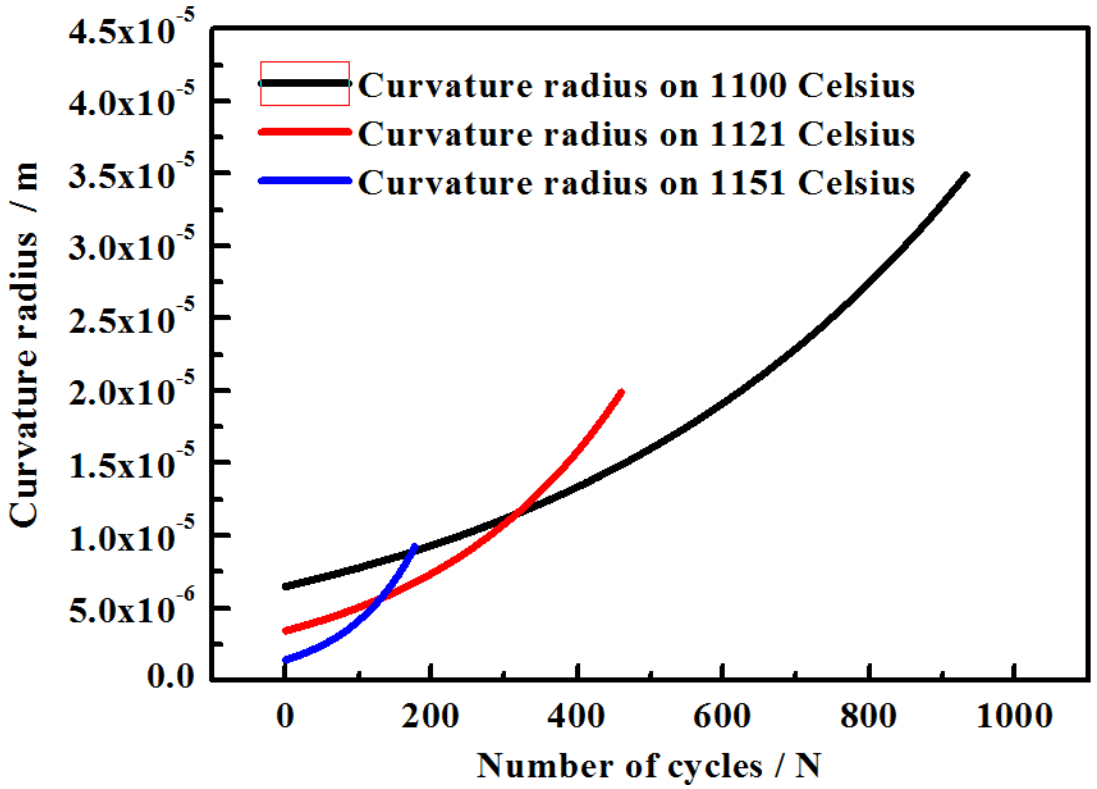

Figure 4-5 Local curvature radius as function of thermal cycles, the higher temperature corresponds to lower initial wavelength but higher gradient as function of number of cycles

It is expected that the microstructure for longer lifetime specimens would be observed to have a flatter surface (larger radius of curvature) but a slower growth rate for bond coat roughness, consistent with the curvature radius parameters measured on the surface of the bond coat as shown in Figure 4-5. It should be mentioned that the substrate of samples used to measure the curvature radius in [13] are made of Ren é N5. In modelling, we ignore this fact and assume CMSX-4 used as substrate for all calculations. The results of curvature radius are integrated into the stress model and with this capability, the model allows for the evaluation of the influence of interfacial roughness on stress levels.

4.4. Model verification and discussion

4.4.1. The results of calculated thermal stress

The calculated thermal stress in eq 4-1, eq 4-3 and eq 4-4 are shown in Figure 4-6 to Figure 4-8.

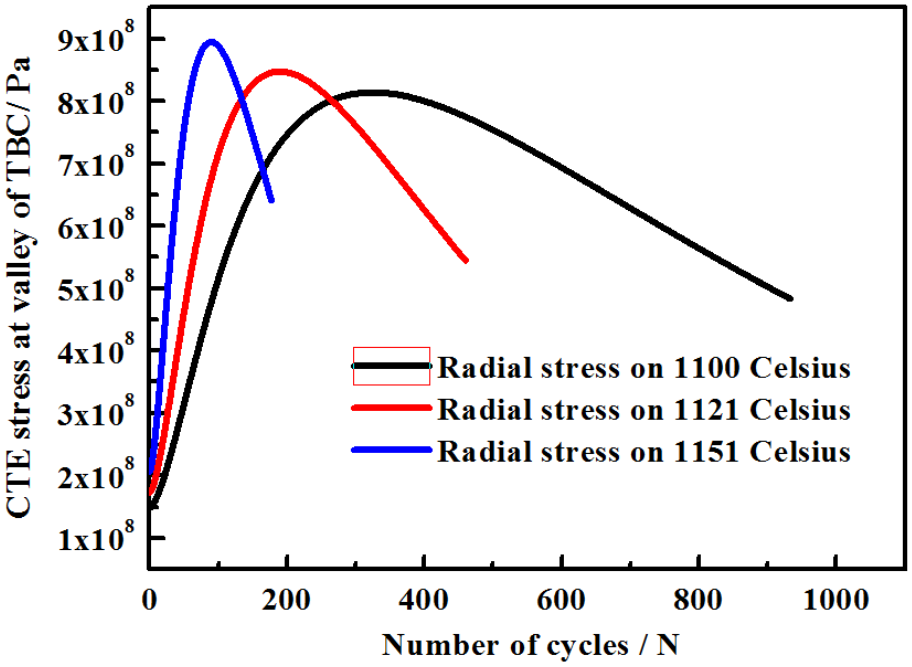

Figure 4-6 thermal stress at valley of topcoat close to TBC/TGO interface where higher stress level could be explained by larger distortion induced by rumpling effect of bond coat for higher temperatures

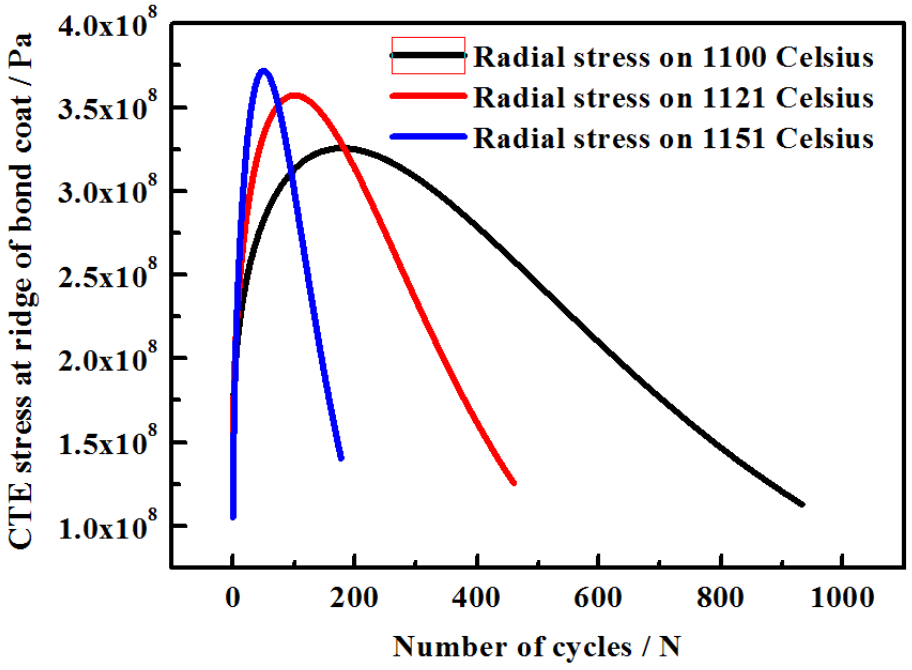

Figure 4-7 thermal stress at ridge of bond coat close to BC/TGO interface where faster stress relaxation are observed due to creep behavior at higher temperature and crack formation at shorter lifetime

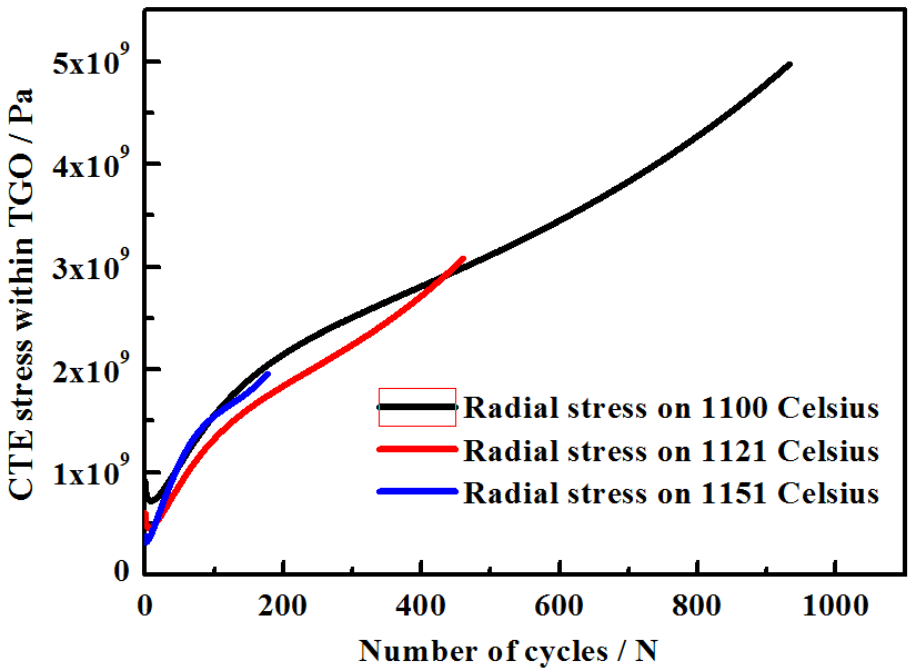

Figure 4-8 thermal stress within TGO indicates the CTE stress level is dominated by the number of thermal cycles

Some observations can be drawn from Figure 4-6 to Figure 4-8. It is evident that a reduction of stress level could be expected in the stress at a valley of the topcoat as well as a ridge of the bond coat. The higher slope in the stress reduction versus thermal cycles plot indicates a dominating process with creep behavior at higher temperature in the bond coat. It is expected that the thermal instability of the bond coat at higher temperatures will cause more strain as a result of creep behavior [98]–[100] at a ridge of the bond coat. This procedure reduced the stress level considerably. However, large strain also facilitates the rumpling effect close to the interface, which in turn increases the maximum stress for higher temperatures, Figure 4-7. On the other hand, the crack nucleation and propagation might be responsible for stress reduction at the topcoat, i.e. the energy stored in the coating is released by a crack running at the interface between topcoat and TGO, reflected by a stress reduction as described in Figure 4-6.

The calculated stress levels at the bond coat and within the TGO are presented in Figure

4-7 and Figure 4-8. It turns out that the stress level calculated at a ridge of the bond coat is smaller than that calculated with the TGO. A possible mechanism which can explain this effect is the difference in creep properties between bond coat and TGO. The creep properties obtained by E.P. Busso et al. are given in [92]. A recompilation of data is presented in Figure 4-9.

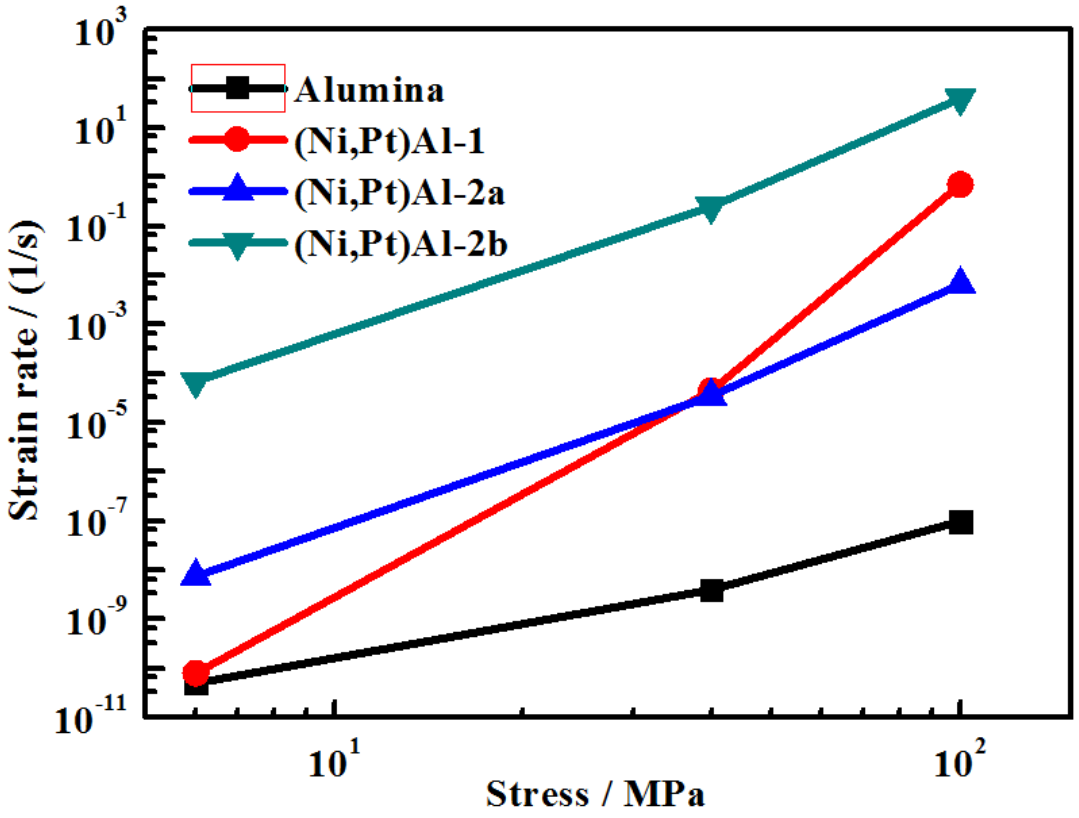

Figure 4-9 Creep properties of different bond coats and TGO, noticed that the lowest strain rate of TGO is presented compared with bond coat materials as function of stress levels which indicates it is more difficult for stress relaxation within TGO than bond coat [92]

The strain rate was hardly influenced by the stress state in the TGO compared with the typical type of bond coat characterized by (Ni, Pt) Al-1 shown in the Figure 4-9. This indicates that a larger stress relaxation might be possible as the thermal cycle proceeds, leading to a significant reduction of stress levels generated at a ridge of the bond coat. Additional influencing factors might be the difference in the fracture toughness. For an EB-PVD system, the fracture toughness for TGO measured in [32] ($3MPa\sqrt{m}$) is nearly constant during the entire lifetime of the EB-PVD specimen, and is considerably larger

than the interfacial fracture toughness measured at the end of lifetime for an EB-PVD specimen [101] ($0.5 MPa\sqrt{m}$ as a mean value). Thus, it is expected that larger stress-related energy release rate within the TGO is necessary as a driving force for fatigue crack growth, compared with the parameters of the bond coat.

4.4.2. The capability of wavelength on stress model in EB-PVD TBCs

In the present approach, it is assumed that the curvature radius is considered to evaluate the width of the roughness in the thermal stress model in EB-PVD TBCs, where the parameter was assumed to be represented by a specific preferred wavelength in a series of models describing the stress distribution in APS-TBC systems. The wavelength given by FFT [9][13] in EB-PVD TBC system was fitted by an exponential function and shows temperature-process-dependent characteristics estimated by

$$W = \alpha \exp(\beta N) \times 10^{-6} \qquad \text{eq 4-10}$$

where $\alpha = -1.55T + 2382.4325; \beta = -2.074 \times 10^{-24} \exp(0.0348T)$

A comparison between the calculated curvature radius given in Figure 4-5 and wavelength presented in Figure 4-10 is made, and it turns out that the value of wavelength parameters are significantly larger than that of the radius.

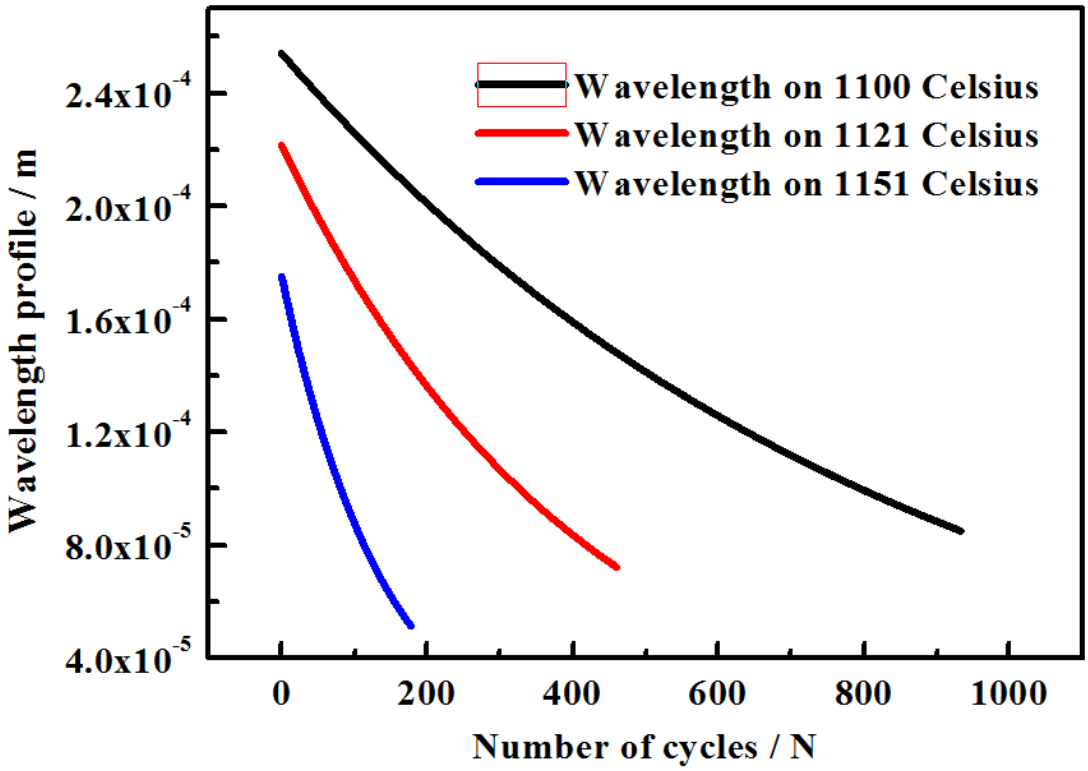

Figure 4-10 Global wavelength as function of thermal cycles and temperature, the higher temperature corresponds to higher initial wavelength but lower gradient as function of number of cycles

Based on the wavelength measuring approach and the failure mechanism of EB-PVD, the wavelength is considered to define the distance between positions for neighboring downward displacements, as shown in Figure 4-11.

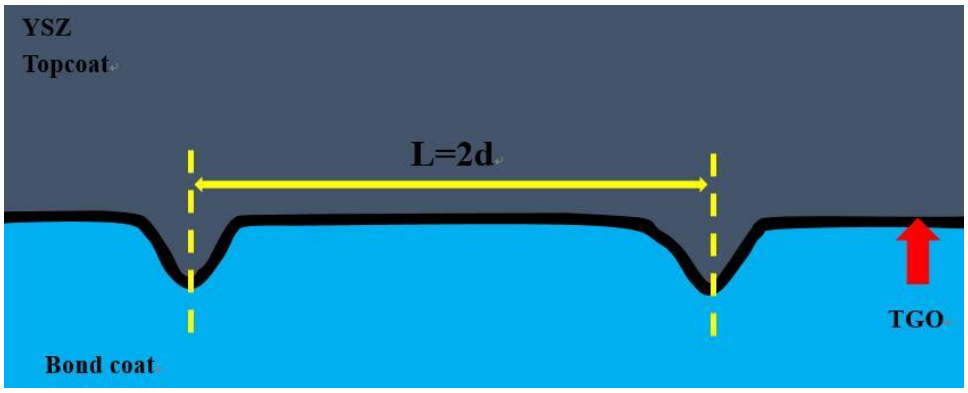

Figure 4-11 Global wavelength parameter which was defined by length of spacing between two imperfections within topcoat

Unlike the sinusoidal interfacial profile of APS-TBCs, the failure mechanism analysis of EB-PVD TBCs is partially based on the flat section of the coating interface between the TGO and the bond coat, which was deliberately designed to reduce the effect of large

imperfections by sand-blasting the bond coat surface before further deposition. Thus, the parameter used in the stress functions should be able to describe local geometrical characteristics (R in the presented stress function) instead of global geometrical characteristics (L). In other words, there is no distinct correlation between the global wavelengths with local stress levels. This fact was already pointed by Mei Wen et al. [9] and D. R. MUMM et al. [93]. However, the redefinition of wavelength is essential for a good performance of a lifetime prediction model, as it gives critical parameters for the global profile of the interface.

4.5. Summary

Based on the two identified possible failure mechanisms of EB-PVD TBC system, imperfection-based stress functions were proposed. Temperature-dependent parameters including the effects of TGO growth, top coat sintering, CTE mismatch and geometrical parameters describing interfacial roughness profile were explored and integrated into the thermal stress models. The results of the stress model were briefly discussed and show that creep behavior and crack extension play a major role in the reduction of stress on the topcoat and bond coat. The difference of creep behavior as well as fracture toughness between TGO and bond coat are responsible for large deviations in stress levels since the curvature radius was approximated and integrated for both stress functions. It was considered that the wavelength measured in EB-PVD TBC system cannot be fully integrated into the stress model as it describes the global characteristics of interfacial profile instead of local characteristics used in stress functions. However, it is noted that wavelength could be essential for lifetime models as the crack length could be reproduced by temperature process-dependent wavelength parameters. Similarly, the stress functions could be taken as a basis for analytical solutions to estimate the lifetime for EB-PVD system.

5. Lifetime prediction based on Electron Beam - Physical Vapor Deposition Thermal Barrier Coating system

This chapter addresses objective 3 (estimate the lifetime and crack growth rate based on EB-PVD TBC system) by using temperature process-dependent model parameters.

The content of this chapter has been submitted for publication in Surface and Coatings Technology in 2016.

[a]*BC. Zhang,* [b*]*K. Chen,* [a] *N. Baddour,* [c] *P. C. Prakash*

[a] *Department of Mechanical Engineering, the University of Ottawa, Ottawa, Canada*

[b] *Structures, Materials and Manufacturing Laboratory, Aerospace Portfolio, National Research Council Canada, Ottawa, Canada*

[c] *Gas Turbine Laboratory, Aerospace Portfolio, National Research Council Canada, Ottawa, Canada*

**Corresponding author*

Aerospace Portfolio

National Research Council Canada

Ottawa, Ontario, K1A 0R6

Canada

Fax 1-613-949-8165

E-mail: kuiying.chen@nrc-cnrc.gc.ca

ABSTRACT

Using experimentally measured temperature-process-dependent model parameters, the failure analysis and life prediction were conducted for Electron Beam Physical Vapor Deposition Thermal Barrier Coatings (EB-PVD TBCs) with Pt-modified β-NiAl bond coats deposited on Ni-base single crystal superalloys. The failure analysis and life model were applied to two failure modes, A and B, identified experimentally for thermal cyclic processes. The rumpling effect and the associated roughness of the constituent coating layers were shown to play a key role in evaluating the coating's failure and life. The experimentally-determined temperature-dependent thickness of thermally grown oxide (TGO), interfacial roughness, elastic moduli of constituent coatings and their coefficients of thermal expansion were incorporated into the life model. The maximum average rumpling amplitude of the bond coat/TGO interface associated with bond coat rumpling was used in the failure analysis and life evaluation for failure mode A. The maximum interface strength determined experimentally was applied to fitting stress model parameters of the topcoat. The global wavelength related to interface rumpling and its radius curvature were identified as essential parameters for life evaluation, and the life results for failure mode A were verified by existing burner rig test data. For failure mode B, the crack growth rate along the topcoat/TGO interface was calculated using the experimentally measured average interfacial fracture toughness.

Keywords: EB-PVD thermal barrier coating, life prediction, failure mechnism and analysis, temperature-process-dependent model parameters, stress, interfacial toughness.

5.1. Introduction

Electron Beam Physical Vapor Deposition Thermal Barrier Coatings (EB-PVD TBCs) have been used as thermal isolators between substrates and hot burning gas in turbine engines for decades [1]–[4]. These coating systems normally comprise 7~8 wt % yittria-stabilized zirconia (YSZ) topcoat, a thermally grown oxide (TGO), a metallic bond coat (BC) and substrate. Compared with plasma-sprayed thermal barrier coatings, a relative high strain tolerance during thermal cyclic processes in EB-PVD TBCs can result [55]–[60]. This is due to the columnar microstructure of the topcoat, where a large strain is developed because of a mismatch between the coefficients of thermal expansion of the top coat and substrate. Pt-modified nickel aluminide or MCrAlY (M = Ni or Co) bond coat deposited on the substrate provides strong mechanical bonding between the topcoat and substrate [61]–[63]. A TGO scale formed on the bond coat during the thermal exposure period prevents the bond coat from further oxidation [64]–[69]. It was realized that failure of TBC systems is mainly caused by the TGO scale, where a large compressive stress is generated due to progressive oxidation of the bond coat [70]–[75]. Meanwhile, cracks nucleate from sites where transient mixed oxides, for example spinel, are formed [76][77][79]–[83][94]. Based on the identified failure mechanisms, a number of life models of EB-PVD TBCs have been proposed. A recent summary given by Simlelark [102] suggested that the life of EB-PVD TBCs can be evaluated using an exponential-like formula with temperature-dependent parameters. A few cyclic life data of EB-PVD TBCs were collected and compiled, where a general trend of life was given

by a logarithmic formula at elevated temperatures. A model proposed by Courcier *et al* [9] divided the life of EB-PVD TBCs into two periods that are related to progressive damage generated during thermal cyclic process. Parameters describing the interfacial damage during both dwell period and upon cooling are integrated into the life model, where the TGO thickness as well as the accumulated plastic strain were used to evaluate the associated damage.

Evans *et al*. [10] introduced a mechanics-based life model in which the failure of TBC was indicated by crack coalescence in residually-stressed film. The critical TGO thickness was estimated when failure occurred. The life could be evaluated by combining the critical thickness of TGO and parabolic TGO growth kinetics. Zhang *et al*. [103] developed an analytical life model where damage accumulation was considered to be the main factor of TBC failure in terms of TGO growth. The failure occurred at the TGO/bond coat interface, as well as within the topcoat, and fatigue stress was used as an essential quantity to evaluate the life during thermal cycles.

In this paper, two possible failure mechanisms of EB-PVD TBCs are analyzed [10][13] and corresponding life models are developed. Most importantly, measured temperature-dependent model parameters [89] are applied. It is shown that the capability of the life model is improved by using such temperature-process-dependent model parameters. In addition, a newly-proposed stress model is used to describe the stress at the valley location of the top coat, where both CTE mismatch strain and TGO growth strain are considered to be critical contributors to the residual stress in the vicinity of the top coat/TGO interface. The crack growth rate along the top coat/TGO interface was subsequently evaluated using the measured average fracture toughness.

5.2. Failure mechanism analysis

5.2.1. Grit blasting process-dependent failure modes A and B

The failure mechanism of EB-PVD TBCs with a Pt-modified bond coat depends on the sand blasting process involved for the bond coat, and based on that, two failure modes A and B are identified experimentally for Pt-modified β-NiAl bond coat of EB-PVD TBCs. Therefore, Prior to YSZ top coat deposition, the Pt-modified β-NiAl bond coat is normally treated using a grit blasting process to flatten the bond coat surface in order to reduce the interfacial roughness between the bond coat and the topcoat. Meanwhile, the sand blasting process is also used to compact the bond coat layer and substrate layer. For the TBCs with flattened and compacted bond coats, large roughness at the interface likely generated during bond coat deposition, no longer exists between the topcoat and TGO. As a result, large creep is hardly observed during high temperature dwell time. On the other hand, a small downward displacement of the TGO/bond coat interface due to rumpling can affect the life of EB-PVD TBC. Failure and life of EB-PVD TBCs were analyzed on the basis of rumpling of the coating interface during the thermal cyclic process, during which cracks nucleate and propagate above the rumpling sites where voids form and grow at the topcoat/TGO interface as indicated in Figure 5-1. Mode A is used to describe the failure process for TBCs with grit-blasted bond coats.

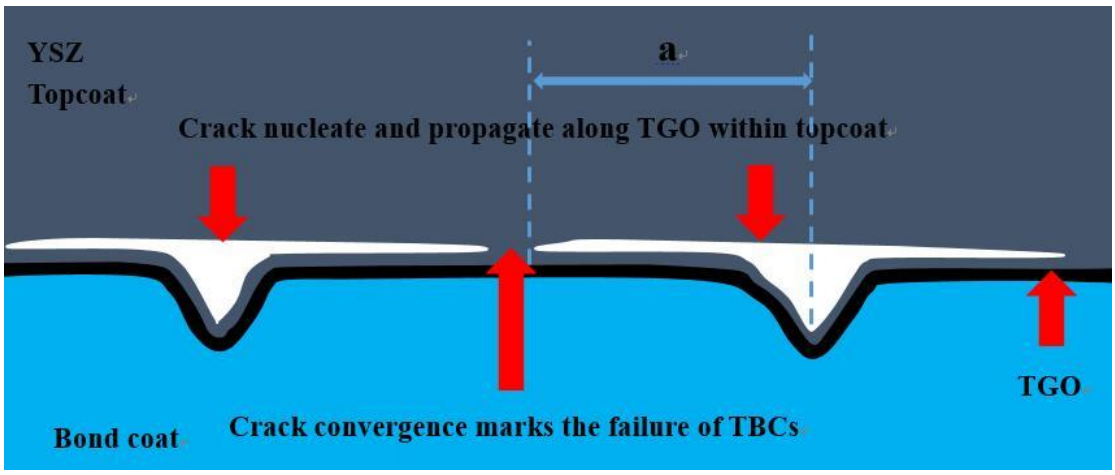

Figure 5-1 Schematic diagram of Failure mode A, noticed that the convergence of neighboring cracks marks the failure of TBCs

Based on the bond coat roughness profile measured experimentally [104], the sand-blasted process eliminates the large peak and valley of the surface. It also generates a certain amount of small peaks and valleys, more so than on surfaces without sand-blasting, Figure 5-2.

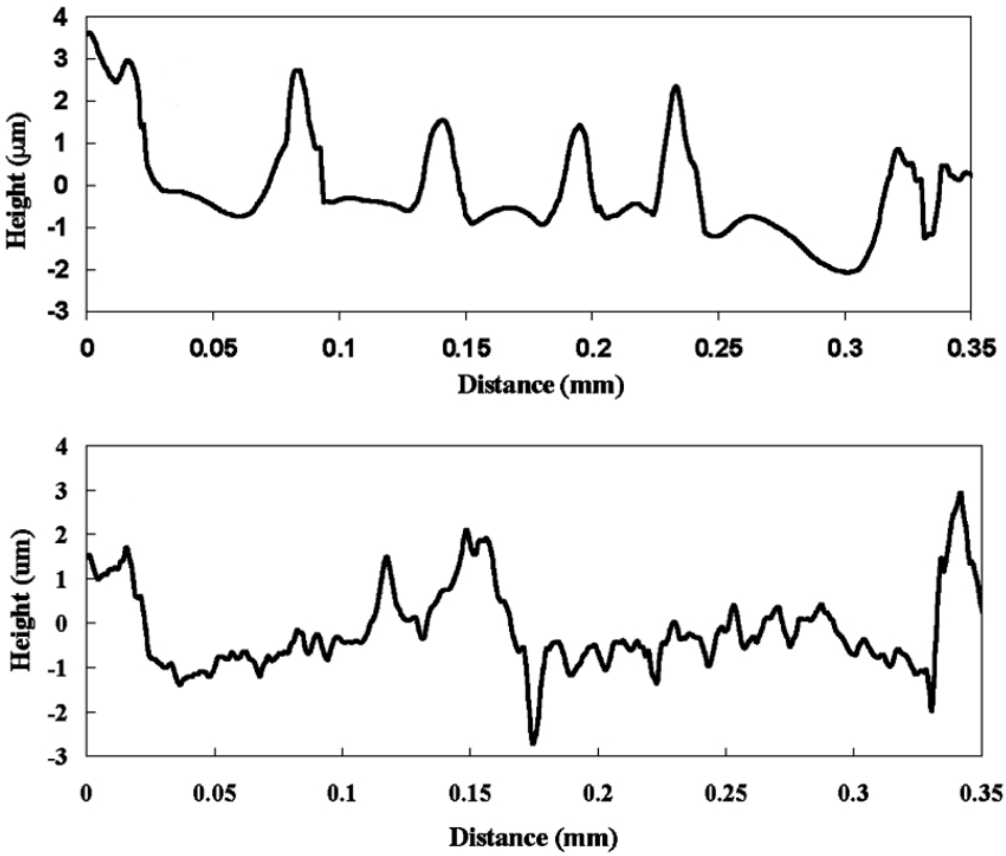

Figure 5-2 BC surface roughness profile with (up) / without (down) sand blasting process [104]

Figure 5-2 indicates that more small rumpling behavior (downward displacement) could be expected at a sand-blasted bond coat surface, which will in turn increase the amount of voids within the topcoat/TGO interface.

For failure mode A, a large number of voids are generated at the top coat/TGO interface, and cracks nucleate incurred by interface rumpling at the valley of the bond coat, followed by a downward displacement of the TGO into the bond coat. As the thermal cycle proceeds, larger voids form and grow as a result of increasing downward displacement of the TGO. Horizontal cracks start to propagate along the TGO/topcoat interface, and spallation of the top coat occurs when these neighboring cracks coalescence. This indicates failure of EB-PVD TBCs, Figure 5-3.

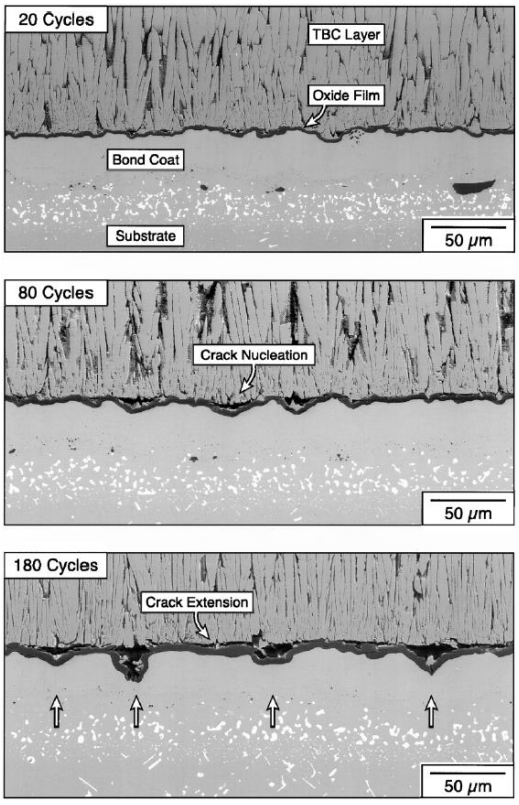

Figure 5-3 Crack nucleate / propagate from the voids at topcoat and TGO interface as thermal cycle proceeds [1]

For the TBCs without a sand-blasted bond coat, a relatively larger roughness can be

expected from the interface of the TGO/bond coat. This results in failure mode B, where cracks nucleate at the ridge of the bond coat due to the out-of-plane tensile stress generated at the rough interface. As cracks at the ridge of the bond coat meet the horizontal cracks from voids at the topcoat, a large in-plane stress is generated by the cooling process, leading to out-of-plane tensile stress within the TGO. This results in the cracks on the two sides of the boundaries convergence together, Figure 5-4 and Figure 5-5.

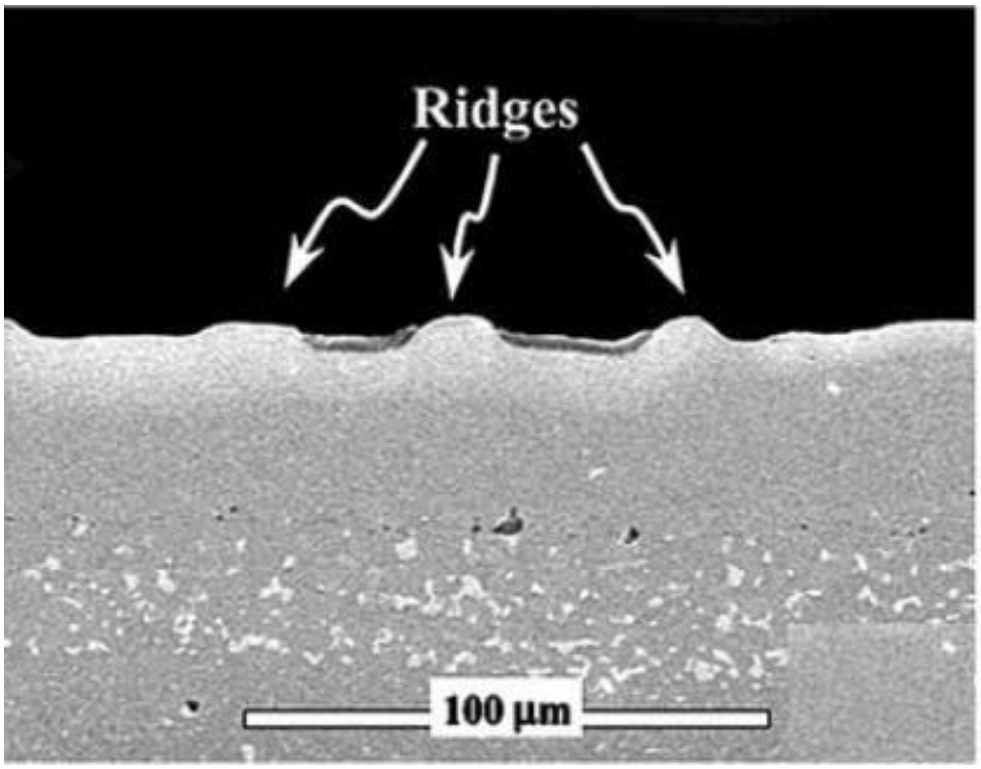

Figure 5-4 the ridge of bond coat and valley of topcoat could be sites where crack nucleates in EB-PVD TBCs due to the rumpling effect of bond coat [90]

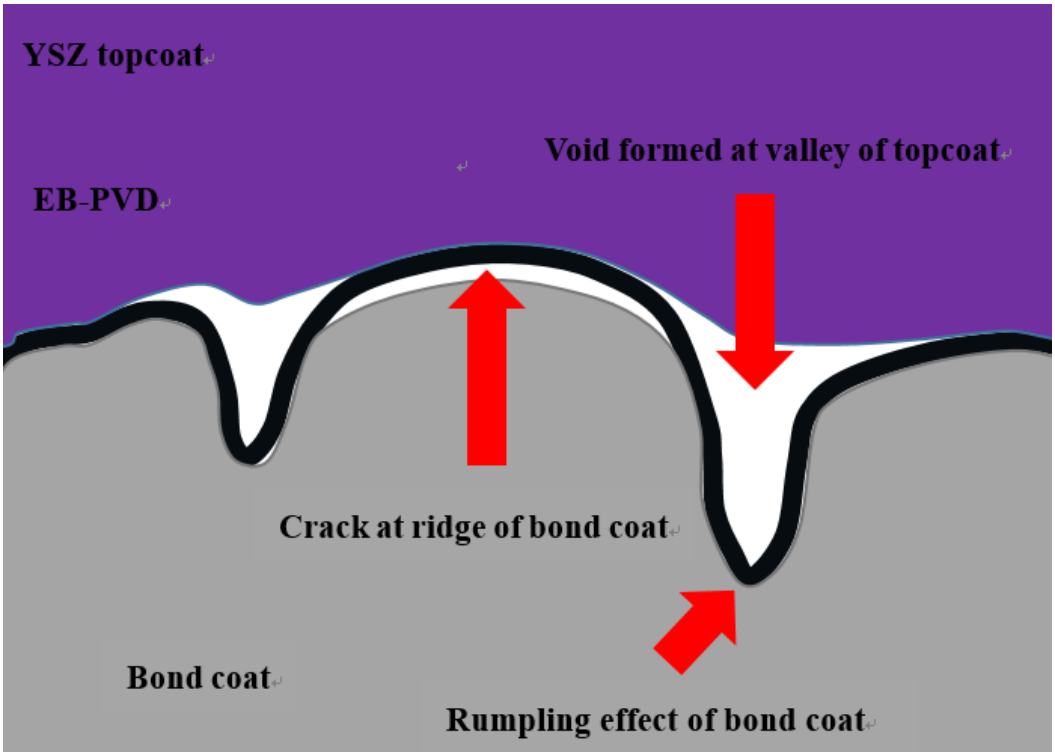

Figure 5-5 SEM indicates the failure was due to the separation generated by crack nucleating and propagating from the at ridge of bond coat [90]

5.2.2. Analysis of correlation between grit blasting process-dependent failure modes to life of EB-PVD TBCs

Figure 5-6 indicates a possible correlation between grit blasting process-dependent failure modes and life of EB-PVD TBCs [104].

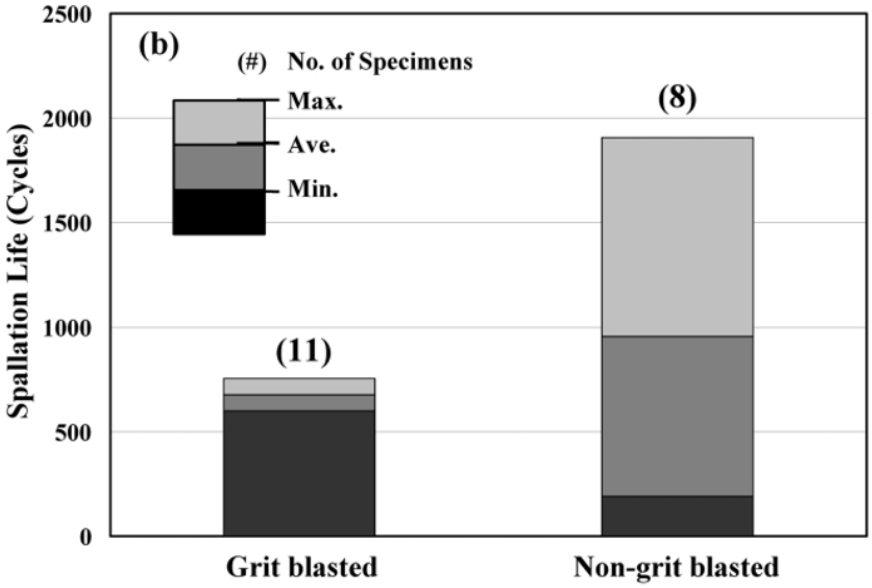

Figure 5-6 Life of EB-PVD TBCs measured by specimen with / without grit blasted BC [104]

It is evident that a relatively flattened surface is one of the essential characteristics that narrows the scatter of lifetime measured from failed grit-blasted TBCs and is more consistent with an engineering coating. The reason for the discrepancy between the life corresponding to respective failure mode can be explained as follows. For the specimen with the grit blasting process, the crack is located within the topcoat and there are less layer-dependent factors that can affect the lifetime based on failure mode A, thus a narrow scatter for measured lifetime can be expected. However, for the specimen without the grit blasting process, there are multiple-cracks that initiate from peaks of roughness at the TGO/bond coat interface, which then propagate and penetrate the TGO and finally meet the voids at the topcoat/TGO interface.

5.3. Life model for failure mode A

5.3.1. The life model

As discussed in the preceding sections, the voids generated at the TGO/top coat interface as a result of bond coat rumpling are the major cause of horizontal crack nucleation and propagation. Failure mode A of an EB-PVD Pt-modified bond coat is schematically shown in Figure 5-1. Based on analysis of the rumpling effect, the stress intensity at a crack tip of the top coat near the TGO was evaluated as [1][13],

$$K \approx \frac{E_{TBC}(dA/dN)}{2\sqrt{\pi}(1-\nu_{TBC}^{\ 2})\sqrt{L}}\left(\frac{L}{a}\right)^{1.5} N \qquad \text{eq 5-1}$$

where K, E_{TBC} and ν_{TBC} stand for the stress intensity factor, Young's modulus and Poisson's ratio of the topcoat, while dA/dN represents the rumpling rate of the TGO/topcoat interface. N is the number of thermal cycles, a is the crack length within the topcoat above the TGO shown in Figure 5-1. L represents the global wavelength,

in which $L = 2d$.

In the present research, it is assumed that the rumpling rate *dA*/*dN* of the TGO/top coat interface follows the same rate as the *dA*/*dN* of the TGO/bond coat interface, shown in Figure 5-1. According to this assumption, the life model allows us to examine the influence of the interfacial rumpling amplitude on the life of EB-PVD TBC.

It can be seen that the stress intensity *K* of eq 5-1 at the crack tip of the top coat does not depend on the properties of either TGO or bond coat. *K* only involves properties of the top coat, although both the TGO and bond coat can show a strong effect on the stress distribution in the top coat. This effect can be accomplished by incorporating temperature-process-dependent model parameters into the life model [89]**.** To evaluate TBC's life, eq 5-1 can be rewritten as,

$$dA \approx \frac{\sqrt{\pi}(1-\nu_{TBC}{}^2)Ka^{1.5}}{E_{TBC}Nd}\,dN \qquad \text{eq 5-2}$$

In the present life evaluation of TBC, the sintering effect of Young's modulus, E_{TBC}, of the top coat was also taken into account. Both E_{TBC} and wavelength *d* are temperature-dependent with thermal cycles. Integrating eq 5-2 gives the maximum rumpling amplitude *A* in which failure occurs, such that

$$\int_{A_0(T)}^{A_f(T,N)} dA \approx \sqrt{\pi}(1-\upsilon_{TBC}{}^2)K_{IC}^{TBC}a^{1.5}\int_0^{N_f}\frac{1}{E_{TBC}(T,N)Nd(T,N)}dN \qquad \text{eq 5-3}$$

where $\sqrt{\pi}(1-\upsilon_{TBC}{}^2)K_{IC}^{TBC}a^{1.5}$ is referred to as a temperature-process-dependent fitting parameter. It was observed through SEM [89] that the coating's life was finished almost at a constant average rumpling amplitude $A_f(T, N) \cong 4.2$ μm for coatings tested at three selected temperatures. This observation on the average rumpling amplitude was applied

in the present life evaluation, and when the upper limit of integration on the left hand side of eq 5-3 is chosen as 4.2 μm, the life cycle N_f can be determined numerically.

5.3.2. The model parameters

The life data for EB-PVD TBC deposited on the Pt-modified NiAl bond coat from burner rig test [89] was used in life prediction using eq 5-1. The related model parameters at different constituent layers are listed in Table 5-1.

Table 5-1 Related parameters in lifetime prediction model

TBC

Parameters	Young's modulus	Coefficient of thermal expansion	Poisson's ratio
Abbreviation	E_{TBC}	α_{TBC}	ν_{TBC}

TGO

Parameters	Coefficient of thermal expansion	TGO thickness
Abbreviation	α_{TGO}	d_{TGO}

Bond coat

Parameters	Young's modulus	Coefficient of thermal expansion	Ridge position for stress calculation	Amplitude of interfacial rumpling
Abbreviation	E_{BC}	α_{BC}	y_{BC}	A
Parameters	Poisson's ratio	Curvature radius	Residual stress model parameters	
Abbreviation	ν_{BC}	R	a_{BC}, b_{BC}, c_{BC}	

Others

Parameters	Crack length	Global wavelength
Abbreviation	a	$L=2d$

The rumpling amplitude *A* of the bond coat is a geometrical parameter used to describe the mean value of the rumpling amplitude of imperfections. The amplitude was measured using SEM at specific cyclic stages [89] as a root mean square (RMS), where the rumpling amplitude *A* can be defined and calculated as [94]

$$A = \sqrt{2}RMS \qquad \text{eq 5-4}$$

A recompilation of data for rumpling amplitude *A* is presented in Figure 5-7.

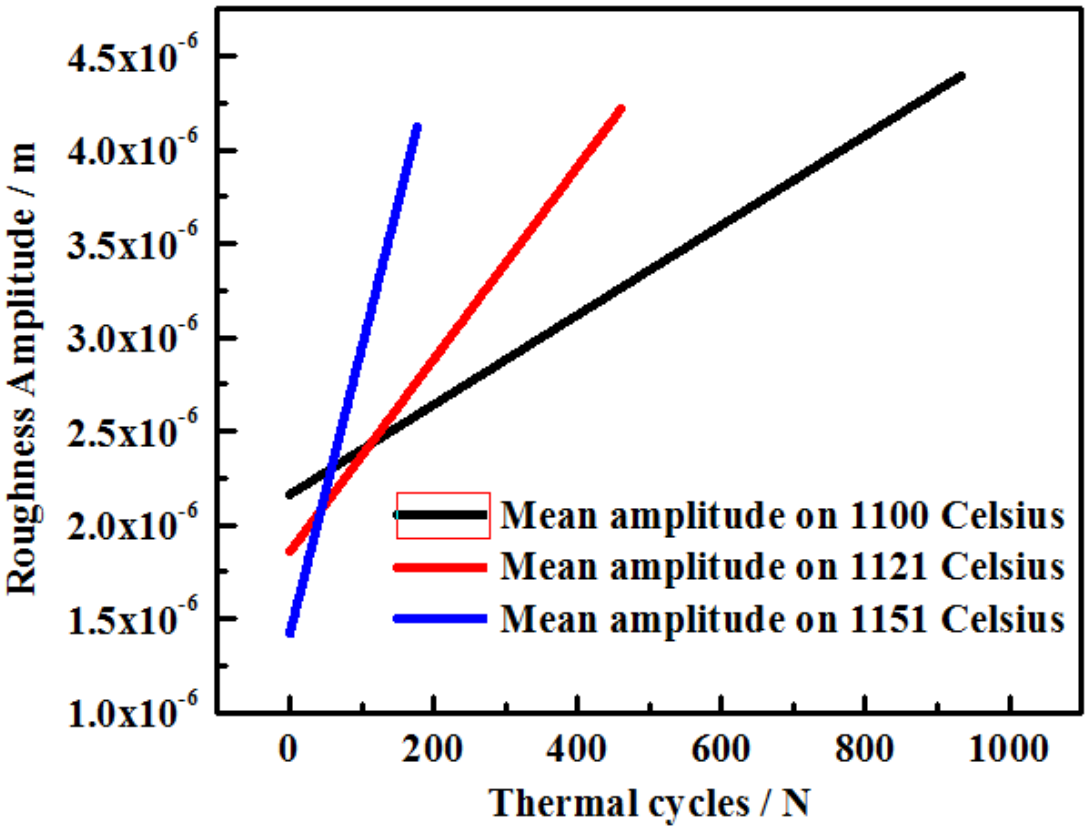

Figure 5-7 Bond coat rumpling amplitude as a significant parameter in lifetime prediction model I, an increase of rumpling gradient was found as temperature goes higher [89]

By fitting the rumpling amplitude *A* to the temperature-process-dependent data, *A* can be expressed as,

$$A = \sqrt{2}(RMS_{slope}N + RMS_{\text{int}}) \times 10^{-6} \qquad \text{eq 5-5}$$

where $RMS_{slope} = 3.559 \times 10^{-25} \exp(0.03635T)$ and $RMS_{\text{int}} = -0.01032T + 15.7$.

It was recognized that the YSZ topcoat of EB-PVD TBC illustrates a considerable sintering effect during a high temperature exposure period, which leads to an increase of Young's moduli [105] of the topcoat as a result of the closure of vertical columnar microstructure as well as pores and segmentation cracks. This sintering effect of the topcoat can be described via a formula describing the sintering effect of the APS-TBC topcoat, given by

$$\mathrm{E_{TBC}(t)} = \frac{\beta \mathrm{E^0_{TBC}} \mathrm{E^\infty_{TBC}}}{\beta \mathrm{E^0_{TBC}} + \mathrm{E^\infty_{TBC}} - \mathrm{E^0_{TBC}}} \text{ with } \beta = 1 + A_{\sin t} \exp\left(-\frac{E_{\sin t}}{\kappa_B T}\right) t^n \qquad \text{eq 5-6}$$

where $A_{\sin t}$, $E_{\sin t}$ and n are the sintering coefficient, sintering activation energy and sintering exponent of the top coat, respectively. E^0_{TBC} and E^∞_{TBC} are used to describe the initial bulk modulus and the final modulus after completion of sintering. Using the temperature-dependent Young's modulus at 1200℃ [105], sintering model parameters $A_{\sin t}, E_{\sin t}$ and n for the EB-PVD TBC topcoat were fitted and plotted with the testing data in Figure 5-8, in which the sintering model parameters are listed in Table 5-2.

Table 5-2 Young's modulus related parameters for topcoat

YSZ related parameters	$A_{\sin t}$	$E_{\sin t}$	n	E^0_{TBC}	E^∞_{TBC}
Value	2.38677×10^7	$4.15788eV$	1.53461	$20GPa$	$192GPa$

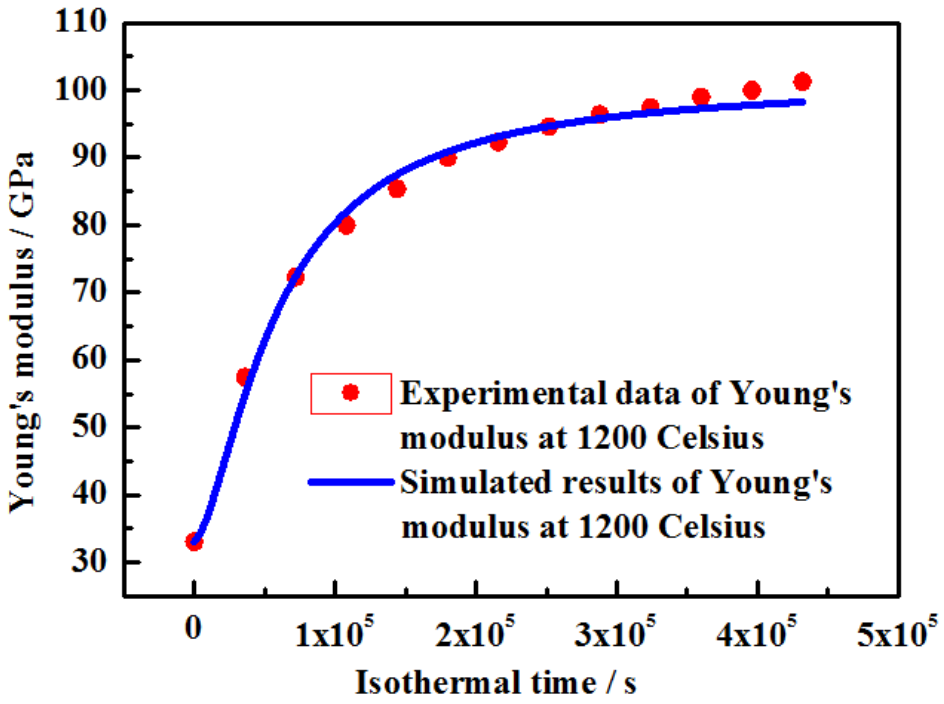

Figure 5-8 A comparison between the experimental data and modelling results for Young's modulus of EB-PVD topcoat in 1200℃

It was suggested that the global wavelength *L*, describing a separation of the rumpling sites in the TGO/bond coat interface, plays an important role in determining the life for failure mode *A* in EB-PVD TBCs. The wavelength calculated by Fast Fourier Transform (FFT) [13][89] in EB-PVD TBC system was approximately expressed by an exponential formulation versus thermal cycles *N* and exposure temperature (*T*). In the present research, a comparison between the measured wavelength given in Figure 5-9 and the measured local curvature radius presented in Figure 5-10 is made, and indicates that the value of wavelength parameters are significantly larger than that of the radius.

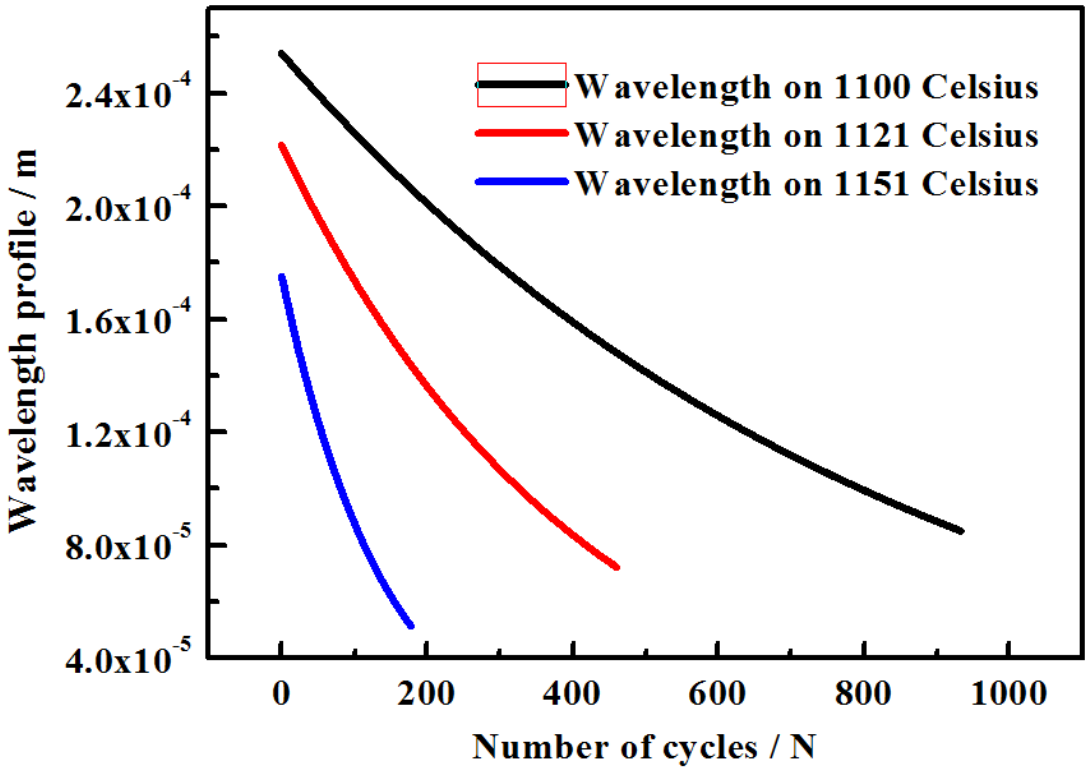

Figure 5-9 Global wavelength as function of thermal cycles and temperature, the higher temperature corresponds to higher initial wavelength but lower gradient as function of number of cycles

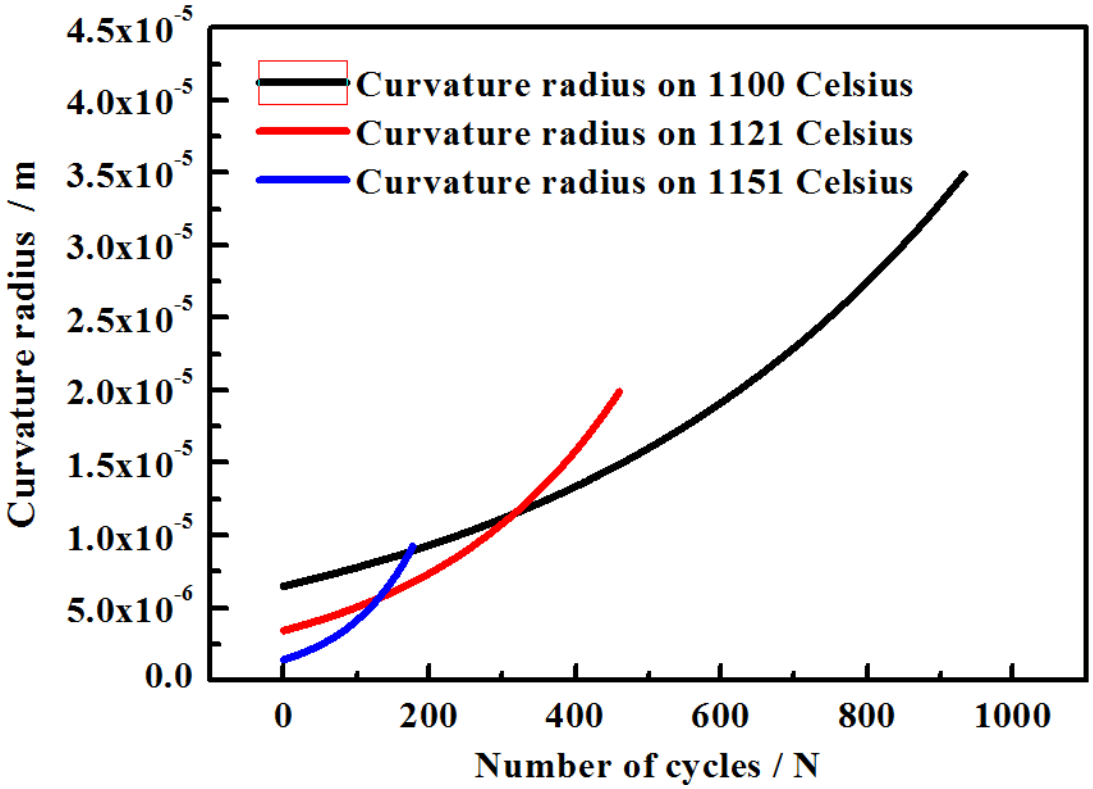

Figure 5-10 Local curvature radius as function of thermal cycles, the higher temperature corresponds to lower initial wavelength but higher gradient as function of number of cycles

The mean curvature radius $R_{T,}$ measured at the bond coat/TGO interface from the cross section of specimens at specific stages during thermal cycles, is used to estimate the size of local imperfections.

In an APS-TBC system, a sinusoidal-like interfacial profile of the TGO/bond coat or TGO/top coat interface has been assumed, and a sinusoidal function is used to describe such an interface. In the failure analysis and life prediction of these APS-TBC systems, the shape parameters, such as the amplitude *A* and the wavelength *L* and their ratios *A/L*, were incorporated to calculate stresses at different coating layers or interfaces. However, in the failure analysis of EB-PVD TBC with Pt-modified β-NiAl as the bond coat, the TGO/bond coat or TGO/topcoat interface was initially flatten compared to the APS-TBC system. Although the wavelength *L* was still used to describe such an interface profile, it cannot be used to estimate the local stress at specific coating layers or interfaces [13][89]. This may indicate that no such relationship exists between the global wavelength *L* and the local stress during thermal cycles of EB-PVD TBC systems.

5.3.3. Results of life prediction of failure mode A

In the present paper, the parameter $\sqrt{\pi}(1-\upsilon_{TBC}{}^2)K_{IC}^{TBC}a^{1.5}$ in the life model of eq 5-3 was fitted to the burner rig test data at three temperatures, 1100°C, 1121°C and 1151°C, respectively. Figure 5-11 shows that this temperature-dependent model parameter is well described by a Gaussian-type function,

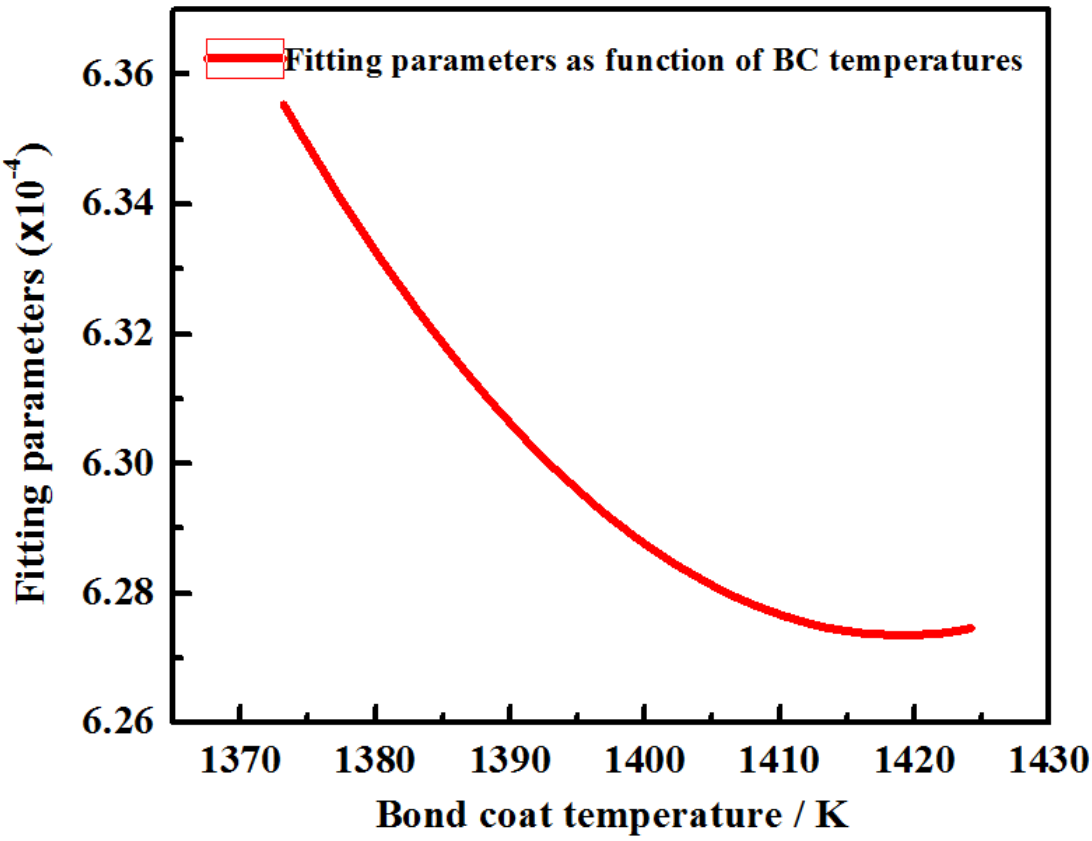

Figure 5-11 Fitting parameters for Lifetime prediction model as function of bond coat temperatures, the order of magnitude is 10^{-4}

$$\sqrt{\pi}(1-\upsilon_{TBC}{}^{2})K_{IC}^{TBC}a^{1.5} \approx 1\Big/\left\{1594\exp\left[-\left(\frac{\mathrm{T}-1419}{402.7}\right)^{2}\right]\right\} \qquad \text{eq 5-7}$$

where the bond coat temperature T was used as a reference temperature. Using the fitted model parameters of eq 5-7, the life prediction of EB-PVD TBC Pt-modified NiAl bond coat system was conducted between 1100℃ to 1151℃. Figure 5-12 shows the calculated life, along with burger rig test results.

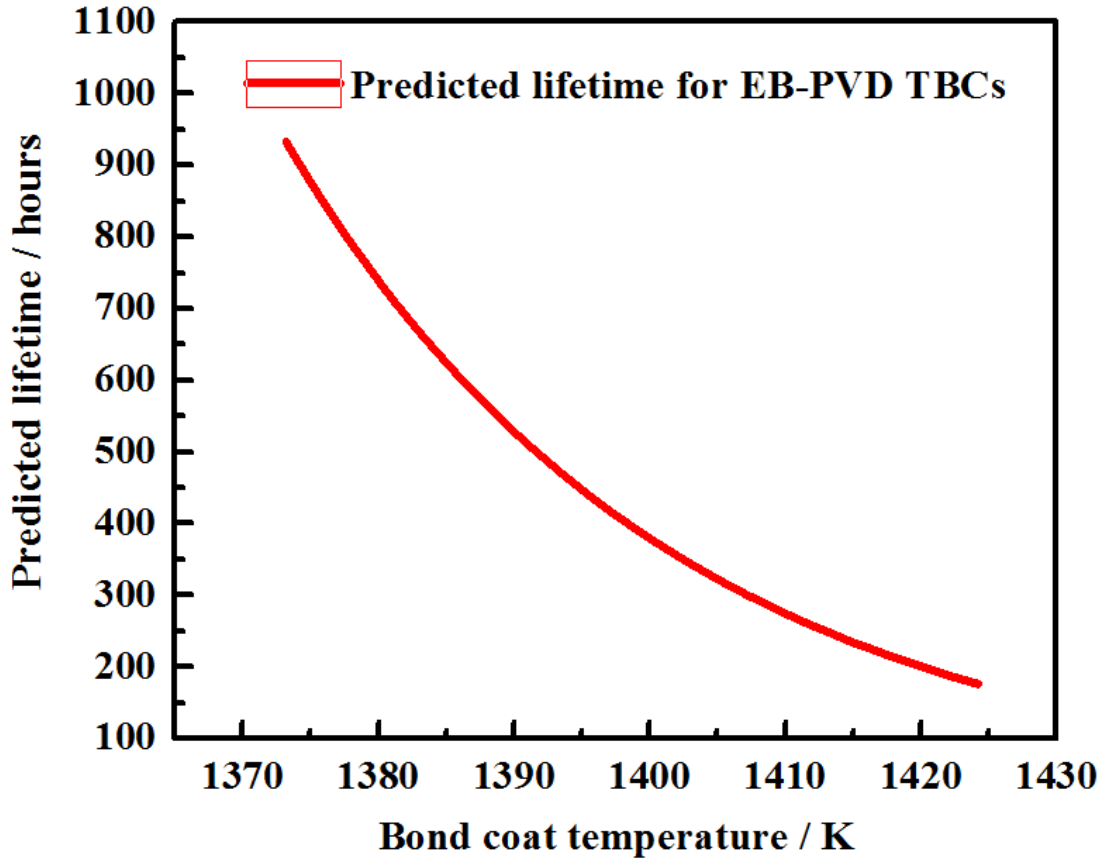

Figure 5-12 Predicted lifetime for Lifetime prediction model I as function of bond coat temperatures

5.4. Crack growth rate of failure mode B

In addition to the life model of failure mode *A*, cracks can nucleate within topcoat, penetrate the TGO layer and propagate along the TGO/bond coat interface during thermal cycles, shown in Figure 5-13 for failure mode B.

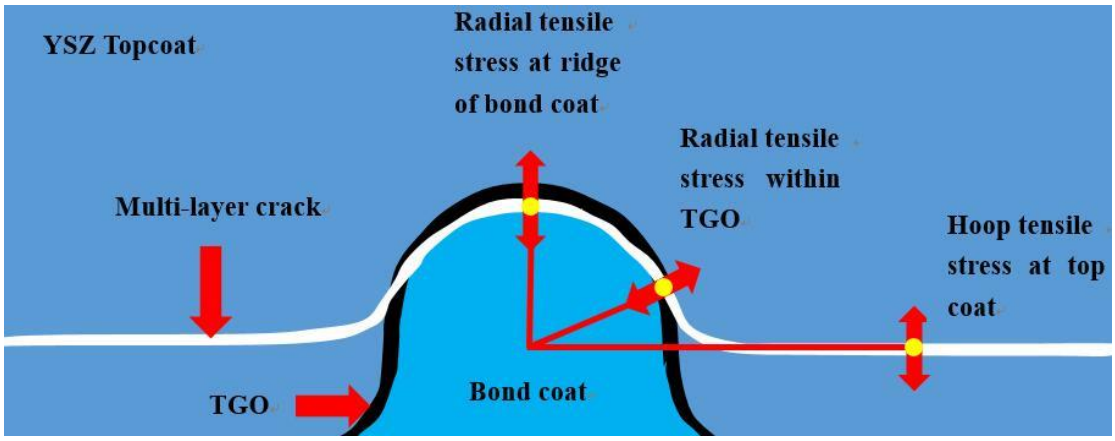

Figure 5-13 Schematic diagram for failure mode B, noticed that crack initiated from bond coat penetrate the TGO and convergence with the existed crack within topcoat

It is evident that the hoop cracks at the TGO/bond coat interface or within TGO scale

nucleate as a result of the hoop tensile stress generated within topcoat layer due to the CTE mismatch or TGO growth stress, whereas the very large stress intensity at inner front of topcoat play an essential role in promoting crack penetrating the TGO layer and coalescence within bond coat close to interface. The life model in eq 5-3 is not capable of evaluating the crack growth rate at specific coating layers or their interfaces. In the following sections, the crack growth rate is formulated along the top coat/TGO interface, and evaluated using the newly proposed stress model and experimentally measured average topcoat / TGO interface fracture toughness.

5.4.1. Stress model of the TBC/TGO interface

According to [1], the stress level for the hoop stress is a half of that radial stress, where a model describing the radial stress was formulated at the TBC/TGO interface due to the CTE mismatch between the topcoat and TGO,

$$\sigma_{\text{valley}} = \alpha\Lambda\left[(\alpha_{TGO}-\alpha_{BC})(\beta\frac{d_{TGO}A}{y_{TBC}R}-1)+(\alpha_{TGO}-\alpha_{TBC})\right](e^{\gamma\frac{A}{R}}-1) \qquad \text{eq 5-8}$$

where α_{TGO}, α_{BC} and α_{TBC} are the temperature-dependent CTEs of TGO, bond coat and top coat, respectively. d_{TGO} presents the thickness of TGO, A is the amplitude of the interfacial rumpling amplitude, y_{TBC} is the valley location of the top coat, R is the curvature radius of the ridge in the bond coat. α, β, γ are temperature-dependent residual stress model parameters. Λ is a factor that combines elastic moduli of bond coat and TGO and temperature change ΔT during cooling process, where $\Lambda = 4\kappa\mu\Delta T/(\kappa+4\mu/3)$ with $\mu = E_{TBC}/2(1+\upsilon)$, and $\kappa = E_{TBC}/3(1-2\upsilon)$. υ is the Poisson ratio of the top coat. The temperature-dependent Young's modulus E_{TBC} was applied,

and the temperature-dependent residual stress model parameters ofα, β, γ are fitted to the FEA calculated stresses at specific temperatures. A stress due to TGO dilatational growth is described as [10],

$$\sigma_{TGO}^{TBC} = \frac{E_{TBC}(m-1)}{3(1-\upsilon_{TBC})m}\left(\frac{h_{TGO}}{R}\right)\left(\frac{R}{r}\right)^3 \qquad \text{eq 5-9}$$

where *m* is the ratio of new TGO volume to the consumed bond coat volume, and taken as 1.28 in the calculations [50], [92].

5.4.2. Crack growth rate evaluation

Based on the formula developed in [10], the stress intensity factor *K* can be used to describe the crack propagation along the topcoat /TGO interface,

$$\frac{K}{\sigma^*\sqrt{R}} = \frac{3}{2(1+\upsilon)\sqrt{\pi}}\left(\frac{R}{a}\right)^{1.5} \qquad \text{eq 5-10}$$

This stress intensity factor for crack tip within topcoat layer is related to the curvature radius *R*, a local geometry parameter describing the shape of TGO/bond coat interface. Temperature-process-dependent curvature radius *R* will be incorporated into eq 5-10 to evaluate the crack growth rate along the TGO/bond coat interface. The stress σ^* includes the residual stress due to a difference of CTE between the top coat and TGO, and also includes the TGO growth stress σ_{TGO}^{TBC}. The crack growth rate derived from eq 5-10 takes the form,

$$\frac{da}{dN} = \frac{1}{(1+\nu_{TBC})K\sqrt{\pi}a^{0.5}}\frac{d\left(\sigma^* R'^2\right)}{dN} \qquad \text{eq 5-11}$$

where,

$$a^{0.5} = \left[\frac{3}{2(1+\nu_{TBC})\sqrt{\pi}K}\right]^{\frac{1}{3}} [\sigma^* R'^2]^{\frac{1}{3}} \qquad \text{eq 5-12}$$

$$\sigma^* = \sigma_{valley} + \sigma_{TGO}^{TBC} \qquad \text{eq 5-13}$$

The curvature radius R' comprises the geometry R and the TGO thickness d_{TGO}, such that

$$R' = R + d_{TGO} \qquad \text{eq 5-14}$$

Equations eq 5-11 to eq 5-14 will be combined to study the crack growth rate along the top coat/TGO interface.

5.4.3. Model parameters

To evaluate the crack growth rate along the top coat/TGO interface, in addition to the parameters used in life model eq 5-3, temperature-process-dependent geometry parameters are also needed for crack growth evaluation. The geometry parameters are mainly used to describe the stresses located at the TGO, bond coat and the TGO/bond coat interface during high temperature exposure period. As discussed in the preceding sections, the bond coat curvature radius R is a geometrical factor used to describe the mean value of the radius of imperfections. The curvature radius parameter R was measured from the TGO/bond coat interface profiles at selected stages of thermal cycles extracted from the cross-sectional micrographs [85][89][91][93], where the trend of local roughness versus thermal cycles can be estimated, Figure 5-10. This measured curvature radius R_T is essential for crack growth rate estimation as it gives the temperature-process dependent curvature radius using in stress models.

The temperature-process-dependent bond coat roughness at three selected temperatures

was fitted to the experimental data, and is well represented by,

$$R_T = \alpha e^{\beta N} \times 10^{-6} \qquad \text{eq 5-15}$$

where the pre-factor is $\alpha = 3.667\times10^{18}\exp(-0.02977T)$ and exponent parameter is given by $\beta = 9.613\times10^{-24}\exp(-0.03401T)$. The TGO growth was assumed to follow a parabolic growth law. For the given test data of TGO growth thickness, d_{TGO} at three selected temperatures was used to fit the TGO thickness versus temperature T and exposure time t according to

$$d_{TGO} = (A_{TGO}t^{0.5} + d_0)\times10^{-6} \qquad \text{eq 5-16}$$

where A_{TGO} is the parabolic growth rate and d_0 is the initial thickness of TGO layer fitted to the test data, and the fitting parameters are represented as $A_{TGO} = 1.97\exp\{-[(T-1641)/1613]^2\}$ and $d_0 = -0.003539T + 5.661$. The measured TGO thickness d_{TGO} and the calculated data are shown in Figure 5-14.

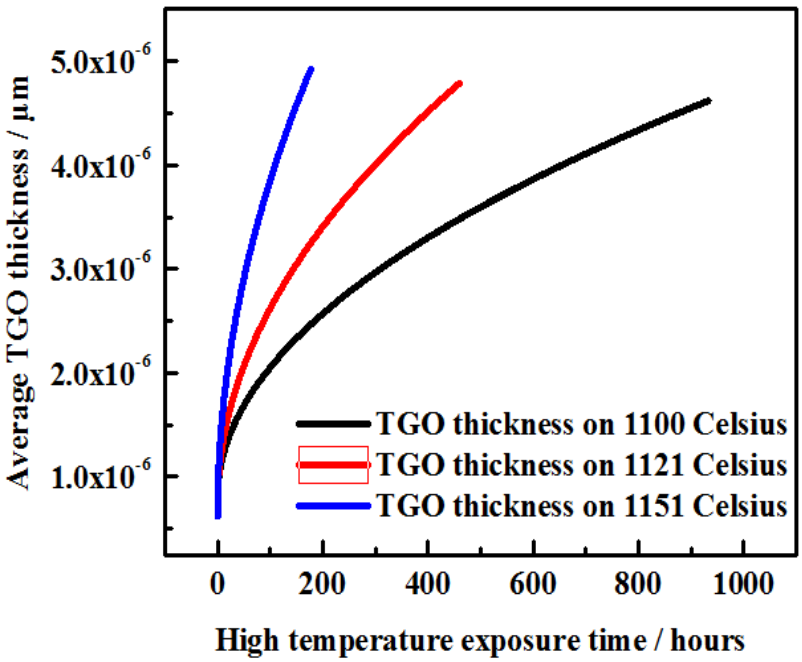

Figure 5-14 Average TGO thickness as function of high temperature exposure time, the TGO growth is consistent with parabolic growth kinetics

The measured temperature-dependent Young's moduli of TGO and bond coat [92] are

listed in Table 5-3,

Table 5-3 Measured Young's modulus of TGO and bond coat as function of temperatures [42]

T(K)	293	473	673	873	1073	1273	1373
E_{TGO} (GPa)	400	390	380	370	355	325	320
E_{BC} (GPa)	426	412	396	362	284	202	114

They are fitted by polynomial functions in Pa, and are given by

$$E_{BC} = (123.9 - 0.02329T) \times 10^9 \quad \text{eq 5-17}$$

$$E_{TGO} = (448 - 0.07506T) \times 10^9 \quad \text{eq 5-18}$$

The temperature-dependent linear CTEs of topcoat, TGO and bond coat are also used in the crack growth rate evaluation. The measured CTEs of bond coat are listed in Table 5-4 [92].

Table 5-4 Coefficient of thermal expansion for topcoat, TGO and bond coat [42]

T(K)	293	473	673	873	1073	1273	1373
$\alpha_{TGO}/10^{-6}(K^{-1})$	8.0	8.2	8.4	8.7	9.0	9.3	9.5
$\alpha_{BC}/10^{-6}(K^{-1})$	12.3	13.2	14.2	15.2	16.3	17.2	17.7
T(K)	293	473	773	973	1173	1373	1373
$\alpha_{TBC}/10^{-6}(K^{-1})$	9.7	9.8	9.9	9.9	10.0	10.1	10.1

It was observed that a variation of CTEs of bond coat and TGO was obtained, and these changes could be related to aluminum depletion in the bond coat and mixed oxide forms in TGO during high temperature cycles. However, the CTE of the topcoat varies slightly, and these three CTEs are fitted linearly with the temperature, such that

$$\alpha_{TBC} = (0.000363T + 9.615) \times 10^{-6} \quad \text{eq 5-19}$$

$$\alpha_{TGO} = (0.001388T + 7.532) \times 10^{-6} \quad \text{eq 5-20}$$

$$\alpha_{BC} = (0.005021T + 10.83) \times 10^{-6} \quad \text{eq 5-21}$$

The residual stress due to a difference of CTEs was calculated using eq 5-8 at the valley of the top coat close to the top coat/TGO interface. It was observed experimentally [90] that the failure stress at the top coat/TGO interface was approximately a constant of 800 MPa for different microstructural morphologies induced at different thermal schemes and temperatures. This maximum failure strength at the top coat/TGO interface was used to fit parameters α, β, γ of the stress model eq 5-8, and the fitted results were listed in Table 5-5.

Table 5-5 Residual stress model parameters

T(℃)/Parameters	Lifetime / hours	α	β	γ
1100	933	6.5	0.132	0.54
1121	460	4.3	0.124	0.48
1151	177	2.4	0.173	0.46

The fracture toughness K of the top coat/TGO interface was measured versus length of crack growth [1], and presented in Figure 5-15 along with a fitting curve. A increase of the fracture toughness was observed as thermal cycling proceeds. In the present, we use the experimentally measured average fracture toughness K_{Ic}^{TBC} approximate to $0.5MPa\sqrt{m}$ as the calculated value. It is expected that the accuracy of crack growth rate evaluation can be improved by using temperature-process-dependent model parameters such as the fracture toughness *K*.

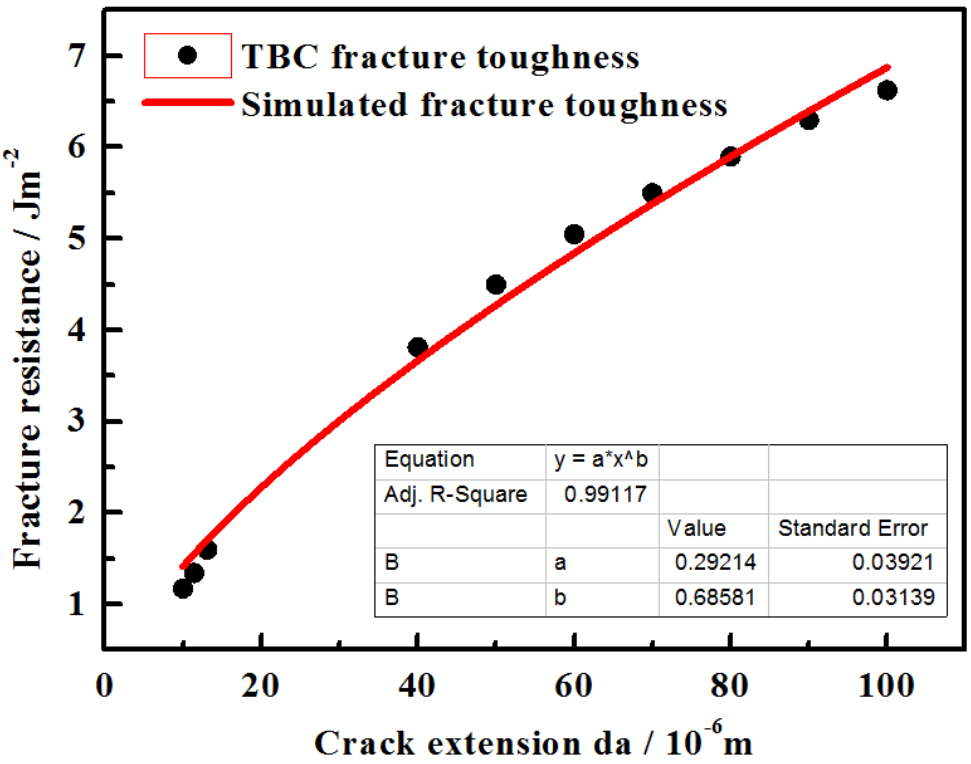

Figure 5-15 Mode I interfacial toughness as a function of crack extension [1]

5.4.4. The crack growth rate *da/dN*

Using the fitted temperature-process-dependent model parameters, the thermal radial stress in eq 5-8 and the stress in eq 5-9 due to dilatational growth of the TGO were calculated and are presented in Figure 5-16 and Figure 5-17 at the valley of the top coat versus exposure time.

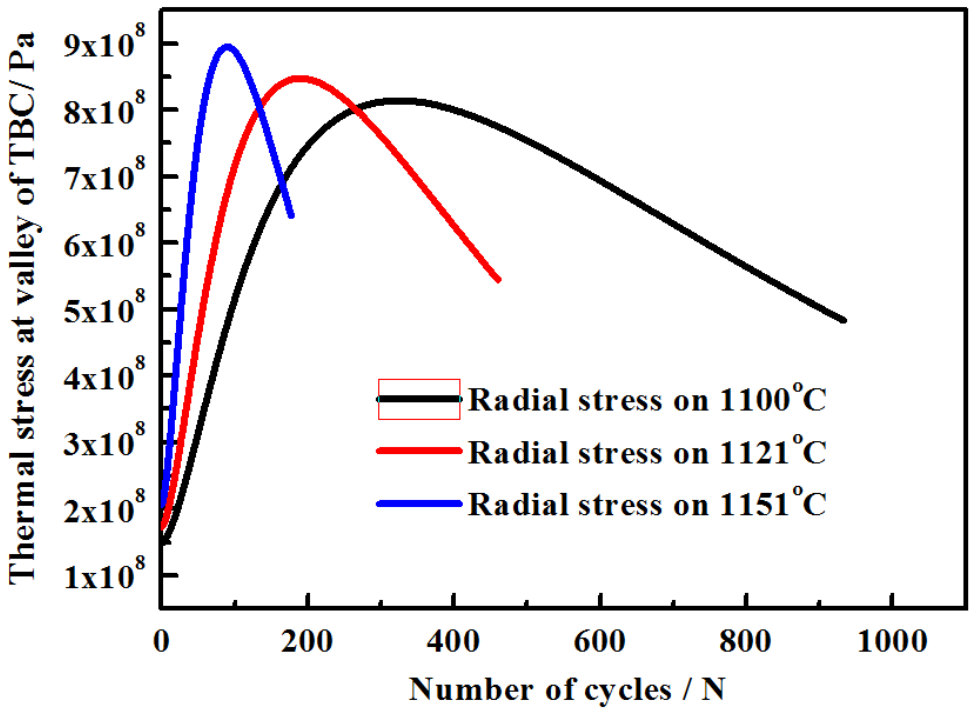

Figure 5-16 thermal stress at valley of topcoat close to TBC/TGO interface where higher stress level could be explained by larger distortion induced by rumpling effect of bond coat for higher temperatures

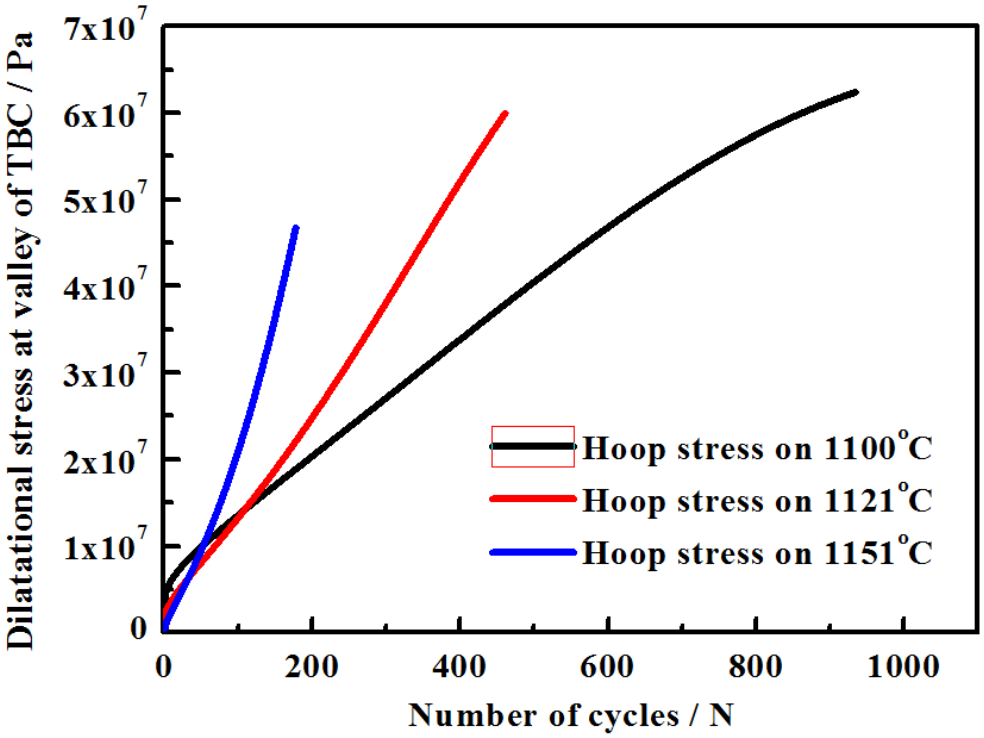

Figure 5-17 Dilatational stress simulation calculated at valley of topcoat coat integrated into lifetime prediction model II as function of number of cycles

It is shown that with the exception of an initial increase of the stress within a short period, it is a common feature that a stress reduction is present after this initial period. A considerable drop in these stresses versus thermal cycles indicates crack nucleation and propagation could be a factor responsible for the stress reduction, i.e., the energy stored is released by cracks at the interface between the top coat and TGO.

The crack growth rate da/dN along the top coat/TGO interface was calculated using eq 5-11 and the exposure-dependent model parameters. The calculation of crack growth rate starts from the valley location of the top coat and after initial 1 cycle, where the result was shown in Figure 5-18.

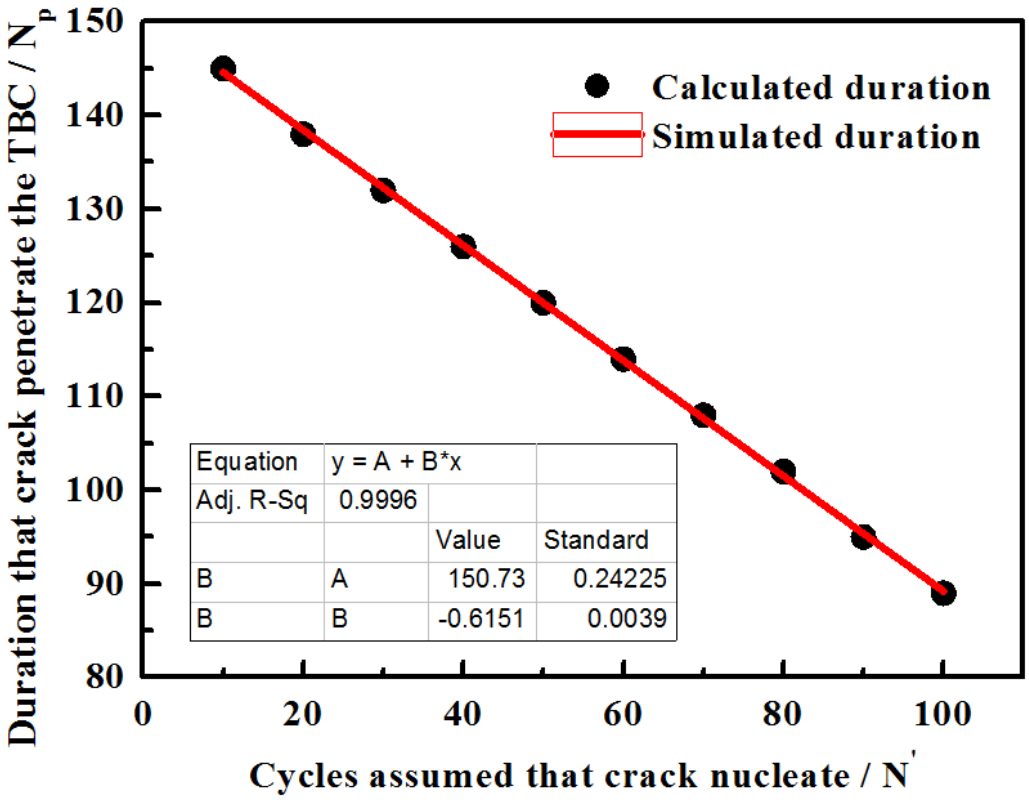

Figure 5-18 Predicted partial lifetime as function of N', it could be reproduced quite nicely by linear fitting

An increase of the crack growth rate was observed versus thermal cycles, despite of an increase of the interfacial fracture toughness K observed as function of crack extension.

This indicates that the thermal and TGO growth stresses plays the most important role as driving forces that promoting the crack nucleation in the early stage of thermal cycles. The integration of eq 5-11 can be applied to studying exposure cycles necessary for a crack growth reaching a certain length, such as the distance between two imperfections within top coat, where the coating failure occurs,

$$\int_0^{d_f-2(R_f+d_{fTGO})} da = \int_{N'}^{Np} f(N)dN \qquad \text{eq 5-22}$$

where *f(N)* represents *da/dN*. The result of integration of crack growth rate using eq 5-22 is shown in Figure 5-19.

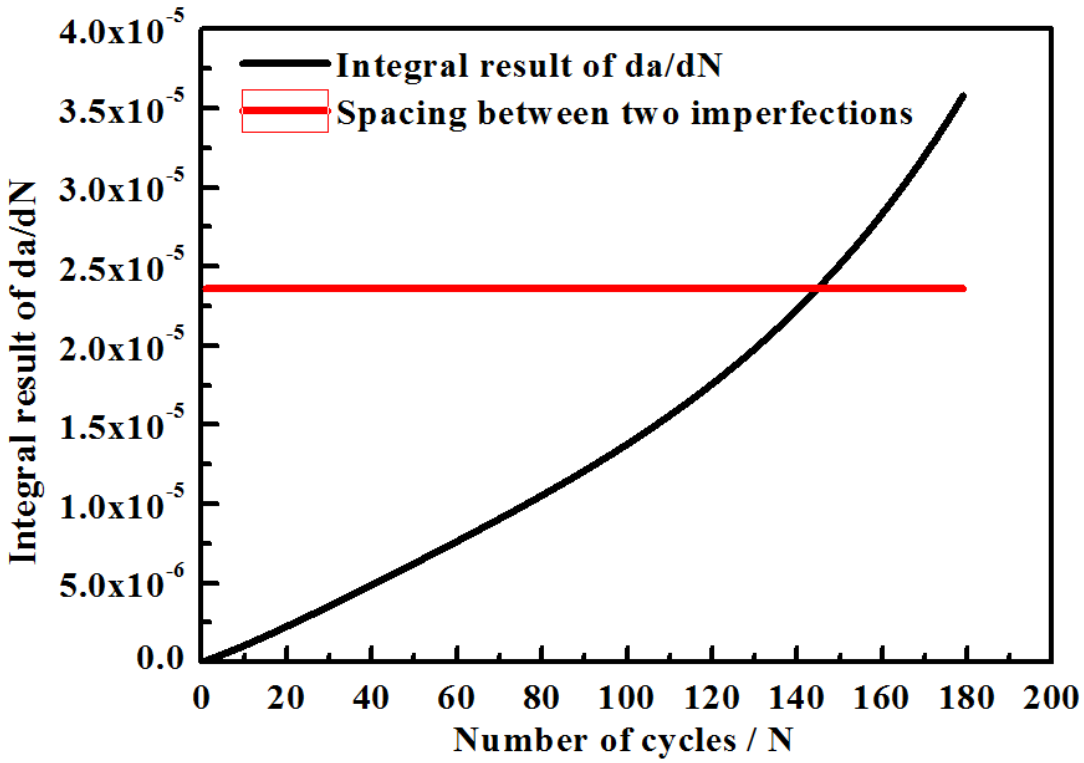

Figure 5-19 integrating results as function of thermal cycle, the integration initiate as N' equals to 10

The derived cycles of N_p from eq 5-22 is 145, indicating a duration that a crack propagates along the top coat/TGO interface from an initial 10 cycles (1 hour per cycle). It should be noticed that there is no direct correlation between the calculated N_p and the entire life N_f of TBC coatings, as predicted in proceeding sections. eq 5-22 only provides

cycles for cracks propagating along the top coat/TGO interface. For the entire TBC coating to fail, cracks need to penetrate the TGO and also propagate along the TGO/bond coat interface, and finally neighboring cracks coalescence within the bond coat.

In crack growth rate analysis, crack length at TGO/TBC between two imperfections was assumed to represent the maximum crack length along the top coat/TGO interface, where the calculated crack length and their proportions versus temperatures are shown in Table 5-6 and Table 5-7.

Table 5-6 Crack length related to failure mode B in terms of temperatures

Temp℃/crack length(μm)	d_{fTGO}	Crack length at BC/TGO	Crack length within TGO	Crack length at TGO/TBC	Sum
		$2\pi R_f/3$	a_{TGO}	$d_f-2(R_f+d_{fTGO})$	
1100	36.01	75.42	18.82	2.83	97.07
1121	19.51	40.86	14.48	23.67	79.01
1151=1424.15K	8.97	18.79	10.61	23.60	53

Table 5-7 Crack length proportionality related to failure mode B in terms of temperatures

Temp℃/Crack length proportionality%	Crack length at BC/TGO	Crack length within TGO	Crack length at TGO/TBC
1100	77.70%	19.39%	2.92%
1121	51.71%	18.33%	29.96%
1151	35.45%	20.02%	44.53%

If a different crack length within top coat was given, then the estimated duration for crack penetration could be varied. A longer time is expected for a crack propagating along the top coat/TGO interface as the crack length increases.

The value of N' representing the starting point for a crack propagation along the TGO/bond coat interface could also affect Np. The calculations demonstrate that as N' increases, Np decreases, Figure 5-18. This could be attributed to the critical effect on increasing of residual stress at early stage of thermal cycles, which in turn leads to an increase of the crack growth rate da/dN. It is difficult to determine at which cycle N' that a crack starts to propagate along the top coat/TGO interface. As discussed previously, the estimation of a crack growth rate at 1151oC relies on the temperature-process-dependent model parameters involved in calculation. It is necessary to point out that eq 5-11 could be only used to estimate crack growth rate at the TGO/topcoat interface provided that the specific stress intensity factor for crack tip within topcoat is given.

5.5. Conclusions

Temperature-process-dependent model parameters were fitted and used in failure analysis and life prediction of electron beam physical vapor deposition thermal barrier coatings (EB-PVD TBCs) of Pt-modified NiAl bond coat on Ni-base single crystal superalloys. In the failure analysis and life prediction of failure mode A, the maximum average rumpling amplitude of the bond coat/TGO interface was used as a failure criterion at three exposure temperatures, in which high exposure temperature leads to a short life, verified using existing burner rig test data. In the life evaluation, the

experimentally determined temperature-dependent thickness of thermally grown oxide (TGO), interfacial roughness, elastic moduli of constituent coatings and their coefficients of thermal expansion were applied in the life model. The global wavelength associated with interface rumpling and its radius curvature were found to play an important role in life evaluation. In estimating crack growth rate along the top coat/TGO interface for failure mode B, the experimentally determined maximum strength 800MPa of the top coat/TGO interface was used to fit stress model parameters of the top coat. Using the experimentally measured average interfacial fracture toughness, the crack growth rate was found to increase, resulting in coating delamination and spallation.

6. Summary and Conclusions

The methodology of lifetime prediction based on failure mechanism analysis of thermal barrier coating system was proposed and applied to evaluate the life for both APS-TBC and EB-PVD TBCs. The experimental data, either the physical or geometrical parameters measured from different stages during thermal cyclic experiments or the lifetime recorded as a function of temperature, was identified. Those parameters played an essential role in determining the temperature-dependent fitting parameters. In APS-TBCs, a non-linear fitting process was selected to estimate the fitting parameter, given that the critical time for stress inversion was calculated as well as enough lifetime data was measured by burner rig test. The temperature-process-dependent fitting parameter for failure mode A in EB-PVD TBCs was also evaluated based on the variation of rumpling amplitude on the interface between the TGO and BC. It was shown in this thesis that the capability for the lifetime prediction model can be improved by using temperature-process-dependent model parameters instead of a mean value for a specific temperature. Meanwhile, the application of analytical solutions to lifetime prediction models was based on newly proposed thermal or dilatational stress model where the stress was determined by the failure mechanism analysis of the coating system followed by FEA such that the sites of maximum stress could be localized and the magnitude of stress could be estimated quantitatively. The stress integrated lifetime prediction model was used in both APS-TBCs and EB-PVD TBCs which consists of energy-released related parameter of crack tip and crack growth rate. The lifetime of TBCs could be evaluated once the temperature-dependent fitting parameter was identified. Moreover,

in APS-TBCs, the interactions of residual stresses representing the top coat, TGO and bond coat were examined. For EB-PVD TBCs, the results of the stress model were briefly discussed such that the creep behavior and crack extension play a major role in the reduction of stress on the topcoat and bond coat.

References

[1] A. G. Evans, D. R. Mumm, J. W. Hutchinson, G. H. Meier, and F. S. Pettit, ‘Mechanisms controlling the durability of thermal barrier coatings’, *Prog. Mater. Sci.*, vol. 46, no. 5, pp. 505–553, 2001.

[2] E. Tzimas, H. Müllejans, S. D. Peteves, J. Bressers, and W. Stamm, ‘Failure of thermal barrier coating systems under cyclic thermomechanical loading’, *Acta Mater.*, vol. 48, no. 18–19, pp. 4699–4707, 2000.

[3] S. Guo and Y. Kagawa, ‘Effect of loading rate and holding time on hardness and Young’s modulus of EB-PVD thermal barrier coating’, *Surf. Coat. Technol.*, vol. 182, no. 1, pp. 92–100, 2004.

[4] U. Schulz, M. Menzebach, C. Leyens, and Y. Q. Yang, ‘Influence of substrate material on oxidation behavior and cyclic lifetime of EB-PVD TBC systems’, *Surf. Coat. Technol.*, vol. 146–147, pp. 117–123, 2001.

[5] N. P. Padture, M. Gell, and E. H. Jordan, ‘Thermal Barrier Coatings for Gas-Turbine Engine Applications’, *Science*, vol. 296, no. 5566, pp. 280–284, Apr. 2002.

[6] W. Beele, G. Marijnissen, and A. van Lieshout, ‘The evolution of thermal barrier coatings — status and upcoming solutions for today’s key issues’, *Surf. Coat. Technol.*, vol. 120–121, pp. 61–67, 1999.

[7] G. Moskal, ‘The porosity assessment of thermal barrier coatings obtained by APS method’, *J. Achiev. Mater. Manuf. Eng.*, vol. 20, no. 1–2, pp. 483–486, Jan. 2007.

[8] S. Guo and Y. Kagawa, ‘Effect of thermal exposure on hardness and Young’s modulus of EB-PVD yttria-partially-stabilized zirconia thermal barrier coatings’,

Ceram. Int., vol. 32, no. 3, pp. 263–270, 2006.

[9] C. Courcier, V. Maurel, L. Rémy, S. Quilici, I. Rouzou, and A. Phelippeau, 'Interfacial damage based life model for EB-PVD thermal barrier coating', *Surf. Coat. Technol.*, vol. 205, no. 13–14, pp. 3763–3773, 2011.

[10] A. G. Evans, M. Y. He, and J. W. Hutchinson, 'Mechanics-based scaling laws for the durability of thermal barrier coatings', *Prog. Mater. Sci.*, vol. 46, no. 3–4, pp. 249–271, 2001.

[11] R. A. Miller, 'Oxidation-Based Model for Thermal Barrier Coating Life', *J. Am. Ceram. Soc.*, vol. 67, no. 8, pp. 517–521, 1984.

[12] J. T. Demasi and M. Ortiz, 'Thermal barrier coating life prediction model development, phase 1', Dec. 1989.

[13] D. R. Mumm, A. G. Evans, and I. T. Spitsberg, 'Characterization of a cyclic displacement instability for a thermally grown oxide in a thermal barrier system', *Acta Mater.*, vol. 49, no. 12, pp. 2329–2340, 2001.

[14] R. Vaßen, S. Giesen, and D. Stöver, 'Lifetime of Plasma-Sprayed Thermal Barrier Coatings: Comparison of Numerical and Experimental Results', *J. Therm. Spray Technol.*, vol. 18, no. 5–6, p. 835, Sep. 2009.

[15] Z. Lu, S.-W. Myoung, Y.-G. Jung, G. Balakrishnan, J. Lee, and U. Paik, 'Thermal Fatigue Behavior of Air-Plasma Sprayed Thermal Barrier Coating with Bond Coat Species in Cyclic Thermal Exposure', *Materials*, vol. 6, no. 8, pp. 3387–3403, Aug. 2013.

[16] X. Zhang, K. Zhou, W. Xu, J. Song, C. Deng, and M. Liu, 'Reaction Mechanism

and Thermal Insulation Property of Al-deposited 7YSZ Thermal Barrier Coating', *J. Mater. Sci. Technol.*, vol. 31, no. 10, pp. 1006–1010, 2015.

[17] G. Dwivedi, V. Viswanathan, S. Sampath, A. Shyam, and E. Lara-Curzio, 'Fracture Toughness of Plasma-Sprayed Thermal Barrier Ceramics: Influence of Processing, Microstructure, and Thermal Aging', *J. Am. Ceram. Soc.*, vol. 97, no. 9, pp. 2736–2744, 2014.

[18] J. Zhang and V. Desai, 'Evaluation of thickness, porosity and pore shape of plasma sprayed TBC by electrochemical impedance spectroscopy', *Surf. Coat. Technol.*, vol. 190, no. 1, pp. 98–109, 2005.

[19] J. R. Nicholls, M. J. Deakin, and D. S. Rickerby, 'A comparison between the erosion behaviour of thermal spray and electron beam physical vapour deposition thermal barrier coatings', *Wear*, vol. 233–235, pp. 352–361, 1999.

[20] S. Kyaw, A. Jones, and T. Hyde, 'Predicting failure within TBC system: Finite element simulation of stress within TBC system as affected by sintering of APS TBC, geometry of substrate and creep of TGO', *Eng. Fail. Anal.*, vol. 27, pp. 150–164, 2013.

[21] C.-J. Li, Y. Li, G.-J. Yang, and C.-X. Li, 'A Novel Plasma-Sprayed Durable Thermal Barrier Coating with a Well-Bonded YSZ Interlayer Between Porous YSZ and Bond Coat', *J. Therm. Spray Technol.*, vol. 21, no. 3–4, pp. 383–390, Mar. 2012.

[22] X. Zhao and P. Xiao, 'Thermal Barrier Coatings on Nickel Superalloy Substrates', *Mater. Sci. Forum*, vol. 606, pp. 1–26, 2009.

[23] R. W. Steinbrech and D. Basu, 'Ceramic Based Thermal Barrier Coating (TBC) for

Gas Turbine Application: Elastic Behaviour of Plasma Sprayed TBC', *Trans. Indian Ceram. Soc.*, vol. 62, no. 4, pp. 192–199, 2003.

[24] S. L, M. G, M. B, and G. T, 'Characterisation of air plasma sprayed TBC coating during isothermal oxidation at 1100°C', *ResearchGate*, vol. 21, no. 2, Apr. 2007.

[25] R. Ghasemi, R. Shoja-Razavi, R. Mozafarinia, and H. Jamali, 'Comparison of microstructure and mechanical properties of plasma-sprayed nanostructured and conventional yttria stabilized zirconia thermal barrier coatings', *Ceram. Int.*, vol. 39, no. 8, pp. 8805–8813, 2013.

[26] T. Patterson, A. Leon, B. Jayaraj, J. Liu, and Y. H. Sohn, 'Thermal cyclic lifetime and oxidation behavior of air plasma sprayed CoNiCrAlY bond coats for thermal barrier coatings', *Surf. Coat. Technol.*, vol. 203, no. 5–7, pp. 437–441, 2008.

[27] M. Schweda, T. Beck, and L. Singheiser, 'Thermal cycling damage evolution of a thermal barrier coating and the influence of substrate creep, interface roughness and pre-oxidation', *Int. J. Mater. Res.*, vol. 103, no. 1, pp. 40–49, 2012.

[28] W. X. Zhang, X. L. Fan, and T. J. Wang, 'The surface cracking behavior in air plasma sprayed thermal barrier coating system incorporating interface roughness effect', *Appl. Surf. Sci.*, vol. 258, no. 2, pp. 811–817, 2011.

[29] R. Vaßen, G. Kerkhoff, and D. Stöver, 'Development of a micromechanical life prediction model for plasma sprayed thermal barrier coatings', *Mater. Sci. Eng. A*, vol. 303, no. 1–2, pp. 100–109, 2001.

[30] W. R. Chen, X. Wu, B. R. Marple, R. S. Lima, and P. C. Patnaik, 'Pre-oxidation and TGO growth behaviour of an air-plasma-sprayed thermal barrier coating', *Surf.*

Coat. Technol., vol. 202, no. 16, pp. 3787–3796, 2008.

[31] W. R. Chen, X. Wu, B. R. Marple, and P. C. Patnaik, 'The growth and influence of thermally grown oxide in a thermal barrier coating', *Surf. Coat. Technol.*, vol. 201, no. 3–4, pp. 1074–1079, 2006.

[32] A. Rabiei and A. G. Evans, 'Failure mechanisms associated with the thermally grown oxide in plasma-sprayed thermal barrier coatings', *Acta Mater.*, vol. 48, no. 15, pp. 3963–3976, 2000.

[33] W. R. Chen, X. Wu, and D. Dudzinski, 'Influence of Thermal Cycle Frequency on the TGO Growth and Cracking Behaviors of an APS-TBC', *J. Therm. Spray Technol.*, vol. 21, no. 6, pp. 1294–1299, Oct. 2012.

[34] M. Karadge, X. Zhao, M. Preuss, and P. Xiao, 'Microtexture of the thermally grown alumina in commercial thermal barrier coatings', *Scr. Mater.*, vol. 54, no. 4, pp. 639–644, 2006.

[35] J. Moon, H. Choi, H. Kim, and C. Lee, 'The effects of heat treatment on the phase transformation behavior of plasma-sprayed stabilized ZrO2 coatings', *Surf. Coat. Technol.*, vol. 155, no. 1, pp. 1–10, 2002.

[36] M. Jinnestrand and H. Brodin, 'Crack initiation and propagation in air plasma sprayed thermal barrier coatings, testing and mathematical modelling of low cycle fatigue behaviour', *Mater. Sci. Eng. A*, vol. 379, no. 1–2, pp. 45–57, 2004.

[37] J. R. VanValzah and H. E. Eaton, 'Cooling rate effects on the tetragonal to monoclinic phase transformation in aged plasma-sprayed yttria partially stabilized zirconia', *Surf. Coat. Technol.*, vol. 46, no. 3, pp. 289–300, 1991.

[38] F. H. Yuan, Z. X. Chen, Z. W. Huang, Z. G. Wang, and S. J. Zhu, 'Oxidation behavior of thermal barrier coatings with HVOF and detonation-sprayed NiCrAlY bondcoats', *Corros. Sci.*, vol. 50, no. 6, pp. 1608–1617, 2008.

[39] M. Ranjbar-Far, J. Absi, G. Mariaux, and F. Dubois, 'Simulation of the effect of material properties and interface roughness on the stress distribution in thermal barrier coatings using finite element method', *Mater. Des.*, vol. 31, no. 2, pp. 772–781, 2010.

[40] A. C. Karaoglanli, K. M. Doleker, B. Demirel, A. Turk, and R. Varol, 'Effect of shot peening on the oxidation behavior of thermal barrier coatings', *Appl. Surf. Sci.*, vol. 354, Part B, pp. 314–322, 2015.

[41] W. R. Chen, X. Wu, B. R. Marple, and P. C. Patnaik, 'Oxidation and crack nucleation/growth in an air-plasma-sprayed thermal barrier coating with NiCrAlY bond coat', *Surf. Coat. Technol.*, vol. 197, no. 1, pp. 109–115, 2005.

[42] J. Kimmel, Z. Mutasim, and W. Brentnall, 'Effects of Alloy Composition on the Performance of Yttria Stabilized Zirconia–Thermal Barrier Coatings', p. V004T02A014, 1999.

[43] W. Nowak, D. Naumenko, G. Mor, F. Mor, D. E. Mack, R. Vassen, L. Singheiser, and W. J. Quadakkers, 'Effect of processing parameters on MCrAlY bondcoat roughness and lifetime of APS–TBC systems', *Surf. Coat. Technol.*, vol. 260, pp. 82–89, 2014.

[44] Y. Bai, C. Ding, H. Li, Z. Han, B. Ding, T. Wang, and L. Yu, 'Isothermal Oxidation Behavior of Supersonic Atmospheric Plasma-Sprayed Thermal Barrier Coating

System', *J. Therm. Spray Technol.*, vol. 22, no. 7, pp. 1201–1209, Aug. 2013.

[45] M. Tanaka, M. Hasegawa, and Y. Kagawa, 'Detection of Micro-Damage Evolution of Air Plasma-Sprayed Y₂O₃-ZrO₂ Thermal Barrier Coating through TGO Stress Measurement', *Mater. Trans.*, vol. 47, no. 10, pp. 2512–2517, 2006.

[46] D. Liu, M. Seraffon, P. E. J. Flewitt, N. J. Simms, J. R. Nicholls, and D. S. Rickerby, 'Effect of substrate curvature on residual stresses and failure modes of an air plasma sprayed thermal barrier coating system', *J. Eur. Ceram. Soc.*, vol. 33, no. 15–16, pp. 3345–3357, 2013.

[47] P. Song, *Influence of Material and Testing Parameters on the Lifetime of TBC Systems with MCrAlY and NiPtAl Bondcoats*. Forschungszentrum Jülich GmbH Zentralbibliothek Verlag, 2012.

[48] R. Eriksson, H. Brodin, S. Johansson, L. Östergren, and X.-H. Li, 'Influence of isothermal and cyclic heat treatments on the adhesion of plasma sprayed thermal barrier coatings', *Surf. Coat. Technol.*, vol. 205, no. 23–24, pp. 5422–5429, 2011.

[49] A. Fossati, M. D. Ferdinando, A. Lavacchi, A. Scrivani, C. Giolli, and U. Bardi, 'Improvement of the Oxidation Resistance of CoNiCrAlY Bond Coats Sprayed by High Velocity Oxygen-Fuel onto Nickel Superalloy Substrate', *Coatings*, vol. 1, no. 1, pp. 3–16, Nov. 2010.

[50] T. Beck, R. Herzog, O. Trunova, M. Offermann, R. W. Steinbrech, and L. Singheiser, 'Damage mechanisms and lifetime behavior of plasma-sprayed thermal barrier coating systems for gas turbines — Part II: Modeling', *Surf. Coat. Technol.*,

vol. 202, no. 24, pp. 5901–5908, 2008.

[51] E. P. Busso, H. E. Evans, L. Wright, L. N. McCartney, J. Nunn, and S. Osgerby, ‘A software tool for lifetime prediction of thermal barrier coating systems’, *Mater. Corros.*, vol. 59, no. 7, pp. 556–565, 2008.

[52] M. Ahrens, R. Vaßen, and D. Stöver, ‘Stress distributions in plasma-sprayed thermal barrier coatings as a function of interface roughness and oxide scale thickness’, *Surf. Coat. Technol.*, vol. 161, no. 1, pp. 26–35, 2002.

[53] D. Renusch, M. Schorr, and M. Schütze, ‘The role that bond coat depletion of aluminum has on the lifetime of APS-TBC under oxidizing conditions’, *Mater. Corros.*, vol. 59, no. 7, pp. 547–555, 2008.

[54] F. Traeger, M. Ahrens, R. Vaßen, and D. Stöver, ‘A life time model for ceramic thermal barrier coatings’, *Mater. Sci. Eng. A*, vol. 358, no. 1–2, pp. 255–265, 2003.

[55] J. R. Nicholls, K. J. Lawson, A. Johnstone, and D. S. Rickerby, ‘Methods to reduce the thermal conductivity of EB-PVD TBCs’, *Surf. Coat. Technol.*, vol. 151–152, pp. 383–391, 2002.

[56] R. A. Miller, ‘Thermal barrier coatings for aircraft engines: history and directions’, *J. Therm. Spray Technol.*, vol. 6, no. 1, p. 35.

[57] P. Morrell and D. S. Rickerby, ‘Advantages/Disadvantages of Various TBC Systems as perceived by the Engine Manufacturer’, *ResearchGate*.

[58] C. H. Liebert, R. E. Jacobs, S. Stecura, and C. R. Morse, ‘Durability of zirconia thermal-barrier ceramic coatings on air-cooled turbine blades in cyclic jet engine operation’, Sep. 1976.

[59] S. Alperine, M. Derrien, Y. Jaslier, and R. Mevrel, ‘Thermal barrier coatings: The thermal conductivity challenge’, *NATO Workshop Therm. Barrier Coat.*, vol. AGARD-R-823, p. paper 1, 1998.

[60] T. E. Strangman and J. Schienle, ‘Tailoring Zirconia Coatings for Performance in a Marine Gas Turbine Environment’, p. V002T03A010, 1989.

[61] H. Xu, S. Gong, and L. Deng, ‘Preparation of thermal barrier coatings for gas turbine blades by EB-PVD’, *Thin Solid Films*, vol. 334, no. 1–2, pp. 98–102, 1998.

[62] A. Hesnawi, H. Li, Z. Zhou, S. Gong, and H. Xu, ‘Isothermal oxidation behaviour of EB-PVD MCrAlY bond coat’, *Vacuum*, vol. 81, no. 8, pp. 947–952, 2007.

[63] M. Movchan and Y. Rudoy, ‘Composition, structure and properties of gradient thermal barrier coatings (TBCs) produced by electron beam physical vapor deposition (EB-PVD).’, *Mater. Des.*, vol. 19, no. 5–6, pp. 253–258, 1998.

[64] V. K. Tolpygo and D. R. Clarke, ‘The effect of oxidation pre-treatment on the cyclic life of EB-PVD thermal barrier coatings with platinum–aluminide bond coats’, *Surf. Coat. Technol.*, vol. 200, no. 5–6, pp. 1276–1281, 2005.

[65] K. S. Murphy, K. L. More, and M. J. Lance, ‘As-deposited mixed zone in thermally grown oxide beneath a thermal barrier coating’, *Surf. Coat. Technol.*, vol. 146–147, pp. 152–161, 2001.

[66] H. Svensson, J. Angenete, and K. Stiller, ‘Microstructure of oxide scales on aluminide diffusion coatings after short time oxidation at 1050 °C’, *Surf. Coat. Technol.*, vol. 177–178, pp. 152–157, 2004.

[67] S. Laxman, B. Franke, B. W. Kempshall, Y. H. Sohn, L. A. Giannuzzi, and K. S.

Murphy, ‘Phase transformations of thermally grown oxide on (Ni,Pt)Al bondcoat during electron beam physical vapor deposition and subsequent oxidation’, *Surf. Coat. Technol.*, vol. 177–178, pp. 121–130, 2004.

[68] Z. Xu, L. He, X. Zhong, R. Mu, S. He, and X. Cao, ‘Thermal barrier coating of lanthanum–zirconium–cerium composite oxide made by electron beam-physical vapor deposition’, *J. Alloys Compd.*, vol. 478, no. 1–2, pp. 168–172, 2009.

[69] H. Guo, S. Gong, K. Aik Khor, and H. Xu, ‘Effect of thermal exposure on the microstructure and properties of EB-PVD gradient thermal barrier coatings’, *Surf. Coat. Technol.*, vol. 168, no. 1, pp. 23–29, 2003.

[70] J. Liu, J. W. Byeon, and Y. H. Sohn, ‘Effects of phase constituents/microstructure of thermally grown oxide on the failure of EB-PVD thermal barrier coating with NiCoCrAlY bond coat’, *Surf. Coat. Technol.*, vol. 200, no. 20–21, pp. 5869–5876, 2006.

[71] Y. H. Sohn, K. Vaidyanathan, M. Ronski, E. H. Jordan, and M. Gell, ‘Thermal cycling of EB-PVD/MCrAlY thermal barrier coatings: II. Evolution of photo-stimulated luminescence’, *Surf. Coat. Technol.*, vol. 146–147, pp. 102–109, 2001.

[72] D. M. Lipkin, H. Schaffer, F. Adar, and D. R. Clarke, ‘Lateral growth kinetics of α-alumina accompanying the formation of a protective scale on (111) NiAl during oxidation at 1100 °C’, *Appl. Phys. Lett.*, vol. 70, no. 19, pp. 2550–2552, May 1997.

[73] V. K. Tolpygo and D. R. Clarke, ‘Competition Between Stress Generation and Relaxation During Oxidation of an Fe-Cr-Al-Y Alloy’, *Oxid. Met.*, vol. 49, no. 1–2, pp. 187–212.

[74] V. K. Tolpygo and D. R. Clarke, ‘Wrinkling of α-alumina films grown by thermal oxidation—I. Quantitative studies on single crystals of Fe–Cr–Al alloy’, *Acta Mater.*, vol. 46, no. 14, pp. 5153–5166, 1998.

[75] V. K. Tolpygo, J. R. Dryden, and D. R. Clarke, ‘Determination of the growth stress and strain in α-Al2O3 scales during the oxidation of Fe–22Cr–4.8Al–0.3Y alloy’, *Acta Mater.*, vol. 46, no. 3, pp. 927–937, 1998.

[76] E. Y. Lee, R. R. Biederman, and R. D. Sisson, ‘Proceedings of the 2nd International Symposium on High Temperature Corrosion of Advanced Materials and CoatingsDiffusional interactions and reactions between a partially stabilized zirconia thermal barrier coating and the NiCrAlY bond coat’, *Mater. Sci. Eng. A*, vol. 120, pp. 467–473, 1989.

[77] Y. H. Sohn, J. H. Kim, E. H. Jordan, and M. Gell, ‘Thermal cycling of EB-PVD/MCrAlY thermal barrier coatings: I. Microstructural development and spallation mechanisms’, *Surf. Coat. Technol.*, vol. 146–147, pp. 70–78, 2001.

[78] M. H. Li, Z. Y. Zhang, X. F. Sun, H. R. Guan, W. Y. Hu, and Z. Q. Hu, ‘Oxidation and Degradation of EB–PVD Thermal–Barrier Coatings’, *Oxid. Met.*, vol. 58, no. 5–6, pp. 499–512.

[79] M. H. Li, X. F. Sun, S. K. Gong, Z. Y. Zhang, H. R. Guan, and Z. Q. Hu, ‘Phase transformation and bond coat oxidation behavior of EB-PVD thermal barrier coating’, *Surf. Coat. Technol.*, vol. 176, no. 2, pp. 209–214, 2004.

[80] M. Li, X. Sun, W. Hu, and H. Guan, ‘Thermocyclic behavior of sputtered NiCrAlY/EB-PVD 7 wt.%Y2O3–ZrO2 thermal barrier coatings’, *Surf. Coat.*

Technol., vol. 200, no. 12–13, pp. 3770–3774, 2006.

[81] E.Y. Lee, 'Life prediction and failure mechanisms for thermal barrier coatings', *PhD Diss.*, vol. Worcester Polytechnic Institute, 1991.

[82] J. Allen Haynes, E. Douglas Rigney, M. K. Ferber, and W. D. Porter, 'Oxidation and degradation of a plasma-sprayed thermal barrier coating system', *Surf. Coat. Technol.*, vol. 86, pp. 102–108, 1996.

[83] C. A. Calow and I. T. Porter, 'The solid state bonding of nickel to alumina', *J. Mater. Sci.*, vol. 6, no. 2, pp. 156–163.

[84] T. Xu, M. Y. He, and A. G. Evans, 'A numerical assessment of the durability of thermal barrier systems that fail by ratcheting of the thermally grown oxide', *Acta Mater.*, vol. 51, no. 13, pp. 3807–3820, 2003.

[85] I. T. Spitsberg, D. R. Mumm, and A. G. Evans, 'On the failure mechanisms of thermal barrier coatings with diffusion aluminide bond coatings', *Mater. Sci. Eng. A*, vol. 394, no. 1–2, pp. 176–191, 2005.

[86] S.-S. Kim, Y.-F. Liu, and Y. Kagawa, 'Evaluation of interfacial mechanical properties under shear loading in EB-PVD TBCs by the pushout method', *Acta Mater.*, vol. 55, no. 11, pp. 3771–3781, 2007.

[87] D. S. Balint, S.-S. Kim, Y.-F. Liu, R. Kitazawa, Y. Kagawa, and A. G. Evans, 'Anisotropic TGO rumpling in EB-PVD thermal barrier coatings under in-phase thermomechanical loading', *Acta Mater.*, vol. 59, no. 6, pp. 2544–2555, 2011.

[88] N. M. Yanar, M. Helminiak, G. H. Meier, and F. S. Pettit, 'Comparison of the Failures during Cyclic Oxidation of Yttria-Stabilized (7 to 8 Weight Percent)

Zirconia Thermal Barrier Coatings Fabricated via Electron Beam Physical Vapor Deposition and Air Plasma Spray', *Metall. Mater. Trans. A*, vol. 42, no. 4, pp. 905–921, Nov. 2010.

[89] M. Wen, E. H. Jordan, and M. Gell, 'Effect of temperature on rumpling and thermally grown oxide stress in an EB-PVD thermal barrier coating', *Surf. Coat. Technol.*, vol. 201, no. 6, pp. 3289–3298, 2006.

[90] K. Vaidyanathan, E. H. Jordan, and M. Gell, 'Surface geometry and strain energy effects in the failure of a (Ni, Pt)Al/EB-PVD thermal barrier coating', *Acta Mater.*, vol. 52, no. 5, pp. 1107–1115, 2004.

[91] L. Zhou, S. Mukherjee, K. Huang, Y. W. Park, and Y. Sohn, 'Failure characteristics and mechanisms of EB-PVD TBCs with Pt-modified NiAl bond coats', *Mater. Sci. Eng. A*, vol. 637, pp. 98–106, 2015.

[92] E. P. Busso, Z. Q. Qian, M. P. Taylor, and H. E. Evans, 'The influence of bondcoat and topcoat mechanical properties on stress development in thermal barrier coating systems', *Acta Mater.*, vol. 57, no. 8, pp. 2349–2361, 2009.

[93] S. Sridharan, L. Xie, E. H. Jordan, M. Gell, and K. S. Murphy, 'Damage evolution in an electron beam physical vapor deposited thermal barrier coating as a function of cycle temperature and time', *Mater. Sci. Eng. A*, vol. 393, no. 1–2, pp. 51–62, 2005.

[94] V. K. Tolpygo, D. R. Clarke, and K. S. Murphy, 'Evaluation of interface degradation during cyclic oxidation of EB-PVD thermal barrier coatings and correlation with TGO luminescence', *Surf. Coat. Technol.*, vol. 188–189, pp. 62–

70, 2004.

[95] K. W. Schlichting, N. P. Padture, E. H. Jordan, and M. Gell, ‘Failure modes in plasma-sprayed thermal barrier coatings’, *Mater. Sci. Eng. A*, vol. 342, no. 1–2, pp. 120–130, 2003.

[96] D. R. Clarke and W. Pompe, ‘Critical radius for interface separation of a compressively stressed film from a rough surface’, *Acta Mater.*, vol. 47, no. 6, pp. 1749–1756, 1999.

[97] C. H. Hsueh and E. R. J. Fuller, ‘Analytical modeling of oxide thickness effects on residual stresses in thermal barrier coatings’, *Scr. Mater.*, vol. 42, no. 8, 2000.

[98] T. Strangman, D. Raybould, A. Jameel, and W. Baker, ‘Damage mechanisms, life prediction, and development of EB-PVD thermal barrier coatings for turbine airfoils’, *Surf. Coat. Technol.*, vol. 202, no. 4–7, pp. 658–664, 2007.

[99] V. K. Tolpygo, D. R. Clarke, and K. S. Murphy, ‘Oxidation-induced failure of EB-PVD thermal barrier coatings’, *Surf. Coat. Technol.*, vol. 146–147, pp. 124–131, 2001.

[100] R. Kitazawa, H. Kakisawa, and Y. Kagawa, ‘Anisotropic TGO morphology and stress distribution in EB-PVD Y2O3-ZrO2 thermal barrier coating after in-phase thermo-mechanical test’, *Surf. Coat. Technol.*, vol. 238, pp. 68–74, 2014.

[101] X. Zhao, J. Liu, D. S. Rickerby, R. J. Jones, and P. Xiao, ‘Evolution of interfacial toughness of a thermal barrier system with a Pt-diffused γ/γ′ bond coat’, *Acta Mater.*, vol. 59, no. 16, pp. 6401–6411, 2011.

[102] J. L. Smialek, ‘Compiled furnace cyclic lives of EB-PVD thermal barrier

coatings', *Surf. Coat. Technol.*, vol. 276, pp. 31–38, 2015.

[103] Y. Y. Zhang, H. X. Deng, H. J. Shi, H. C. Yu, and B. Zhong, 'Failure characteristics and life prediction for thermally cycled thermal barrier coatings', *Surf. Coat. Technol.*, vol. 206, no. 11–12, pp. 2977–2985, 2012.

[104] L. Xie, Y. Sohn, E. H. Jordan, and M. Gell, 'The effect of bond coat grit blasting on the durability and thermally grown oxide stress in an electron beam physical vapor deposited thermal barrier coating', *Surf. Coat. Technol.*, vol. 176, no. 1, pp. 57–66, 2003.

[105] X. Zhao, X. Wang, and P. Xiao, 'Sintering and failure behaviour of EB-PVD thermal barrier coating after isothermal treatment', *Surf. Coat. Technol.*, vol. 200, no. 20–21, pp. 5946–5955, 2006.

[106] X. Wang, C. Wang, and A. Atkinson, 'Interface fracture toughness in thermal barrier coatings by cross-sectional indentation', *Acta Mater.*, vol. 60, no. 17, pp. 6152–6163, 2012.